Final Report for AOARD Grant FA2386-12-1-4006

Surface Modification and Nanojunction Fabrication with Molecular Metal Wires

December 21, 2012

Name of Principal Investigators:

Taiwan PI and co-PI:	Shie-Ming Peng	Co-PI:	Chun-hsien Chen
− e-mail address:	smpeng@ntu.edu.tw		chhchen@ntu.edu.tw
− Institution:	National Taiwan University		National Taiwan University
− Mailing Address:	No. 1, Sec. 4, Roosevelt Rd. Taipei, Taiwan 10617		No. 1, Sec. 4, Roosevelt Rd. Taipei, Taiwan 10617
− Phone:	+886-2-3366 1655		+886-2-3366 4191
− Fax:	+886-2-8369 3765		

US PI:	Tong Ren
− e-mail address:	tren@purdue.edu
− Institution:	Purdue University
− Mailing Address:	560 Oval Drive West Lafayette, IN 47907
− Phone:	765-494-5466

Period of Performance: 11/28/2011 – 11/27/2012

Report Documentation Page

Form Approved
OMB No. 0704-0188

1. REPORT DATE	2. REPORT TYPE	3. DATES COVERED
08 JAN 2013	**Final**	**01-12-2011 to 30-11-2012**

4. TITLE AND SUBTITLE
Surface Modification and Nanojunction Fabrication with Molecular Metal Wires

5a. CONTRACT NUMBER
FA23861214006

5b. GRANT NUMBER

5c. PROGRAM ELEMENT NUMBER

6. AUTHOR(S)
Shie-Ming Peng

5d. PROJECT NUMBER

5e. TASK NUMBER

5f. WORK UNIT NUMBER

7. PERFORMING ORGANIZATION NAME(S) AND ADDRESS(ES)
National Taiwan University,1 Roosevelt Rd Sec 4,Taipei ,Taiwan,TW,10000

8. PERFORMING ORGANIZATION REPORT NUMBER
N/A

9. SPONSORING/MONITORING AGENCY NAME(S) AND ADDRESS(ES)
AOARD, UNIT 45002, APO, AP, 96338-5002

10. SPONSOR/MONITOR'S ACRONYM(S)
AOARD

11. SPONSOR/MONITOR'S REPORT NUMBER(S)
AOARD-124006

12. DISTRIBUTION/AVAILABILITY STATEMENT
Approved for public release; distribution unlimited

13. SUPPLEMENTARY NOTES

14. ABSTRACT
The long-term research interests of this work focus on behaviors of electron transfer through metal-metal bonds which can be extended with more metal atoms or with axially coordinated functionality and thus evolves into a unique category of functional molecular wires. The work carried out in this AOARD project is the synthesis of novel molecular metal wires, including pentachromium compounds (New J. Chem. 2012, 36, 632), rigid diazaphenoxazine as the equatorial ligands (Dalton Trans. 2012, 41, 3166), a naphthyridine-based ligand to furnish tetranickel metal wires (C. R. Chim. 2012, 15, 159), and diruthenium moieties coordinated axially with ethynyls to form linear π-conjugated molecular wires (Inorg. Chem. 2012, 51, 3261; 2012, 51, 7561; Organometallics 2013, 32, in press).

15. SUBJECT TERMS
Chemical Synthesis, molecular Electronics, Inorganic Chemistry

16. SECURITY CLASSIFICATION OF:			17. LIMITATION OF ABSTRACT	18. NUMBER OF PAGES	19a. NAME OF RESPONSIBLE PERSON
a. REPORT	b. ABSTRACT	c. THIS PAGE			
unclassified	**unclassified**	**unclassified**	**Same as Report (SAR)**	**43**	

Abstract
Our long-term research interests focus on behaviors of electron transfer through metal-metal bonds which can be extended with more metal atoms or with axially coordinated functionality and thus evolves into a unique category of functional molecular wires. The work carried out in this AOARD project is the synthesis of novel molecular metal wires, including pentachromium compounds (*New J. Chem.* **2012**, *36*, 632), rigid diazaphenoxazine as the equatorial ligands (*Dalton Trans.* **2012**, *41*, 3166), a naphthyridine-based ligand to furnish tetranickel metal wires (*C. R. Chim.* **2012**, *15*, 159), and diruthenium moieties coordinated axially with ethynyls to form linear π-conjugated molecular wires (*Inorg. Chem.* **2012**, *51*, 3261; **2012**, *51*, 7561; *Organometallics* **2013**, *32*, in press). Studies show that the ligands perturb the electronic structures and the electron-transport properties of the metal-metal frameworks. Such a long-term contribution to this research field received recognition from Japan Society of Coordination Chemistry with the 2011 International Award (previous awardees: Michael Grätzel, James P. Collman, Jean-Pierre Sauvage, and Harry B. Gray). An account was published in 2012 (*Bull. Jap. Soc. Coord. Chem.* **2012**, *59*, 3) on the synthesis and characterization of molecular metal wires.

Introduction

EMACs (Extended Metal Atom Chains, Scheme 1) represent a unique category of molecular wires because most compounds studied in this research field are limited to carbon-based molecules involving conjugated double bond, triple bonds, and aryl moieties. Instead of transporting through the π-electron conjugated framework of carbon-carbon bonds, the metal-metal chains of EMACs are the conducting pathways. Furthermore, these complexes are similar to the electric wires in our macroscopic world as proposed by Cotton's group and demonstrated by the simulation work of Jin's group (*J. Phys. Chem. C* **2010**, *114*, 3641). Hence, EMACs alone or being further hybridized with organic ligands are particularly attractive in the field of molecular electronics. The summary of our recent advancement and goals of this research can be found in a feature article in *Chem. Commun.* (**2009**, 4323), a monograph in *Nano Redox Sites: Nano-Space Control and its Applications* (ed. T. Hirao, Springer, Berlin, 2006, Ch. 5, pp. 85–117), an account in *Bull. Jpn. Soc. Coord. Chem.* (**2012**, *59*, 3), and a short review in *Comptes Rendus Chim.* (**2009**, *12*, 321, Wire-like Diruthenium -alkynyl Compounds and Charge Mobility Therein).

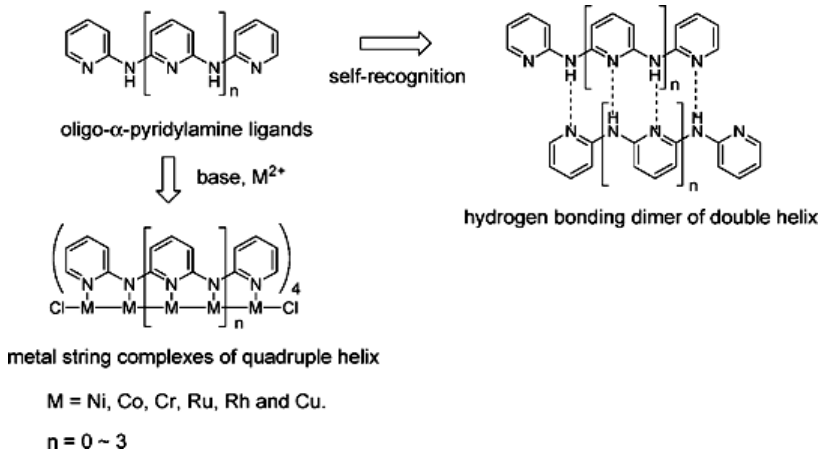

Scheme 1 Oligo- -pyridylamine ligands and metal string complexes (*Chem. Commun.* **2009**, 4323).

The prototypical framework of the metal string complexes consists of a one-dimensional linear transition metal backbone. The metal cores are coordinated by two axial ligands at termini and by four equatorial ligands of oligo-α-pyridylamido anions (Scheme 1). Previous STM measurements showed that resistances ranged from 0.9 MΩ to 24 MΩ for $[Ni_3(dpa)_4(NCS)_2]$, $[Co_3(dpa)_4(NCS)_2]$, $[Cr_3(dpa)_4(NCS)_2]$, $[Ni_5(tpda)_4(NCS)_2]$, $[Co_5(tpda)_4(NCS)_2]$, and $[Cr_5(tpda)_4(NCS)_2]$. The results are qualitatively well correlated with the metal–metal bond orders. Namely, EMACs with stronger metal–metal interaction exhibit higher conductivity.

Metal alkynyl complexes have been considered as building blocks for molecular wires. Diruthenium units prepared in this team are shown efficient electron/hole transport media (recent examples: *J. Am. Chem. Soc.* **2011**, *133*, 15094; *Angew. Chem. Int. Ed.* **2010**, *49*, 954). The attenuation of charge transport properties via the design of axial and equatorial ligands is a current focus of the research.

The measurements in electron/hole transporting through the metal-metal bonds are the first step of the exploration of the tailored metal string complexes to become functional devices in the future molecular electronics. Therefore, the development of synthetic strategies that tune the molecular properties is of paramount importance. During the course of this project, this team demonstrated approaches to adjust the properties of EMACs and diruthenium, including the modification of the ligands which improve the delocalization of unpaired electrons and thus the molecular conductance. The results of these studied are reported by providing the abstract of the corresponding publication. Current progress of heterometallic EMACs is also incorporated in this report.

Experiment:

General procedures for EMAC synthesis. The following describes the preparation of $[Cr_5(\mu_5\text{-dppzda})_4Cl_2]$ and $[Cr_5(\mu_5\text{-dppzda})_4(NCS)_2]$, representing procedures for reactions of, respectively, metallation and the subsequent change of axial ligands. Detailed information, including those for prototypical oligo- -pyridylamido anions and new ligands, are referred to the journal articles listed in the publication list.

$[Cr_5(\mu_5\text{-dppzda})_4Cl_2]$: naphthalene (60 g), anhydrous $CrCl_2$ (0.369 g, 3.0 mmol) and H_2dppzda (0.528 g, 2.0 mmol) were heated at *ca.* 170–180 °C under argon and then a solution of potassium tert-butoxide (0.471 g, 4.2 mmol) in n-butyl alcohol (4 mL) was added dropwise. The reaction was continued for another 6 h and a dark brown solution was obtained. After cooling the product was transferred to hexane to wash out naphthalene, and then CH_2Cl_2 was used to extract the complex. A dark red-brown complex was obtained after evaporation. The product was recrystallized from a CH_2Cl_2–diethyl ether solution. Red-brown crystals were obtained. (269 mg, 39% yield).

$[Cr_5(\mu_5\text{-dppzda})_4(NCS)_2]$: $[Cr_5(\mu_5\text{-dppzda})_4Cl_2]$ (0.690 g, 0.5 mmol) and NaNCS (0.405 g, 5.0 mmol) in a mixed solvent consisting of CH_2Cl_2 (50 mL) and benzene (25 mL) were stirred for 4 d. The solution was filtered and the solvent was removed under reduced pressure. The remaining deep brown solid was dissolved in CH_2Cl_2 and the solution was then layered with hexane. After 2 weeks, deep red crystals were obtained (463 mg, 65% yield).

General procedures for the synthesis of Ru_2 moieties. The following describes the preparation of $[Ru_2(DMBA)_4Cl_2]$ and $[Ru_2(DMBA)_4(NO_3)_2]$. The subsequent procedures for the synthesis of alkynyl derivatives are referred to the corresponding journal articles.

$[Ru_2(DMBA)_4Cl_2]$. The mixture of $Ru_2(OAc)_4Cl$ (0.474 g, 1.00 mmol), *N*,*N*'-dimethylbenzamidine (0.740 g, 5.00 mmol), LiCl (excess), Et_3N (2 mL), and 40 mL of THF was gently refluxed for 2 h in a round-bottom flask. The solvent, THF, was removed and the residue was dissolved in CH_2Cl_2 and filtered through a silica gel pad (2 cm). Further recrystallization from CH_2Cl_2/hexane yielded 0.786-g dark brown crystals (91% based on Ru).

$[Ru_2(DMBA)_4(NO_3)_2]$. $Ru_2(DMBA)_4Cl_2$ (0.172 g, 0.20 mmol) was dissolved in 40 mL THF under argon. Upon the addition of $AgNO_3$ (0.340 g, 2.0 mmol), the color of the solution immediately changed from dark brown to green. After being subject to 21-h stirring, the reaction mixture was filtered through a Celite plug, and the solid residue was extracted with CH_2Cl_2. After removal of the solvent, the product appeared dark green. The solid was rinsed with THF until the filtrate became colorless (yield: 0.160 g, 88%).

Results and Discussion:

The physical properties of EMACs and the $Ru_2(DMBA)_4$ unit are perturbed by newly synthesized ligands. The metal-metal interactions, in terms of electron transporting through the metal framework or mediated by the Ru_2 moiety are examined.

(1) *New. J. Chem.* **2012**, *36*, 632.

Title: Fine Tuning of Pentachromium(II) Metal String Complexes through Elaborate Design of Ligand.

Pentachromoium EMACs $[Cr_5(\mu_5\text{-L})_4X_2]$ (X = Cl^-, L = $dppzda^{2-}$ (**1**), $dpzpda^{2-}$ (**2**); X = NCS^-, L = $dppzda^{2-}$ (**3**), $dpzpda^{2-}$ (**4**)) were designed and synthesized through pyrazine-modulated ligands

instead of the prototypical tripyridyldiamines. The positions of the pyrazine are different in these compounds. X-Ray crystallographic studies revealed a linear metal chain structure consisting of two quadruple Cr–Cr bonds and a separated high spin Cr(II) at an end in crystallized form. A quintet ground state was observed for all pentachromium(II) molecules by magnetic study with *g* values of 2.04–2.18. While the electronic structure remained unchanged after the modification of ligands, electrochemistry showed a significant change in the molecular orbital energy levels of metal string molecules. Observation of the first oxidation peak of **1** at +0.57 V and of **2** at +0.73 V revealed that these complexes are quite resistant to oxidation. Single molecular conductance measurements showed that the complex exhibited good electronic conductance.

(2) *Dalton Trans.* **2012**, *41*, 3166.

Title: New Trinuclear Metal String Complexes Containing Rigid Hdzp Ligands: Synthesis, Structure, Magnetism and DFT Calculation (Hdzp = 1,9-diazaphenoxazine).

Hdzp (1,9-diazaphenoxazine, **1**) is a rigid ligand developed in this study to demonstrate how the ligand rigidity affects the properties of trinickel and tricobalt EMACs, $[Ni_3(dzp)_4(NCS)_2]$ (**2**) and $[Co_3(dzp)_4(NCS)_2]$ (**3**). The rigidity of Hdzp is created by fusing the pyridyl rings by an oxygen bridge (see the left panel of the Figure). Crystallographic analyses (see the Figure for the side view and end view of **2**) show that the rigidity makes **2** and **3** bearing smaller torsion angles and longer metal–metal distances than those trimetallic analogues with the corresponding protopytical dpa^- (dpa^- = dipyridylamido anion). The longer metal–metal distance observed for **2** results in an exchange interaction (J) of -160 cm^{-1} between two high spin Ni(II) ions. The value is slightly smaller that of -160 cm^{-1} for its dpa^- analogue, $[Ni_3(\mu_3\text{-}dpa)_4(NCS)_2]$. The doublet–quartet gap of **3** is smaller than its dpa^- analogue, $[Co_3(\mu_3\text{-}dpa)_4(NCS)_2]$. Hence, **3** shows the spin-crossover behavior even at low temperature.

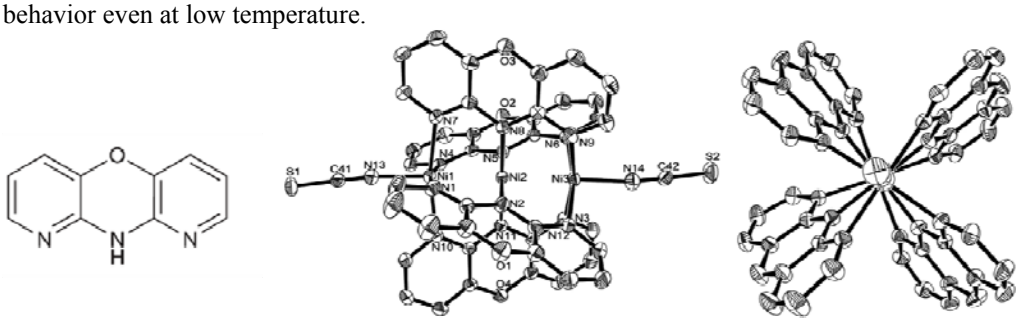

(3) *C. R. Chim.* **2012**, *15*, 159.

Title: Further Studies of $Ni_4(DAniDANy)_4$ ($DAniDANy^{2-}$ = N,N'-bis-p-anisyl-2,7-diamido-1,8-naphthyridine) and its One-electron Oxidation Product: Metal-Metal Sigma Bonding in Ni_4^{9+} Complex.

A new ligand is designed by extending the naphthyridine unit with decorated p-anisyl-amido anions ($DAniDANy^{2-}$ = N,N'-bis-p-anisyl-2,7-diamido-1,8-naphthyridine). Linear tetranickel strings, $[Ni_4(DAniDANy)_4]$ (**1**), and its one-electron oxidized product, $[Ni_4(DAniDANy)_4](PF_6)$ (**2**), were synthesized and studied. Magnetic and EPR measurements show that **1** has a singlet ground state while **2** has a doublet one due to the removal of an electron from the σ* antibonding orbital, supported by crystal structural analyses and DFT calculations. The chemical oxidation of **1** results an increase in the bond order and the formation of Ni-Ni bonds in **2**. Given that the redox process is reversible and thus the conductance, these tetranickel complexes can be considered the shortest even-numbered molecular switches.

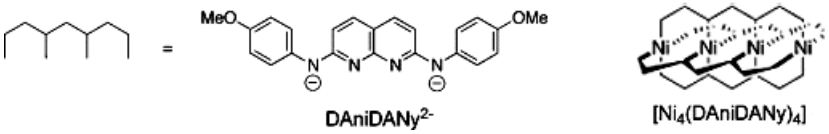

(4) *Eur. J. Inorg. Chem.* **2013**, in press.

Title: Synthesis, Structure, Magnetism, and Single Molecular Conductance of Linear Trinickel String Complexes with Sulfur-Containing Ligands.

We proposed to prepare asymmetric ligands for EMACs. Synthesized herein is a sulfur-containing Hmpta (4-methylpyridylthiazolylamine, **1**) and two linear trinickel EMACs, $[Ni_3(mpta)_4(NCS)_2]$ (**2**)

and $[Ni_3(mpta)_4(CN)_2]$ (**3**). Within the trinickel framework, the two terminal high-spin (S = 1) Ni ions are strongly coupled antiferromagnetically (J = –91 cm^{-1} in **2** and –79 cm^{-1} in **3**). The axial CN^- ligand is basic and strongly pulls the terminal Ni ions away from the central Ni ion, resulting in the Ni–Ni bond lengths (*ca.* 2.52 Å) longer than those in **2** (*ca.* 2.47 Å). The lengthening of the Ni–Ni bond lengths causes **3** to exhibit weaker antiferromagnetic interactions and lower single molecular conductance [R = 11.1 (± 3.9) MΩ for **3**; R = 7.1 (± 1.5) MΩ for **2**].

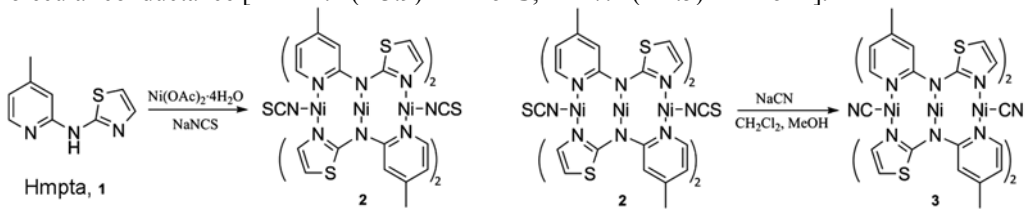

(5) *Inorg. Chem.* **2012**, *51*, 3261.

Title: Diruthenium(III,III) Bis(alkynyl) Compounds with Donor/Acceptor-Substituted *geminal*-Diethynylethene Ligands.

Molecules with extensive π delocalization systems have been intensively studied. Cross-conjugation systems with three unsaturated branches in conjugation attract attentions of physical organic chemists yet are relatively unexplored. Isotriacetylene units, abbreviated as *gem*-DEE from *geminal*-diethynylethene, are interesting because of the phenomenon of *quantum interference* predicted by computational modeling (by van Duyne, Ratner and coworkers *J. Am. Chem. Soc.* **2008**, *130*, 17301). Integration of a redox-rich Ru_2 moiety with *gem*-DEE would provide a channel to probe the effect of *cross-conjugation* and *quantum interference*. Reported herein are the preparation and characterization of *trans*-$Ru_2(DMBA)_4(X\text{-}gem\text{-}DEE)_2$ [DMBA = N,N'-dimethylbenzamidinate; X = H (**1**), Si^iPr_3 (**2**), Fc (**3**); 4-$C_6H_4NO_2$ (**4**), and 4-$C_6H_4NMe_2$ (**5**)]. The compounds were characterized by spectroscopic and voltammetric techniques as well as the single-crystal X-ray diffraction studies of **2** and **3**. Both the single-crystal structural data of **2** and **3** and the spectroscopic/voltammetric data indicate that the *gem*-DEE ligands are similar to simple acetylides in their impact on the molecular and electronic structures of the $Ru_2(DMBA)_4$ core. Density functional theory calculations revealed more extensive π delocalization in aryl-donor-substituted *gem*-DEEs and that the hole-transfer mechanism will likely dominate the charge delocalization in Ru_2-*gem*-DEE-based wires.

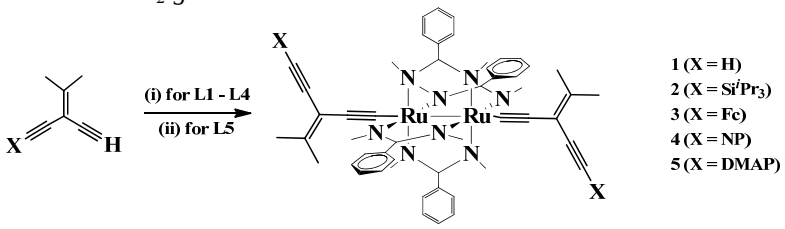

(6) *Inorg. Chem.* **2012**, *51*, 7561.

Title: Diruthenium(III,III) Ethynyl-phenyleneimine Molecular Wires: Preparation *via* On-Complex Schiff Base Condensation.

$Ru_2(DMBA)_4$ is superior to other diruthenium polyynyls in the richness in redox properties as well as in the facile formation of *bis*-alkynyl adducts. *trans*-$Ru_2(DMBA)_4(C{\equiv}C{-}C_6H_4\text{-}4\text{-}CHO)_2$, **1**, was prepared from the reaction between $Ru_2(DMBA)_4(NO_3)_2$ and $HC{\equiv}C{-}C_6H_4$-4-CHO under the weak base conditions. The aldehyde groups of **1** undergo a condensation reaction with $NH_2C_6H_4$-4-Y (Y = H and NH_2) to afford *trans*-$Ru_2(DMBA)_4(C{\equiv}C{-}C_6H_4\text{-}4\text{-}CH{=}N{-}C_6H_4\text{-}4'\text{-}Y)_2$ (Y = H (**2**) and NH_2 (**3**)). $Ru_2(DMBA)_4(C{\equiv}C{-}C_6H_4\text{-}4\text{-}N{=}C(Me)Fc)_2$, **4**, was also prepared from the reaction between $Ru_2(DMBA)_4(NO_3)_2$ and $HC{\equiv}C{-}C_6H_4{-}N{=}C(Me)Fc$. X-ray crystallography of **1** and **2** revealed significant deviation from an idealized D_{4h} geometry in the coordination sphere of the Ru_2 core. Voltammetric measurements revealed four one electron redox processes for **1**−**3**: the Ru_2 centered oxidation and reduction, and a pair of reductions of the imine or aldehyde groups. **4** displays an additional oxidation attributed to the Fc groups. DFT calculations were performed on model compounds to gain a more thorough understanding of the interaction of the organic functional groups across the Ru_2 bridge.

(7) *Organometallics* **2013**, in preparation.

Title: Diruthenium Alkynyl Compounds with Phosphonate Capping Groups.

In the above-manuscript, we described the synthesis of *trans*-(4-$Me_3Si(CH_2)_2$S-Ph-C≡C)-$Ru_2(ap)_4$-C≡C-4-Ph-P(O)(O^tBu)$_2$ (**1**) and *trans*-$Ru_2(DMBA)_4$(C≡C-4-Ph-P(O)(O^tBu)$_2$)$_2$ (**2**). The former contains both a thiol and a phosphonate capping groups at the opposite ends of the molecule, and hence can be readily incorporated into a Au/molecule/SiO_2 (metal-molecule-insulator) junction. The latter has phosphonate capping groups on both ends and can be sandwiched in an oxide/molecule/oxide junction. Voltammetric and spectroscopic evidences indicated that the addition of phophonate caps does not alter the electronic structures of the Ru_2 moiety.

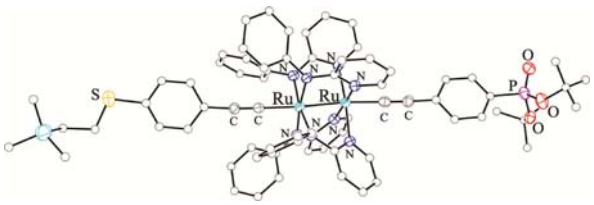

trans-(4-$Me_3Si(CH_2)_2$S-Ph-C≡C)-$Ru_2(ap)_4$-C≡C-4-Ph-P(O)(O^tBu)$_2$

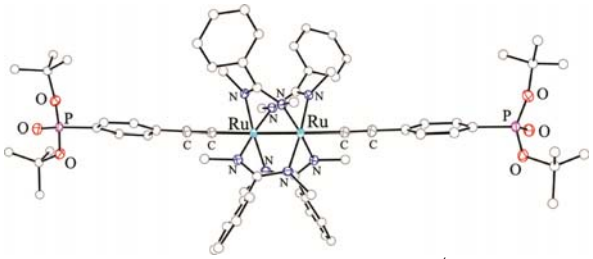

trans-$Ru_2(DMBA)_4$(C≡C-4-Ph-P(O)(O^tBu)$_2$)$_2$

(8) Preparation of Heterometal EMACs (still on-going).

The synthetic strategies for the preparation of tri-/penta-nuclear heterometal EMACs include (i) self-assembly by thermodynamic control, (ii) stepwise formation by kinetic control which involves sequential addition of different metal ions, and (iii) separation and purification by chemical treatment or column chromatography. Examples for (i) are $CoPdCo(dpa)_4Cl_2$, $CoNiCo(dpa)_4Cl_2$, $CoCoRh(dpa)_4Cl_2$; for (ii), $NiCoRh(dpa)_4Cl_2$ and $[NiCoRh(dpa)_4Cl](PF_6)$ (see the diagram); for (ii + chemical treatment), $NiNiCo(dpa)_4Cl_2$; for (iii + chromatography separation), $NiRhNi(dpa)_4(NCS)_2$, $NiRhRh(dpa)_4(NCS)_2$. In addition to x-ray crystallographic analysis, these EMACs have been characterized by mass spec, NMR, and SQUID. The protocols are useful for penta-nuclear heterometal EMACs because the formation of homometallic ones takes place concomitantly. In addition, suitable reaction precursors are difficult to prepare and the reactivity of the 2nd-row transition metals are poor. Thus far prepared pentametal EMACs are $Ru_2Ni_3(tpda)_4(NCS)_2$, $Ru_2Co_3(tpda)_4(NCS)_2$, $Rh_2Ni_3(tpda)_4(NCS)_2$, and $Rh_3Ni_2(tpda)_4(NCS)_2$.

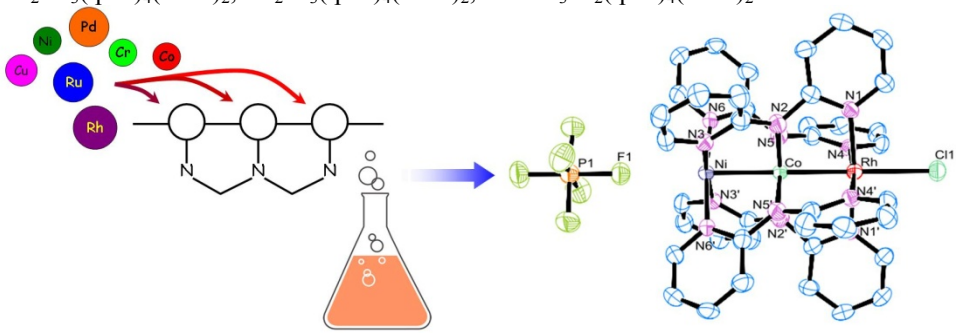

(9) Rigid ligands for novel EMACs (still on-going).

The design of new ligands will always be our continuous effort to explore interesting chemistry of EMACs. For example, the ligand (anphthyridyl) shown below confers trinickel and tricopper EMACs with unprecedented oxidation states of Ni_3^{3+} and Cu_3^{2+}, respectively.

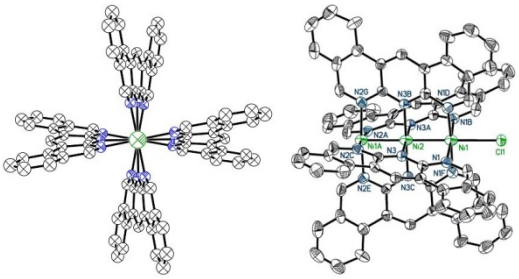

Crystal structure of $[Ni_3(\mu_3\text{-dbay})_4Cl]Cl_2$

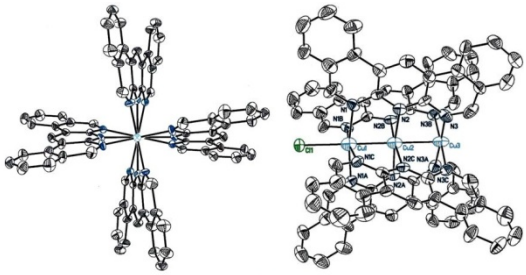

Crystal structure of $[Cu_3(\mu_3\text{-dbay})_4Cl]I$

(10) *Angew. Chem. Int. Ed.* **2013**, accepted.

Title: Tactile-Feedback Stabilized Molecular Junctions for the Measurements of Molecular Conductance.

The fundamental understanding of intrinsic properties for molecular electronics is expedited by the advancement of measurement platforms for single-molecule conductance. The most prevalent approaches are break-junction (BJ) methods, such as MCBJ (mechanically controllable) and STM BJ (scanning tunneling microscopy), which involve a pair of metal electrodes engaging the routine of being pushed towards and then pulled apart from one another. Such routines warrant the momentary development of gaps with the dimension suitable to host molecules. The time scale generally falls in hundredths to tenths of a second, making it difficult to study time-dependent properties. Herein, we integrate an additional force-based control to adjust the junction spacing. Stable junctions on the order of minutes are accessible and allow the study of single-molecule conductance from truly one molecular junction, as opposed to those from collective dataset acquired at millisecond timescale.

Concluding Remarks:

Based on the prototypical oligo-α-pyridylamine, we continue our efforts on the development of new families of pyrazine- and naphthyridine-modulated ligands by substituting the pyridine (py) rings. Ligands of oxygen-fused Hdzp (1,9-diazaphenoxazine), anphthyridyl, and sulfur-incorporated thiazolyl are prepared to study the effect of ligand rigidity and asymmetry. For $[Ru_2(DMBA)_4]$ units, novel *bis*-alkynyl derivatives have been designed and prepared. As a mediating bridge, the electron transfer efficiency is shown tunable by the axial ligands. In the coming year, we will continue (1) the exploration of conductive behaviors for the novel metal complexes, (2) theoretical studies of the underlying physics that control the electron transfer and transport processes, and (3) the measurement platform from metal-molecule-metal configuration to semiconductor-molecule-metal set of connections.

List of Publications:

a) papers published in peer-reviewed journals,

1. "The Road to Molecular Metal Wires: The Past and Recent Advances of Metal String Complexes", Liu, I. P.-C.; Chen, C.-h.; Peng, S.-M.* *Bull. Jap. Soc. Coord. Chem.* **2012**, *59*, 3–10.
2. "Fine Tuning of Pentachromium(II) Metal String Complexes through Elaborate Design of Ligand", Wang, W.-Z.; Ismayilov, R. H.; Lee, G.-H.; Huang, Y.-L. Yeh, C.-Y.; Fu, M.-D.; Chen, C.-h.; Peng, S.-M.* *New. J. Chem.* **2012**, *36*, 632–637.
3. "New Trinuclear Metal String Complexes Containing Rigid Hdzp Ligands: Synthesis, Structure, Magnetism and DFT Calculation (Hdzp = 1,9-diazaphenoxazine)", Cheng, M.-C.; Liu, I. P.-C.; Hsu, C.-H.; Lee, G.-H.; Chen, C.-h.; Peng, S.-M.* *Dalton Trans.* **2012**, *41*, 3166–3173.
4. "Further Studies of $Ni_4(DAniDANy)_4$ ($DAniDANy^{2-}$ = N,N'-*bis*-*p*-anisyl-2,7-diamido-1,8-naphthyridine) and its One-electron Oxidation Product: Metal-Metal Sigma Bonding in Ni_4^{9+} Complex", Huang, G.-C.; Hua, S.-A.; Liu, I. P.-C.; Chien, C.-H.; Kuo, J.-H.; Lee, G.-H.; Peng, S.-M.* *C. R. Chim.* **2012**, *15*, 159–162.
5. "*trans*-$[Fe(cyclam)(C_2R)_2]^+$: A New Family of Iron(III) Bis-Alkynyl Compounds", Cao, Z.; Forrest, W. P.; Gao, Y.; Fanwick, P. E.; Ren, T.* *Organometallics* **2012,** *31*, 6199–6206.

6. "Diruthenium(III,III) Ethynyl-phenyleneimine Molecular Wires: Preparation via On-Complex Schiff Base Condensation",
   Cummings, S. P.; Cao, Z.; Fanwick, P. E.; Kharlamova, A.; Ren, T.* *Inorg. Chem.* **2012,** *51*, 7561−7568.
7. "Diruthenium(III,III) Bis(alkynyl) Compounds with Donor/Acceptor-Substituted *geminal*-Diethynylethene Ligands",
   Forrest, W. P.; Cao, Z.; Hassell, K. M.; Prentice, B. M.; Fanwick, P. E.; Ren, T.* *Inorg. Chem.* **2012**, *51*, 3261−3269.
8. "Synthesis, Structure, Magnetism, and Single Molecular Conductance of Linear Trinickel String Complexes with Sulfur-Containing Ligands",
   Yang, C.-C.; Liu, I. P.-C.; Hsu, Y.-J.; Lee, G.-H.; Chen, C.-h.; Peng, S.-M.* *Eur. J. Inorg. Chem.* **2013**, in press.
9. "New Linear π-Conjugated Diruthenium Compounds Containing Axial Tetrathiafulvalene-acetylide Ligands",
   Cai, X.-M.; Zhang, X.-Y.; Savchenko, J.; Gao, Z.; Ren, T.*; Zuo, J.-L.* *Organometallics* **2013**, in press.
10. "New Diruthenium (II,III) Compounds Bearing Terminal Olefin Groups",
    Savchenko, J.; Fanwick, P. E.; Hope, H.; Gao, Y.; Yerneni, C. K.; Ren, T.* *Inorg. Chim. Acta* **2013**, *394*, in press.
11. "Tactile-Feedback Stabilized Molecular Junctions for the Measurements of Molecular Conductance",
    Chen, I-W. P.; Tseng, W.-H.; Gu, M.-W.; Su, L.-C.; Hsu, C.-H.; Chang, W.-H.; Chen, C.-h.* *Angew. Chem. Int. Ed.* **2013**, in press.

b) papers published in peer-reviewed conference proceedings,
c) papers published in non-peer-reviewed journals and conference proceedings,
d) conference presentations without papers,
e) manuscripts submitted but not yet published, and
f) provide a list any interactions with industry or with Air Force Research Laboratory scientists or significant collaborations that resulted from this work.

DD882: There is no material from this project required to fill in Form DD882 (the inventions disclosure form). The inventions disclosure form is submitted in a separate document.

Important Note: If the work has been adequately described in refereed publications, submit an abstract as described above and refer the reader to your above List of Publications for details. If a full report needs to be written, then submission of a final report that is very similar to a full length journal article will be sufficient in most cases. This document may be as long or as short as needed to give a fair account of the work performed during the period of performance. There will be variations depending on the scope of the work. As such, there is no length or formatting constraints for the final report. Keep in mind the amount of funding you received relative to the amount of effort you put into the report. For example, do not submit a $300k report for $50k worth of funding; likewise, do not submit a $50k report for $300k worth of funding. Include as many charts and figures as required to explain the work.

Attachments: Publications a2~4, a6~7 listed above.

NJC

Cite this: *New J. Chem.*, 2012, **36**, 632–637

www.rsc.org/njc

PAPER

Fine tuning of pentachromium(II) metal string complexes through elaborate design of ligand†

Wen-Zhen Wang,[abc] Rayyat Huseyn Ismayilov,[bcd] Gene-Hsiang Lee,[bc] Yi-Lin Huang,[e] Chen-Yu Yeh,[e] Ming-Dung Fu,[b] Chun-hsien Chen[b] and Shie-Ming Peng*[bc]

Received (in Victoria, Australia) 11th June 2011, Accepted 31st October 2011
DOI: 10.1039/c1nj20512a

New pentachromoium metal string complexes $[Cr_5(\mu_5\text{-}L)_4X_2]$ ($X = Cl^-$, $L = dppzda^{2-}$ (**1**), $dpzpda^{2-}$ (**2**); $X = NCS^-$, $L = dppzda^{2-}$ (**3**), $dpzpda^{2-}$ (**4**)) were designed and synthesized through pyrazine-modulation of tripyridyldiamine ligand. X-Ray crystallographic studies revealed a linear metal chain structure consisting of two quadruple Cr–Cr bonds and a separated high spin Cr(II) at an end in crystallized form. A quintet ground state was observed for all pentachromium(II) molecules by magnetic study with *g* values of 2.04–2.18. While the electronic structure remained unchanged after the modification of ligands, electrochemistry showed a significant change in the molecular orbital energy levels of metal string molecules. Observation of the first oxidation peak of **1** at +0.57 V and of **2** at +0.73 V revealed that these complexes are quite resistant to oxidation. Single molecular conductance measurements showed that the complex exhibited good electronic conductance.

Introduction

Metal string complexes have attracted much attention in recent decades as they are very important to the fundamental understanding of extended metal–metal interactions and in potential applications as molecular devices, such as molecular wires, voltage-activated switches, and single molecular transistors.[1] The typical structure of this family includes a linear metal chain helically wrapped by four deprotonated oligo-α-pyridylamido ligands. Metal string complexes of many metals including Ni,[2] Co,[3] Cr,[4] Cu,[5] Ru[6] and Rh[6] have been synthesized and structurally characterized. Chromium string complexes are especially interesting with respect to both structure and properties. In chromium string complexes, two kinds of structures, symmetrical and unsymmetrical, were observed. The symmetrical structures exhibit all Cr–Cr bonds with very similar distances of $d_{Cr-Cr} > 2.35$ Å, and the unsymmetrical structures consist of quadruple Cr–Cr bonds with $d_{Cr-Cr} < 2.3$ Å and a separated high spin Cr(II) at an end. Recent research found that a transformation between two kinds of structures might happen in a solution of penta- and heptachromium(II) complexes. Furthermore, chromium complexes are the most conductive molecular wires that have been observed among metal string complexes up to the present time.[7] However, chromium strings are quite unstable and sensitive to both air and moisture, which makes their synthesis and subsequent research relatively difficult. Recently we designed a series of pyrazine-modulated oligo-α-pyridylamino ligands, by including pyrazine instead of pyridine ring(s) in ligands. The introduction of one or more nitrogen-rich pyrazine molecules significantly improves the reactivity of the ligand, and the resulting complexes are more stable than the relevant oligo-α-pyridylamino compounds. While the trichromium(II) complex of pyrazine-modulated oligo-α-pyridylamino ligands showed a symmetrical structure, hapta- and nonachromium(II) complexes showed an unsymmetrical structure.[2d,4c,d] Thus as an intermediate the structure of pentachromium(II) is especially interesting. Here we report a group of carefully designed pentachromium(II) complexes from pyrazine-modulated tripyridyldiamine ligands, N^2,N^6-di(pyridin-2-yl)pyrazine-2,6-diamine (H_2dppzda) and N^2,N^6-di(pyrazin-2-yl)pyridine-2,6-diamine (H_2dpzpda) (Scheme 1). The coordination environment of the middle and terminal chromium of pentachromium(II) metal string complexes was

[a] *Department of Chemistry, Xi'an Shiyou University, 710065, Xi'an, P R China. E-mail: wzwang@xsyu.edu.cn; Fax: +86 29 88382693; Tel: +86 29 88382693*
[b] *Department of Chemistry, National Taiwan University, Taipei, ROC. E-mail: smpeng@ntu.edu.tw; Fax: +886 2 83693765; Tel: +886 2 33661655*
[c] *Institute of Chemistry, Academia Sinica, Taipei, ROC*
[d] *Institute of Chemical Problems of Azerbaijan Academy of Sciences, Baku-1143, Azerbaijan Republic. E-mail: rayyat9193@hotmail.com; Tel: +994 12 4 389654*
[e] *Department of Chemistry, National Chung Hsing University, Taichung, ROC*

† Electronic supplementary information (ESI) available: Magnetism of complexes **1**, **3** and **5**. CCDC reference numbers [829384–829386]. For ESI and crystallographic data in CIF or other electronic format see DOI: 10.1039/c1nj20512a

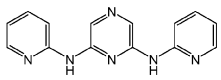

N^2,N^6-di(pyridin-2-yl)pyrazine-2,6-diamine
(H_2dppzda)

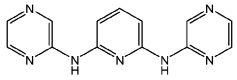

N^2,N^6-di(pyrazin-2-yl)pyridine-2,6-diamine
(H_2dpzpda)

Scheme 1

precisely controlled and the property of complexes was adjusted through introducing pyrazine at different positions of the spacer ligands.

Results and discussion

Syntheses and structures

The ligands were synthesized on the basis of Buchwald's palladium-catalyzed procedures *via* the palladium-catalyzed cross-coupling reaction.[8] The chloride complexes $[Cr_5(\mu_5\text{-dppzda})_4Cl_2]$ (**1**) and $[Cr_5(\mu_5\text{-dpzpda})_4Cl_2]$ (**2**) were synthesized by the reaction of anhydrous $CrCl_2$ with the ligand H_2L in an argon atmosphere at high temperature (180–200 °C) employing naphthalene as a solvent and Bu^tOK as a base to deprotonate the amine group. Thiocyanate species $[Cr_5(\mu_5\text{-dppzda})_4(NCS)_2]$ (**3**) and $[Cr_5(\mu_5\text{-dpzpda})_4(NCS)_2]$ (**4**) were obtained through the substitution of axial chloride ligands from chloride complexes. Terminal pyrazine-modulated pentachromium complexes **2** and **4** are more unstable, and thiocyanate species **4** decomposes quickly in solution.

The crystal structures of **1**, **2** and **3** are shown in Fig. 1–3. The structures of **1** and **2** were revised using Platon/SQUEEZE to smooth the electron density. After revision the R_F and R_W for **1** decreased from 7.96% to 7.08% and from 18.72% to 16.64%, and the R_F and R_W for **2** decreased from 7.47% to 6.70% and 20.07% to 18.74%, respectively. Compounds **1–3** are pentachromium linear metal string complexes. The atoms of axial ligands bonded to the terminal metal atoms, chloride or nitrogen atoms of NCS^-, are collinear with the Cr_5 axis.

Molecules of **1** crystallized in the tetragonal system with space group $I4/m$ (Table 1). There is a four-fold axis along the

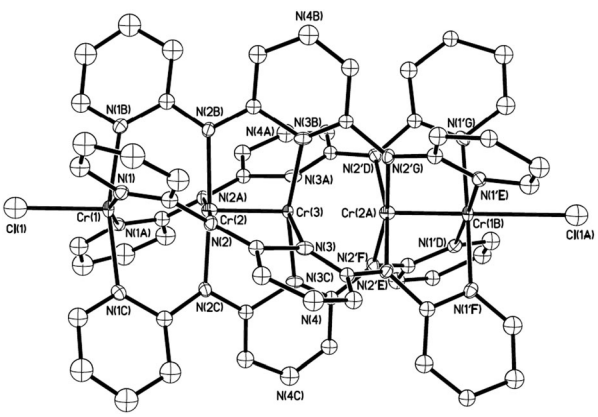

Fig. 1 ORTEP drawing of the structure of **1**. Thermal ellipsoids are drawn at the 30% probability level. The hydrogen atoms have been omitted for clarity. Label A was generated through the symmetry operations A = x, $-y$, z.

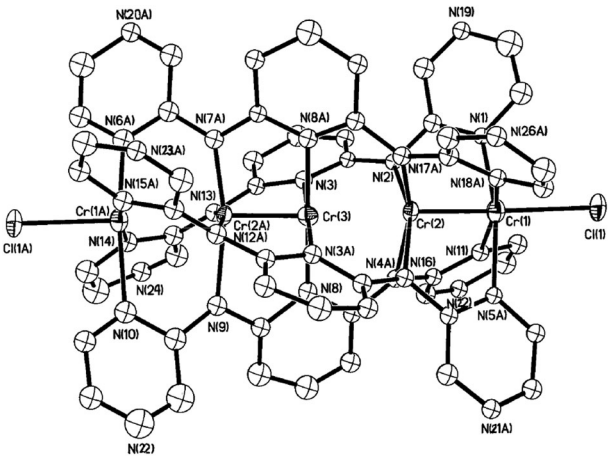

Fig. 2 ORTEP drawing of the structure of **2**. Thermal ellipsoids are drawn at the 30% probability level. The hydrogen atoms have been omitted for clarity. Label A was generated through the symmetry operations A = $-x + 1$, $-y$, $-z + 1$ and label B represents nonsymmetric related positions (disordered positions).

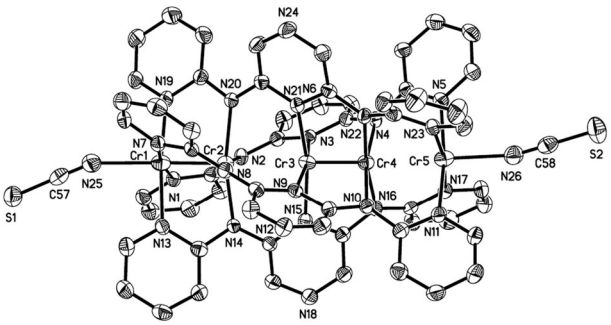

Fig. 3 ORTEP drawing of the structure of **3**. Thermal ellipsoids are drawn at the 50% probability level. The hydrogen atoms have been omitted for clarity.

molecular chain of **1** and a perpendicular mirror through the center of the molecule. Cr(1) and Cr(3) are disordered over two positions and each position is half occupied. The separation between the two disordered Cr atoms is 0.483 Å for Cr(1) and 0.544 Å for Cr(3). In molecules of **2** the Cr(3) atom is at an inversion center, and helical ligands $dpzpda^{2-}$ coordinate around the metal chain with left- and right-turn disorder. Cr(2) is disordered over two positions with a separation of 0.477 Å and each position is half occupied. In **3** Cr(2), Cr(3) and Cr(4) are disordered over two equally occupied positions, distances between two disordered positions are 0.356, 0.288 and 0.368 Å for Cr(2), Cr(3) and Cr(4), respectively. All molecules of **1**, **2** and **3** contain two neighbouring quadruple Cr–Cr bonds and a separate Cr(II) atom, and are asymmetrical structures, the same as those observed in hepta- and non-achromium string complexes.[4c,d] The distances of Cr–Cr bonds are between 1.933(13) to 2.093(6) Å, and the largest Cr to Cr distance in the molecular chain is 2.566(2) Å (Table 2). Thiocyanate complex **3** showed low symmetry and both the shortest and longest Cr–Cr separations were observed in it. The M–M–M bond angles are in a range of 177.1–179.8°. In complexes **1** and **3**, the separated, terminal chromium atom

Table 1 Crystal data for **1–3**

	1·$C_2H_5OC_2H_5$	**2**·$2CH_2Cl_2$	**3**·$2CH_2Cl_2$·$2C_6H_6$
Formula	$C_{60}H_{50}Cl_2Cr_5N_{24}O$	$C_{54}H_{40}Cl_6Cr_5N_{28}$	$C_{72}H_{56}Cl_4Cr_5N_{26}S_2$
Formula weight	1454.14	1553.84	1751.35
Crystal system	Tetragonal	Monoclinic	Monoclinic
Space group	$I4/m$	$P2_1/c$	$P2_1/n$
a/Å	10.5897(6)	10.4539(2)	14.8488(2)
b/Å	10.5897(6)	12.7977(3)	31.4891(4)
c/Å	26.8588(16)	25.2298(5)	15.9630(2)
β/°	90	101.3254(13)	95.5875(6)
V/Å^3/Z	3012.0(3)/2	3309.66(12)/2	7428.44(17)/4
T/K	150(2)	150(2)	150(2)
D_c/Mg m^{-3}	1.603	1.559	1.566
Absorption coefficient/mm^{-1}	1.028	1.098	0.972
Crystal size/mm	0.27 × 0.17 × 0.17	0.20 × 0.20 × 0.05	0.45 × 0.22 × 0.10
θ Range for data collection/°	2.07–27.50	1.65–25.00	1.29–27.50
Reflection collected	15 017	32 994	46 127
Independent reflections	1771 (R_{int} = 0.0426)	5830 (R_{int} = 0.0633)	16 938 (R_{int} = 0.0580)
R_F, $R_W(F^2)$ ($I > 2\sigma(I)$)	0.0796, 0.1872	0.0747, 0.2007	0.0543, 0.1443
R_F, $R_W(F^2)$ (all data)	0.0898, 0.1945	0.1117, 0.2322	0.1169, 0.1684
GOF	1.162	1.045	1.054

Table 2 Selected bond distances (Å) and angles (°) for **1–3**[a]

1			
Cr(1)–Cr(2)	2.529(3)	Cr(2)–Cr(3)	1.973(2)
Cr(3)–Cr(2A)[b]	2.518(2)	Cr(2A)–Cr(1B)[b]	2.046(3)
Cr(1)–$N_{av.}$	2.145(11)	Cr(2)–$N_{av.}$	2.025(6)
Cr(3)–$N_{av.}$	2.044(4)	Cr(1)–Cl(1)	2.314(4)
2			
Cr(1)–Cr(2)	2.070(3)	Cr(2)–Cr(3)	2.482(3)
Cr(3)–Cr(2B)[c]	2.018(3)	Cr(2B)–Cr(1A)[c]	2.535(3)
Cr(1)–$N_{av.}$	2.105(13)	Cr(2)–$N_{av.}$	2.034(10)
Cr(3)–$N_{av.}$	2.046(4)	Cr(1)–Cl(1)	2.4869(15)
3			
Cr(1)–Cr(2)	2.093(6)	Cr(2)–Cr(3)	2.566(12)
Cr(3)–Cr(4)	1.933(13)	Cr(4)–Cr(5)	2.492(6)
Cr(1)–N(25)	2.220(3)	Cr(5)–N(26)	2.206(3)
Cr(1)–$N_{av.}$	2.102(3)	Cr(2)–$N_{av.}$	2.028(8)
Cr(3)–$N_{av.}$	2.039(13)	Cr(4)–$N_{av.}$	2.034(8)
Cr(5)–$N_{av.}$	2.111(3)		
Cr(1)–Cr(2)–Cr(3)	178.2(5)	Cr(2)–Cr(3)–Cr(4)	179.8(8)
Cr(3)–Cr(4)–Cr(5)	177.6(5)	Cr(4)–Cr(5)–N(26)	177.1(2)
N(25)–Cr(1)–Cr(2)	178.5(2)		

[a] Bond lengths of M–N_{av} represent the average value of M–N from the four wrapping ligands and label B represents non-symmetric related positions (disordered positions). [b] Symmetry operation for **1**: A = $x, -y, z$. [c] Symmetry operation for **2**: A = $-x + 1, -y, -z + 1$.

is coordinated to four pyridine nitrogen atoms, and the middle chromium atom in the inner quadruple Cr–Cr bond is coordinated to four pyrazine nitrogen atoms. In complexes **2** and **4**, the separated, terminal chromium atom is coordinated to four pyrazine nitrogen atoms, whereas another terminal chromium atom in the outer quadruple Cr–Cr bond is coordinated to four pyrazine nitrogen atoms.

Two-terminal-pyrazine modulated complex **2** showed a significantly longer Cr–Cl distance (2.4869(15) Å) than the middle pyrazine-modulated one, **1** (2.314(4) Å), but slightly shorter than that in the unmodulated tripyridyldiamido complex $[Cr_5(\mu_5\text{-tpda})_4Cl_2]$ (**5**) (2.499(6)–2.604(5) Å). The Cr–N_{NCS} distance (average 2.213(3) Å) in **3** is slightly shorter than that in the unmodulated tripyridyldiamido complex **5** (2.499(6)–2.604(5) Å).

This is different from cobalt metal string complexes, in which Co–X (X = Cl^- or NCS^-) distances in pyrazine-modulated complexes are always shorter than those in unmodulated species.[3b,d] The Cr–N_{amido} bond distances of **1–3** are shorter than all Cr–$N_{aromatic}$ distances because of the higher negative densities on the amido nitrogen atoms (N(2) and N(4)) after deprotonation of ligands. Among Cr–$N_{aromatic}$ distances central Cr–N_{aro} are shorter than terminal ones. Thus the order of bond distances in **1–3** was observed as Cr(2)–N_{av} < Cr(3)–N_{av} < Cr(1)–N_{av}.

Magnetic properties

The temperature-dependent magnetic susceptibilities were measured in the range 2–300 K for **2** and **3** and in the range 5–300 K for **1**. The magnetic moment at room temperature showed values of 5.00–5.35 μ_B. The magnetic moments decreased slightly upon cooling. As all the quadruple-bonded Cr(II) atoms in molecules are diamagnetic, these results indicate that the magnetic contribution is due to the isolated terminal Cr(II) which showed a high-spin state with four unpaired electrons (spin-only magnetic moment for a quintet ground state of four unpaired electrons is 4.90 μ_B). Therefore the molecule shows four unpaired electrons localized at an end of the molecular chain, the same spin topology with those observed in other chromium(II) metal string complexes of unsymmetrical structure, as shown in Scheme 2. Plots of molar magnetic susceptibility χ_M and $\chi_M T$ *vs.* T and fits of the Curie–Weiss law for $S = 2$ are shown in Fig. 4 for compound **2** and in ESI† for other compounds (Table 3). Diamagnetism corrections for the constituent atoms have been done for all the magnetic data. The θ values indicated both large magnitude of intermolecular interaction and zero-field splitting resulting from a strong interaction of electrons with

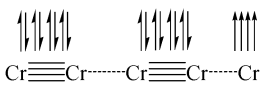

Scheme 2

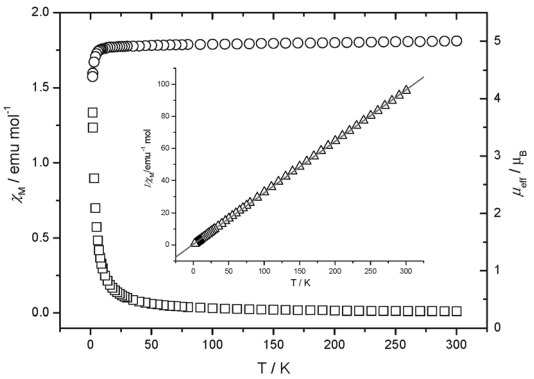

Fig. 4 Plots of molar magnetic susceptibility χ_M (□, left) and μ_{eff} (○, right) *vs.* *T* for compound **2**. Inset: reciprocal dependence of the magnetic susceptibility on temperature. The solid lines result from least-square fits of the Curie–Weiss law. The fitting results are $g = 2.04$ and $\theta = -1.1$ K.

Table 3 Magnetic results for pentachromium complexes

Complexes	**1**	**2**	**3**	**5**
g	2.18	2.04	2.10	2.15
θ/K	2.05	−1.1	−14.3	−11.6

delocalized molecular orbitals, which is consistent with the observed obvious decrease of $\chi_M T$. The larger θ value for complex **3** reflected the low symmetry in the structure of the thiocyanate molecule. The magnetic behaviour of pentachromium was similar to that of the corresponding hepta- and nonachromium complexes suggesting that neither supporting ligands nor axial ligands showed significant effect on the electronic structure of chromium metal string complexes.[4c,d]

Electrochemistry

Both **1** and **2** showed two reversible one-electron oxidation couples, at +0.57 and +0.87 V for **1** and +0.73 and +1.08 V for **2**, respectively (Fig. 5). A reduction peak at −1.31 V was observed for **2**, but no reduction peak appeared in **1**. Compared with tripyridyldiamido chromium complex **5**, which showed 1st and 2nd oxidation peaks at +0.29 and +0.63 V, both **1** and **2** are more stable and are resistant to oxidants due to the electron-withdrawing effect of pyrazine (Table 4).

A previous study revealed that the first oxidation of chromium metal string complexes happens on the terminal chromium atom Cr(1), resulting in the oxidation of separate Cr(II) to Cr(III). In complex with terminal pyrazine modulated ligand H_2dpzpda, Cr(1) is coordinated to four pyrazyl nitrogen atoms other than pyridyl nitrogen atoms. An anodical shift of 0.44 V on the first oxidation of **2** compared to that of **5** is consistent with this observation. The same strand was observed in tri- and heptachromium metal string complexes. For two-terminal-pyrazine modulated ligands, anodic shifts of first oxidation are 0.58 V for $[Cr_3(\mu_3\text{-dpza})_4Cl_2]$ (Hdpza = di(2-pyrazyl)amine) and 0.34 V for $[Cr_7(\mu_7\text{-pzpz})_4Cl_2]$ (H_3pzpz = N^2-(pyrazin-2-yl)-N^6-(6-(pyrazin-2-ylamino)pyridin-2-yl)pyridine-2,6-diamine), which reflects the increase of shift with the portion of pyrazine groups in supporting ligands.[2d,4d]

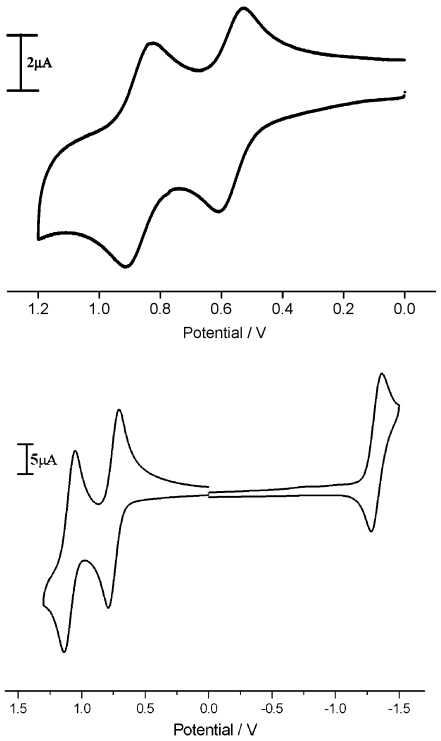

Fig. 5 Cyclic voltammogramms of **1** (top) and **2** (bottom) in CH_2Cl_2 containing 0.1 M TBAP.

Table 4 Comparison of oxidation potentials (V) for chromium(II) metal string complexes

Complexes	1st	2nd
1	0.57	0.87
2	0.73	1.08
5	0.29	0.63
$[Cr_3(\mu_3\text{-dpza})_4Cl_2]$	0.76	1.40
$[Cr_7(\mu_7\text{-pzpz})_4Cl_2]$	0.61	0.88

It is worth noting that although **1** contains a Cr(1) atom of the same coordination environment as **5**, the first oxidation of the former complex anionically shifts 0.28 V from the latter. This indicates the significant effect of the electron-withdrawing pyrazine group on molecular orbital energy levels of the whole metal string molecule.

Single molecular conductance

Research on single molecular conductance found that electronic conductivity of metal string complexes depends on the extent of electron delocalization along the linear metal framework, essentially on the length of molecules and character of metal. The metal string complexes with stronger metal–metal interaction exhibit a better conductivity.

Among metal string complexes chromium strings are the most conductive molecular wires studied so far. The electronic conductivity of **3** was studied by the scanning tunnelling microscopy (STM) break junction method using a gold surface and a gold STM tip as electrodes.[7] The resistance for single molecules of compound **3** is 3.8 ± 0.8 MΩ. This value does not significantly differ from that of **5** and shows a good single molecular conductance of **3**.[7]

Conclusions

A series of new pentachromium(II) metal string complexes were synthesized and studied through fine tuning of ligands by introducing pyrazine instead of pyridyl rings at different position(s) in oligo-α-pyridylamino ligands. The modification stabilized the pentachromium(II) string complexes. X-Ray crystallographic studies revealed that the structure of the complexes is unsymmetric, *i.e.*, the linear metal chain structure consisting of two quadruple Cr–Cr bonds and a separated high spin Cr(II) at an end in crystallized form. A quintet ground state with four unpaired electrons was observed for all pentachromium(II) molecules by magnetic study. Electrochemistry research showed that the modification of ligands resulted in a significant change of the molecular orbital energy levels of metal string molecules. The complex exhibited good electronic conductance.

Experimental section

Materials: all reagents and solvents were obtained from commercial sources and were used without further purification unless otherwise noted. The CH_2Cl_2 used for electrochemistry was freshly distilled prior to use. Tetra-*n*-butylammonium perchlorate (TBAP) was recrystallized twice from ethyl acetate and dried under vacuum. Compound $[Cr_5(\mu_5\text{-tpda})_4Cl_2]$ (**5**) was obtained by a method reported in the literature.[4b]

Physical measurements

Absorption spectra were recorded on a Hewlett Packard 8453 spectrophotometer. IR spectra were performed with a Perkin Elmer FT-IR Spectrometer PARAGON 1000 in the range of 400–4000 cm^{-1}. FAB-MS mass spectra were obtained with a JEOL JMS-700 HF double focusing spectrometer operating in the positive ion detection mode. Molar magnetic susceptibility was recorded on a SQUID system with 2000 Gauss external magnetic field. Electrochemistry was performed with a three-electrode potentiostat (CH Instruments, Model 750A) in CH_2Cl_2 deoxygenated by purging with prepurified nitrogen gas. Cyclic voltammetry was conducted with the use of a home-made three-electrode cell equipped with a BAS glassy carbon (0.07 cm^2) or platinum (0.02 cm^2) disk as the working electrode, a platinum wire as the auxiliary electrode, and a home-made Ag/AgCl (saturated) reference electrode. The reference electrode was separated from the bulk solution by a double junction filled with electrolyte solution. Potentials were reported *vs.* Ag/AgCl (saturated) and referenced to the ferrocene/ferrocenium (Fc/Fc^+) couple which occurs at $E_{1/2}$ = +0.54 V *vs.* Ag/AgCl (saturated). The working electrode was polished with 0.03 μm aluminium on Buehler felt pads and put under ultrasonic radiation for 1 min prior to each experiment. The reproducibility of individual potential values was within ±5 mV. The spectroelectrochemical experiments were accomplished with the use of a 1 mm cuvette, a 100 mesh platinum gauze as the working electrode, a platinum wire as the auxiliary electrode, and a Ag/AgCl (saturated) reference electrode. The experimental procedures and data treatment for the STM (scanning tunnelling microscopy) break-junction method were documented in detail by the groups of Tao and Lindsay.[9] The experiments were carried out with a NanoScope IIIa controller (Veeco, Santa Barbara, CA). A gold STM tip was brought into and out of contact with a gold substrate in toluene (TEDIA) containing 1 mM compound **3** and housed in a dry N_2(g)-filled chamber. Upon the repeated formation of the tip–substrate gap, the isothiocyanate headgroups at the termini of the EMACs bind to the gold electrodes and complete a molecular junction. The current-to-tip stretching profiles were recorded by a Nano-Scope built-in program and exported as ASCII files, which subsequently were used to plot the frequency histograms of the molecular conductance by Origin (version 6.0, Microcal Software). Substrates for STM experiments were 100 nm-thick gold films thermally evaporated onto glass slides pre-deposited with a 5 nm Cr adhesive layer (99.99%, Super Conductor Materials, Suffern, NY). The vacuum pressure was nominally 2×10^{-6} Torr. Prior to placing the glass slide in the bell-jar evaporator (Auto 306, Edwards High Vacuum International, West Sussex, UK), the glass slides were cleaned with piranha solution, rinsed thoroughly with copious deionised water, and oven-dried for 1 h. The piranha solution is a 1 : 3 (v/v) mixture of 30% H_2O_2 and concentrated H_2SO_4, which reacts violently with organics and should be handled with great care.

Preparation of compounds

Synthesis of $[Cr_5(\mu_5\text{-dppzda})_4Cl_2]$ (**1**): naphthalene (60 g), anhydrous $CrCl_2$ (0.369 g, 3.0 mmol) and H_2dppzda (0.528 g, 2.0 mmol) were heated at *ca.* 170–180 °C under argon and then a solution of potassium *tert*-butoxide (0.471 g, 4.2 mmol) in *n*-butyl alcohol (4 mL) was added dropwise. The reaction was continued for another 6 hours and a dark brown solution was obtained. After cooling the product was transferred to hexane to wash out naphthalene, and then CH_2Cl_2 was used to extract the complex. A dark red-brown complex was obtained after evaporation. The product was recrystallized from a CH_2Cl_2–diethyl ether solution. Red-brown crystals were obtained. (269 mg, 39% yield). IR (KBr) ν/cm^{-1} = 3446 m, 1603 m, 1463 s, 1416 s, 1342 s, 1332 s, 1302 m, 1275 m, 1186 m, 1164 m, 1121 m, 1009 m, 774 w, 744 w; UV/Vis (CH_2Cl_2) λ_{max}/nm ($\varepsilon/dm^3\ mol^{-1}\cdot cm^{-1}$) = 237 ($6.87 \times 10^4$), 286 ($9.15 \times 10^4$), 421 ($5.74 \times 10^4$), 560 ($5.25 \times 10^3$), 766 ($5.92 \times 10^3$); MS(FAB): *m*/*z*: 1343 $[Cr_5(\mu_5\text{-dppzda})_4Cl]^+$; EA (%) $[Cr_5(\mu_5\text{-dppzda})_4Cl_2]\cdot C_6H_{14}$: calcd C 50.79, H 3.71, N 22.93; found: C 51.05, H 3.33, N 22.80.

Synthesis of $[Cr_5(\mu_5\text{-dpzpda})_4Cl_2]$ (**2**): compound **2** was synthesized using a procedure similar to that for **1** except that H_2dpzpda was used instead of H_2dppzda (156 mg, 45% yield). IR (KBr) ν/cm^{-1} = 3070 w, 1587 m, 1560 m, 1507 w, 1496 m, 1472 m, 1447 s, 1348 m, 1260 w, 1200 w, 1156 m, 1021 m; UV/Vis (CH_2Cl_2) λ_{max}/nm ($\varepsilon/dm^3\ mol^{-1}\cdot cm^{-1}$) = 238 ($7.23 \times 10^4$), 284($9.38 \times 10^4$), 410 ($5.40 \times 10^4$), 560 ($4.25 \times 10^3$), 679 ($3.86 \times 10^3$), 769 ($3.82 \times 10^3$); MS(FAB): *m*/*z*: 1385 $[Cr_5(\mu_5\text{-dpzpda})_4Cl_2 + H]^+$; EA (%) $[Cr_5(\mu_5\text{-dpzpda})_4Cl_2]\cdot C_6H_6$·diethyl ether: calcd C 48.48, H 3.41, N 25.53; found: 48.54, H 3.08, N 25.56.

Synthesis of $[Cr_5(\mu_5\text{-dppzda})_4(NCS)_2]$ (**3**): $[Cr_5(\mu_5\text{-dppzda})_4Cl_2]$ (0.690 g, 0.5 mmol) and NaNCS (0.405 g, 5.0 mmol) in a mixed solvent consisting of CH_2Cl_2 (50 mL) and benzene (25 mL) were stirred for 4 d. The solution was filtered and the solvent was

removed under reduced pressure. The remaining deep brown solid was dissolved in CH_2Cl_2 and the solution was then layered with hexane. After 2 weeks deep red crystals were obtained (463 mg, 65% yield). IR (KBr) ν/cm^{-1} = 2080 m, 1678 m, 1632 m, 1601 m, 1575 m, 1537 m, 1466 s, 1437 s, 1373 m, 1302 m, 1271 m, 1236 m, 1193 m, 1150 m, 1005 m, 1067 m, 776 m; UV-Vis (CH_2Cl_2) λ_{max}/nm (ε/dm^3 mol^{-1} cm^{-1}) = 230 (6.84 × 10^4), 281 (6.35 × 10^4), 349 (3.57 × 10^4), 420 (3.26 × 10^4), 558 (5.07 × 10^3), 767 (5.94 × 10^3); MS(FAB): m/z: 1310 $[Cr_5(\mu_5\text{-dppzda})_4]^+$; EA (%) $[Cr_5(\mu_5\text{-dppzda})_4(NCS)_2]\cdot 2C_6H_6\cdot 2CH_2Cl_2$: calcd C 49.15, H 3.05, N 22.93; found: C 48.69, H 3.53, N 22.52.

Synthesis of $[Cr_5(\mu_5\text{-dpzpda})_4(NCS)_2]$ (**4**): $[Cr_5(\mu_5\text{-dpzpda})_4Cl_2]$ (0.139 g, 0.1 mmol) and NaNCS (0.081 g, 1.0 mmol) in benzene (80 mL) were stirred for 4 d. The solution was filtered and the solvent was removed under reduced pressure. The remaining deep brown solid was redissolved in benzene and a brown solid was obtained by adding hexane to the solution (62 mg, 43% yield). IR (KBr) ν/cm^{-1} = 2078 m, 1608 m, 1590 m, 1564 m, 1529 m, 1507 m, 1448 s, 1352 m, 1311 m, 1272 m, 1244 m, 1200 m, 1159 m, 1067 m, 1028 m, 1011 m, 903 m, 876 m, 833 m, 780 m, 630 m; UV-Vis (CH_2Cl_2) λ_{max}/nm (ε/dm^3 mol^{-1} cm^{-1}) = 231 (1.41 × 10^5), 264 (1.82 × 10^5), 345 (1.43 × 10^5), 414 (4.77 × 10^4), 560 (4.50 × 10^3), 678 (6.58 × 10^3), 772 (6.02 × 10^3); MS(FAB): m/z: 1429 $[Cr_5(\mu_5\text{-dpzpda})_4(NCS)_2 + H]^+$; EA (%) $[Cr_5(\mu_5\text{-dpzpda})_4(NCS)_2]\cdot 2C_6H_6\cdot C_6H_{14}$: calcd C 51.73, H 3.74, N 25.14; found: C 52.03, H 4.01, N 25.58.

Crystal structure determination

The chosen crystals were mounted on a glass fiber. Data collection was carried out on a BRUKER SMART APEXCCD diffractometer for **1** and a NONIUS Kappa CCD diffractometer for **2** and **3** at 150(2) K using Mo-Kα radiation (λ = 0.71073 Å) and a liquid nitrogen low-temperature controller. Cell parameters were retrieved and refined using the Bruker SAINT for **1** and DENZO-SMN software for **2** and **3** on all reflections. Data reduction was performed on the Bruker SAINT for **1** and DENZO-SMN software for **2** and **3**. Semi-empirical absorption was based on symmetry-equivalent reflections and absorption corrections were applied. All the structures were solved using SHELXLS-97[10a] and refined with SHELXL-97[10b] by full-matrix least squares on F^2 values. The number of atoms is refined as isotropic only (for ligand). We tried to refine it as anisotropic, and the refined result showed unreasonable bond distance, angle and thermal because of structural disorder. In complex **1**, a 4/m symmetry exists in the midst of Cr(3) and Cr(3)', resulting in the supporting ligand with left-turn and right-turn disordered structures, and both Cr(1) and Cr(3) are disordered over two positions. The site occupancy factors of two structures are refined and very close to 0.50. In complex **2**, the Cr(3) atom is at the invert center, resulting in the disordered structures of left-turn and right-turn of supporting ligands. The Cr(2) atom is disordered over two equally occupied positions. In both structures of **1** and **2**, the solvents are diffused and disordered. Hence we tried to smooth the electron density in this region. The SQUEEZE function in the PLATON package was then applied to remove the solvents' electron density, thereby improving the final cycle of refinement, converging at values of R_1 (wR_2) from 7.96% (18.72%) to 7.08% (16.64%) for **1**, and from 7.47% (20.07%) to 6.70% (18.74%) for **2**, respectively.

Acknowledgements

We thank the National Science Council and the Ministry of Education of the Republic of China for financial support. We are also grateful to Mr Wei-Min Lee and Ko-Chun Lin for their help with magnetic measurement and Dr Isiah Po-Chun Liu for his help in structural discussion.

Notes and references

1 I. P.-C. Liu, W.-Z. Wang and S.-M. Peng, *Chem. Commun.*, 2009, 4323.
2 (*a*) S.-M. Peng, C.-C. Wang, Y.-L. Jang, Y.-H. Chen, F.-Y. Li, C.-Y. Mou and M.-K. Leung, *J. Magn. Magn. Mater.*, 2000, **209**, 80; (*b*) X. López, M.-Y. Huang, G.-C. Huang, S.-M. Peng, F.-Y. Li, M. Bénard and M.-M. Rohmer, *Inorg. Chem.*, 2006, **45**, 9075; (*c*) J. F. Berry, F. A. Cotton, P. Lei, T. Lu and C. A. Murillo, *Inorg. Chem.*, 2003, **42**, 3534; (*d*) R. H. Ismayilov, W.-Z. Wang, G.-H. Lee, R.-R. Wang, I. P.-H. Liu, C.-Y. Yeh and S.-M. Peng, *Dalton Trans.*, 2007, 2898; (*e*) R. H. Ismayilov, W.-Z. Wang, G.-H. Lee, C.-Y. Yeh, S.-A. Hua, Y. Song, M.-M. Rohmer†, M. Bénard and S.-M. Peng, *Angew. Chem., Int. Ed.*, 2011, **50**, 2045.
3 (*a*) E.-C. Yang, M.-C. Cheng, M.-S. Tsai and S.-M. Peng, *Chem. Commun.*, 1994, 2377; (*b*) W.-Z. Wang, R. H. Ismayilov, G.-H. Lee, I. P.-C. Liu, C.-Y. Yeh and S.-M. Peng, *Dalton Trans.*, 2007, 830; (*c*) R. Clérac, F. A. Cotton, L. M. Daniels, K. R. Dunbar, K. Kirschbaum, C. A. Murillo, A. A. Pinkerton, A. J. Schutz and X. Wang, *J. Am. Chem. Soc.*, 2000, **122**, 6226; (*d*) W.-Z. Wang, R. H. Ismayilov, R.-R. Wang, Y.-L. Huang, C.-Y. Yeh, G.-H. Lee and S.-M. Peng, *Dalton Trans.*, 2008, 6808.
4 (*a*) J. F. Berry, F. A. Cotton, T. Lu, C. A. Murillo, B. K. Roberts and X. Wang, *J. Am. Chem. Soc.*, 2004, **126**, 7082–7096; (*b*) H.-C. Chang, J.-T. Li, C.-C. Wang, T.-W. Lin, H.-C. Lee, G.-H. Lee and S.-M. Peng, *Eur. J. Inorg. Chem.*, 1999, 1243; (*c*) R. H. Ismayilov, W.-Z. Wang, R.-R. Wang, C.-Y. Yeh, G.-H. Lee and S.-M. Peng, *Chem. Commun.*, 2007, 1121; (*d*) R. H. Ismayilov, W.-Z. Wang, G.-H. Lee, C.-H. Chien, C.-H. Jiang, C.-L. Chiu, C.-Y. Yeh and S.-M. Peng, *Eur. J. Inorg. Chem.*, 2009, 2110.
5 J. F. Berry, F. A. Cotton, P. Lei and C. A. Murillo, *Inorg. Chem.*, 2003, **42**, 377.
6 C.-K. Kuo, J.-C. Chang, C.-Y. Yeh, G.-H. Lee, C.-C. Wang and S.-M. Peng, *Dalton Trans.*, 2005, 3696.
7 (*a*) I.-W. P. Chen, M.-D. Fu, W.-H. Tseng, J.-Y. Yu, S.-H. Wu, C.-J. Ku, C.-H. Chen and S.-M. Peng, *Angew. Chem., Int. Ed.*, 2006, **45**, 5814; (*b*) S.-Y. Lin, I.-W. P. Chen, C.-H. Chen, M.-H. Hsieh, C.-Y. Yeh, T.-W. Lin, Y.-H. Chen and S.-M. Peng, *J. Phys. Chem. B*, 2004, **108**, 959.
8 R. H. Ismayilov, W.-Z. Wang, G.-H. Lee and S.-M. Peng, *Dalton Trans.*, 2006, 478.
9 (*a*) B. Xu and N. J. Tao, *Science*, 2003, **301**, 1221; (*b*) X. Li, J. He, J. Hihath, B. Xu, S. M. Lindsay and N. Tao, *J. Am. Chem. Soc.*, 2006, **128**, 2135.
10 (*a*) G. M. Sheldrick, *SHELXS-97, Program for solution of crystal structures*, University of Göttingen, Germany, 1997; (*b*) G. M. Sheldrick, *SHELXL-97, Program for refinement of crystal structures*, University of Göttingen, Germany, 1997.

Dalton Transactions

Cite this: *Dalton Trans.*, 2012, **41**, 3166

www.rsc.org/dalton

PAPER

New trinuclear metal string complexes containing rigid Hdzp ligands: synthesis, structure, magnetism and DFT calculation (Hdzp = 1,9-diazaphenoxazine)†

Ming-Chuan Cheng,[a,b] Isiah Po-Chun Liu,*[a] Chan-Hsiang Hsu,[a] Gene-Hsiang Lee,[a] Chun-hsien Chen[a] and Shie-Ming Peng*[a,b]

Received 30th June 2011, Accepted 18th August 2011
DOI: 10.1039/c2dt11246a

The synthesis, crystal structure, magnetic properties, and single-molecule conductance of two new trinuclear metal string complexes, $[Ni_3(dzp)_4(NCS)_2]$ (**2**) and $[Co_3(dzp)_4(NCS)_2]$ (**3**), containing the rigid Hdzp ligand (**1**, 1,9-diazaphenoxazine) are reported. X-ray structural analyses show that compounds **2** and **3** exhibit smaller torsion angles and longer metal–metal distances than those exhibited by the corresponding dpa^- analogues (dpa^- = dipyridylamido anion) due to the rigidity of Hdzp ligands. The longer metal–metal distance observed for **2** and **3** results in variations in their magnetic properties. The exchange interaction ($J = -160\ cm^{-1}$) between two high spin (HS) Ni(II) ions in **2** decreases slightly in comparison with those of trinickel dpa^- analogues. The doublet–quartet gap of **3** is smaller than that of $[Co_3(dpa)_4(NCS)_2]$ (**4**), which causes compound **3** to show spin-crossover behavior even at low temperature.

Introduction

Metal string complexes are of considerable significance for their potential applications as molecular wires, since these complexes consist of a linear transition metal framework that can be envisaged as the macroscopic metal wire in miniature at the atomic scale.[1–3] Because of this potential application, more studies have been devoted to the development of metal string complexes in the past two decades.[4–7]

One general approach to synthesize metal string complexes is to utilize oligo-α-pyridylamine ligands (Scheme 1).[6] These ligands contain numerous amino and pyridino groups, which can effectively stabilize the cationic linear transition metal backbone. By using appropriate oligo-α-pyridylamine ligands, a number of trinuclear, pentanuclear, heptanuclear and nonanuclear metal strings can be prepared and characterized successfully.[6]

Although the oligo-α-pyridylamine ligands were practical to create metal string complexes, a main drawback of these ligands was found in the synthesis process of longer metal strings.[8] This drawback arises from the fact that oligo-α-pyridylamine ligands have two types of coordination modes, *syn* and *anti* (Scheme 2). When the oligo-α-pyridylamine ligands coordinate to metal ions by the *syn* mode, the target metal string complexes can be obtained. If the ligands bond to metal ion with the *anti* mode,

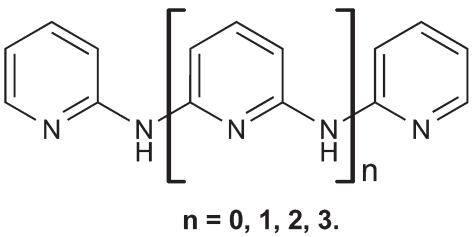

Scheme 1 Oligo-α-pyridylamine ligands.

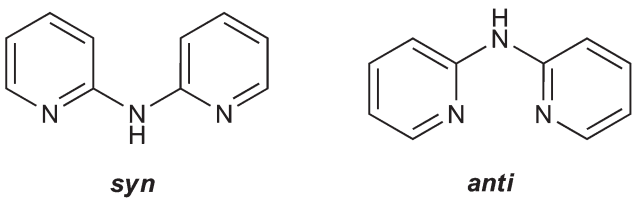

Scheme 2 Examples of two coordination modes of dipyridylamine, *syn* (left) and *anti* (right).

several side products may appear during the reaction. For instance, the *syn–syn–syn–syn* mode of tripyridyldiamine (tpda) leads to the formation of a pentanuclear metal string, $[M_5(tpda)_4Cl_2]$. On the contrary, the *anti–anti–anti–anti* mode of tpda can also coordinate to a metal ion, which forms mononuclear transition metal complexes, $[M(tpdaH_2)Cl_2]$ and $[M(tpdaH_2)_2]^{2+}$.[9,10] The formation of these mononuclear transition metal complexes plays a crucial role for the synthesis of

[a]*Department of Chemistry and Center for Emerging Material and Advanced Devices, National Taiwan University, Taipei, Taiwan. E-mail: smpeng@ntu.edu.tw, isiahliu@yahoo.com.tw*
[b]*Institute of Chemistry, Academia Sinica, Taipei, Taiwan*

†CCDC reference numbers 832185–832187. For crystallographic data in CIF or other electronic format see DOI: 10.1039/c2dt11246a.

longer metal strings. Some reactions prefer to form mononuclear transition metal complexes instead of metal string complexes, which significantly decreases the yield or completely inhibits the formation of longer metal strings.

In order to avoid the potential problem of oligo-α-pyridylamine ligands for synthesizing future longer metal string complexes, we explored the possibility to limit the coordination modes of oligo-α-pyridylamine ligands by binding their pyridine rings. The shortest prototypical ligand, 1,9-diazaphenoxazine (Hdzp) (**1**),[11] was therefore chosen and synthesized in this work (Scheme 3). The two pyridine rings in Hdzp are bound by an oxygen atom, which only allows the coordination conformation of this ligand to be *syn*. The limitation of *syn* coordination mode indicates that the Hdzp ligand can only form target metal string complexes. In this work, we have therefore described the synthesis, structure, magnetic behavior, DFT calculation and conductance of new trinuclear metal strings, $[Ni_3(dzp)_4(NCS)_2]$ (**2**) and $[Co_3(dzp)_4(NCS)_2]$ (**3**), containing the Hdzp ligands. This is the first time that the "fused" tridendate ligand has been used to synthesize metal strings. It is believed that this strategy is an important initial point for developing future longer metal string complexes.

Results and discussion

Synthesis

The overall synthetic routes to compounds **1–3** are summarized in Scheme 4. The ligand, 1,9-diazaphenoxazine (Hdzp) (**1**), was prepared by reacting 2-amino-3-hydroxypyridine and 2-chloro-3-nitropyridine in DMSO. Treatment of Hdzp with $Ni(OAc)_2{\cdot}4H_2O$, followed by excess of NaNCS, generated compound **2**. Similar to the above methods, treatment of Hdzp with the $CoCl_2$ in the presence of *t*-BuOK, followed by excess of NaNCS, generated compound **3**.

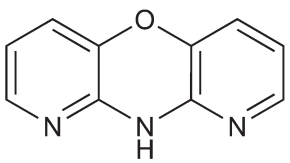

Hdzp

Scheme 3 The Hdzp ligand (**1**).

Molecular structures

The crystallographic data for compounds **1–3** are listed in Table 1. The labelled ORTEP plots of **1–3** are depicted in Fig. 1–3, respectively. Selected bond distances and angles of **1–3** are reported in Table 2.

Compound **1** crystallizes in the monoclinic system with space group $P2_1/n$. Because of crystal packing forces, two molecules are linked by two hydrogen bonds. The two pyridine rings of **1** are essentially coplanar.

Compounds **2** and **3** crystallize in the triclinic $P\bar{1}$ space group. Both complexes show an approximate D_4 geometry, having a linear symmetrical trimetal framework surrounded by four dzp^- ligands. In complex **2**, the coordination environment of the central Ni ion is in a square planar arrangement with short Ni–N bond lengths (~1.907 Å), indicative of low-spin electronic configurations ($S = 0$). The two terminal Ni ions are roughly square pyramidal with long Ni–N bond distances (~2.07 Å), displaying high-spin characteristics ($S = 1$).[12–15] As described above, the two pyridine rings of **1** are nearly coplanar. However, the dzp^- ligands in **2** are not planar. The observed torsion angle N–Ni–Ni–N (Scheme 5) for adjacent Ni(II) is ~17.94° (Table 2), which results from a helical arrangement of the four dzp^- ligands. It should be recalled that the origin of the torsion angle in trinuclear dpa^- complexes is attributed to the repulsion of two hydrogen atoms on two pyridine rings of dpa^- ligand.[16,17] Although the torsion angle in **2** is smaller than that in similar trinickel dpa^- complexes (~22.5°), it still suggests that the β-H repulsion is not a crucial factor for ligand distortion.[18] The Ni–Ni bond distances in **2** are ~2.48 Å, which are 0.05 Å longer than those in $[Ni_3(dpa)_4(NCS)_2]$ (**5**).[19] Since the rigidity of the dzp^- ligand resulting from the C–O–C bonds may increase the strain of the bite angle (Fig. 1, N1–N2–N3), it may also lead to the lengthening of the Ni–Ni distances in **2**.

A similar trend is found for the tricobalt family. Compound **3** shows longer Co–Co distances (~2.40 Å) and smaller torsion angles (~14.03°) in comparison with those in $[Co_3(dpa)_4(NCS)_2]$ (**4**) (Co–Co distances = ~2.31Å, torsion angles = ~23.9°).[20] It is noteworthy that two crystalline forms, symmetrical

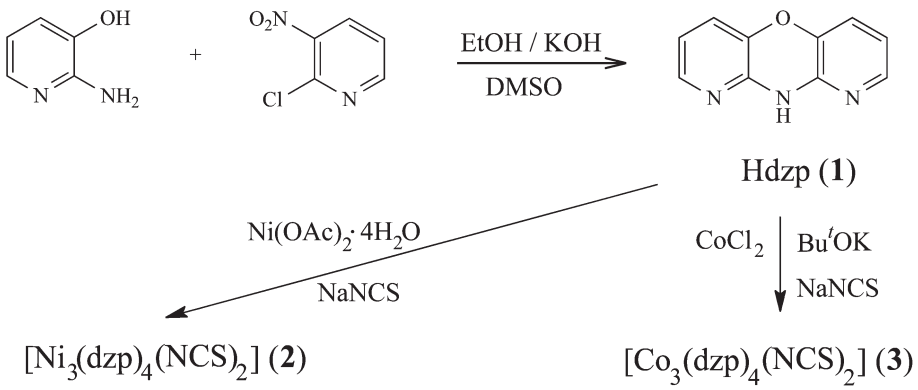

Scheme 4 Synthesis of compounds **1**, **2** and **3**.

Table 1 X-ray crystallographic data for compounds **1–3**

Compound	**1**	**2**·$CHCl_3$·$2Et_2O$	**3**·$3.5CH_2Cl_2$·0.5hexane
Formula	$C_{10}H_7N_3O$	$C_{51}H_{45}Cl_3N_{14}Ni_3O_6S_2$	$C_{48.5}H_{38}Cl_7Co_3N_{14}O_4S_2$
Formula weight	185.19	1296.61	1369.99
Temperature/K	150(2)	150(2)	150(2)
Crystal system	Monoclinic	Triclinic	Triclinic
Space group	$P2_1/n$	$P\bar{1}$	$P\bar{1}$
a/Å	6.9523(2)	12.8397(2)	13.2548(2)
b/Å	16.7982(4)	14.0455(3)	13.6957(2)
c/Å	7.5968(2)	17.5224(4)	16.9851(3)
α/°	90	110.9505(9)	109.9557(9)
β/°	113.7211(13)	94.3680(12)	93.5481(8)
γ/°	90	107.3184(12)	106.9729(9)
V/Å^3, Z	812.25(4), 4	2757.57(10), 2	2726.89(7), 2
Absorption coefficient/mm^{-1}	0.104	1.298	1.381
Reflection collected	5453	33146	35563
Independent reflections	1845	12570	12459
R_1, wR_2 [$I > 2\sigma(I)$]	0.0439, 0.1147	0.0580, 0.1763	0.0784, 0.2328
R_1, wR_2 (all data)	0.0645, 0.1254	0.0793, 0.1924	0.1234, 0.2652
Goodness-of-fit on F^2	1.019	1.044	1.048

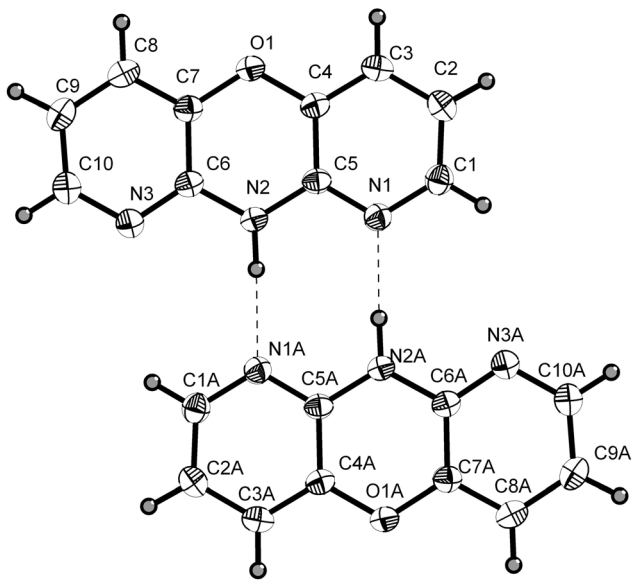

Fig. 1 ORTEP view of the molecular structure of Hdzp (**1**) (50% probability).

[*s*-$Co_3(dpa)_4(Cl)_2$] and unsymmetrical [*u*-$Co_3(dpa)_4(Cl)_2$],[21,22] for the tricobalt dpa$^-$ analogues can be obtained by modifying the crystallization conditions. The [*s*-$Co_3(dpa)_4(Cl)_2$] contains a symmetrical tricobalt framework with identical Co–Co bond lengths (2.34 Å). The [*u*-$Co_3(dpa)_4(Cl)_2$] contains an unsymmetrical tricobalt framework with two different Co–Co bond lengths (2.30 and 2.47 Å). Attempting to obtain the unsymmetrical [*u*-$Co_3(dzp)_4(NCS)_2$] in this work, however, is unsuccessful. A rational explanation for this failure is due to the larger bite angle of the Hdzp ligand. Since the large bite angle of Hdzp tends to elongate the metal–metal bond distances, it may be difficult for Hdzp to stabilize very short Co–Co bond distances (~2.29 Å) needed for forming the unsymmetrical tricobalt compound. Compound **3** with dzp$^-$ ligand always shows a symmetrical linear tricobalt framework associated with longer Co–Co bond distances.

Magnetic properties

Magnetic susceptibility measurements for compounds **2** and **3** were made on polycrystalline samples in the temperature range 4–300 K. The temperature dependence of the $\chi_M T$ values against T of **2** and **3** are shown in Fig. 4 and 5, respectively.

The $\chi_M T$ value of **2** at 300 K is *ca.* 1.30 cm^3 K mol^{-1}, smaller than the expected value of two independent S = 1 magnetic centers (2.00 cm^3 K mol^{-1}). This character is typical of the magnetic properties of trinickel string complexes, indicating that the two high-spin (HS) Ni(II) ions are strongly antiferromagnetically coupled.[23] The $\chi_M T$ values of **2** decrease rapidly with decreasing temperature, also suggesting the presence of the strong antiferromagnetic interaction between two S = 1 magnetic centers. An analysis of $\chi_M T$ values was carried out using the Heisenberg Hamiltonian defined in eqn (1):

$$\hat{H} = -JS_1S_2 + g\beta HS \quad (1)$$

where $S_1 = S_2 = 1$, g is the Landé factor, and β is the Bohr magneton.[23] The best fit gives g = 2.25, and J = −160 cm^{-1}, showing a strong antiferromagnetic interaction. Note that the unpaired electrons on two terminal Ni(II) ions couple directly through the d_{z^2} orbital of the central Ni(II) ion by spin polarization mechanism.[24] Comparison of the coupling constant of **2** with those of trinickel dpa$^-$ analogues (J = ~ −210 cm^{-1}), it is clear that the elongation of Ni–Ni distances in **2** decreases the spin polarization mechanism and the strength of the antiferromagnetic interaction.[24]

The $\chi_M T$ value for **3** is 0.99 cm^3 K mol^{-1} at 300 K, which then decreases as the temperature lowers, and reaches the minimum (0.54 cm^3 K mol^{-1}) below 25 K. This feature is similar to those of the tricobalt analogues, indicating the presence of a spin-crossover process (S = 1/2 ⇆ S = 3/2).[20] At low temperature, the spin state of **3** is essentially doublet (S = 1/2, theoretical $\chi_M T$ value = 0.38 cm^3 K mol^{-1}). As the temperature increases, the spin state of **3** gradually changes to S = 3/2. At 300 K, the $\chi_M T$ value for **3** is smaller than that expected for S = 3/2 (1.88 cm^3 K mol^{-1}), which shows that the saturation is still not reached. A notable magnetic behavior of **3** is that its $\chi_M T$

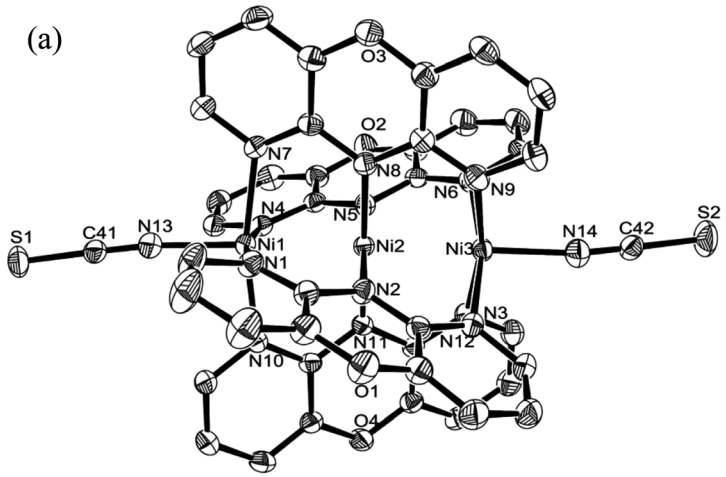

Fig. 2 ORTEP view of the molecular structure of $[Ni_3(dzp)_4(NCS)_2]$ (**2**) (50% probability): (a) side view, (b) end view. All atoms are drawn at the 50% probability level and hydrogen atoms are omitted for clarity.

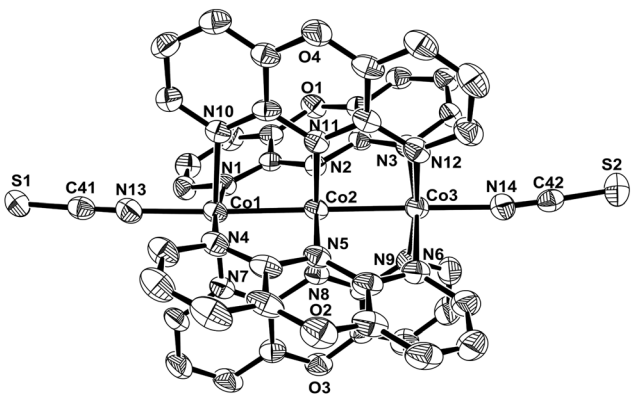

Fig. 3 ORTEP view of the molecular structure of $[Co_3(dzp)_4(NCS)_2]$ (**3**) (50% probability). All atoms are drawn at the 50% probability level and hydrogen atoms are omitted for clarity.

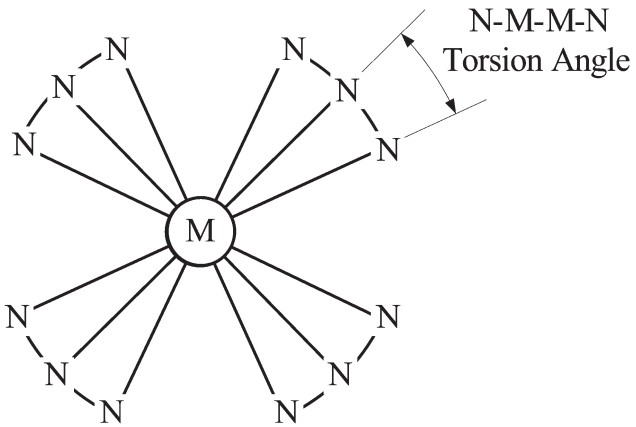

Scheme 5 Illustration of N–M–M–N torsion angles.

versus T curve does not appear a plateau related to the S = 1/2 state, even at very low temperature. Considering that the $\chi_M T$ values of $[Co_3(dpa)_4(NCS)_2]$ (**4**) reach this plateau below 200 K,[20] the energy gap between S = 1/2 and S = 3/2 of **3** is proposed to be smaller than that of **4**. The smaller gap of **3** results in the remaining population of S = 3/2 state at low temperature, which leads to slight higher $\chi_M T$ values and a continuous descending curve.

Table 2 Selected bond lengths (Å) and angles (deg) for compounds **1–3**

Hdzp (**1**)			
N1···H···N2A	2.910	N2···H···N1A	2.910
N(2)–C(5)	1.3767 (15)	O(1)–C(7)	1.3880 (14)
N(2)–C(6)	1.3836 (14)	O(1)–C(4)	1.3899 (13)
C(3)–N(1)–N(3)–C(8)	1.89		
$[Ni_3(dzp)_4(NCS)_2]$ (**2**)			
Ni(1)···Ni(2)	2.4770(6)	Ni(1)–N(13)	1.992(4)
Ni(2)···Ni(3)	2.4766(6)	Ni(3)–N(14)	1.989(4)
Ni(1)–N_{av} (outer)	2.076(3)	Ni(1)–Ni(2)–Ni(3)	178.99(3)
Ni(3)–N_{av} (outer)	2.073(3)	Ni(2)–Ni(1)–N(13)	178.37 (11)
Ni(2)–Ni_{av} (central)	1.907(3)	Ni(2)–Ni(3)–N(14)	179.07 (11)
N–Ni–Ni–N $Torsion_{av}$[a]	17.94		
$[Co_3(dzp)_4(NCS)_2]$ (**3**)			
Co(1)–Co(2)	2.4007 (10)	Co(1)–N(13)	2.053(5)
Co(2)–Co(3)	2.3959 (10)	Co(3)–N(14)	2.042(5)
Co(1)–N_{av} (outer)	1.995(5)	Co(1)–Co(2)–Co(3)	179.12(4)
Co(3)–N_{av} (outer)	1.982(5)	Co(2)–Co(1)–N(13)	178.14 (14)
Co(2)–Co_{av} (central)	1.902(4)	Co(2)–Co(3)–N(14)	179.42 (15)
N–Co–Co–N $Torsion_{av}$[a]	14.03		

[a] The definition of torsion angle is illustrated in Scheme 5.

DFT calculations

In the previous paragraph, the magnetic measurements suggest that the energy gap between S = 1/2 and S = 3/2 states of $[Co_3(dzp)_4(NCS)_2]$ (**3**) is smaller than that of $[Co_3(dpa)_4(NCS)_2]$ (**4**).

Since this gap directly relates to the spin-crossover behavior that is considered to have potential applications as a molecular memory,[25,26] it is important to study the magneto-structure correlation of **3** in detail. To obtain further insights into the electronic structure of **3** and **4**, a series of DFT calculations were performed.

The geometry of compounds **3** and **4** was fully optimized in both the $S = 1/2$ and $S = 3/2$ states. The optimized structural parameters and relative energies of **3** and **4** are listed in Tables 3 and 4, respectively. The qualitative MOs sequence of tricobalt strings near the Fermi level is shown in Scheme 6. The electronic configuration ($e^4b_2^2a_2^1$) that gives rise to the $^2A_2$ state has been shown to be the ground state of compounds **3** and **4**, which is similar to that of tricobalt dpa$^-$ analogues.[27,28]

For the singlet–triplet spin-crossover of **3** and **4**, DFT calculations suggest that this process involves the spin transition of an electron from the π anti-bonding orbital (e) to the σ anti-bonding orbital (a_1). The calculated energy needed for this spin transition (energy difference between $^2A_2$ and ^4E, Tables 3 and 4) of **3** and **4** are 0.750 and 0.825 eV, respectively. Compound **3** has a

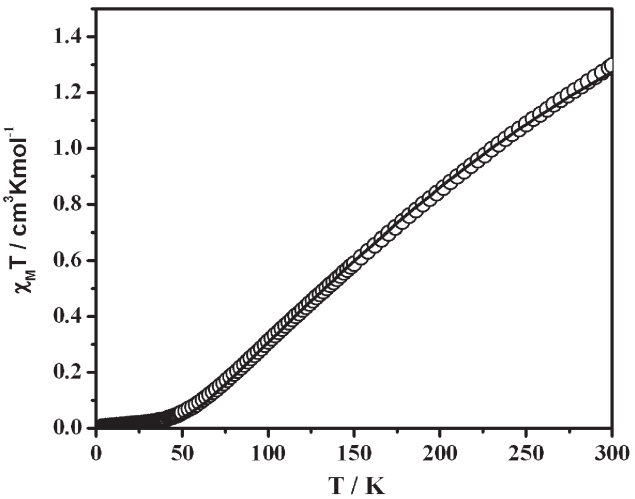

Fig. 4 Plot of $\chi_M T$ *versus* T of complex **2**. The solid line represents the best theoretical fit.

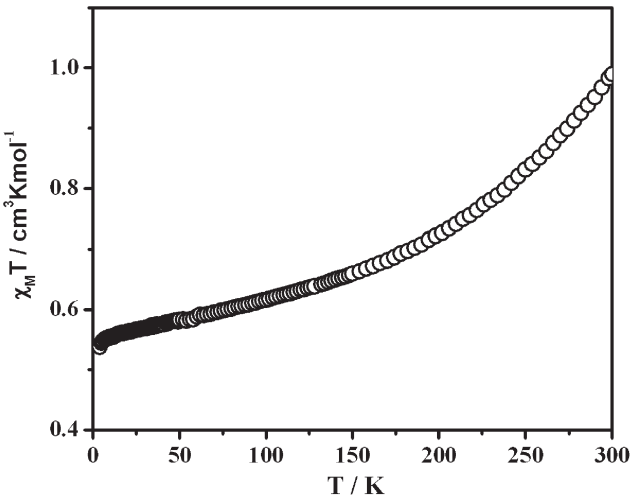

Fig. 5 Plot of $\chi_M T$ *versus* T of complex **3**.

Table 3 Relevant geometrical parameters (distances in Å) and results computed for **3**

	$S = 1/2$			$S = 3/2$	
	$^2A_2$ $e^4b_2^2a_2^1$	$^2E_2$ $e^3b_2^2a_2^2$	$^2B_2$ $e^4b_2^1a_2^2$	^4E $e^3b_2^2a_2^1a_1^1$	$^4B_1$ $e^4b_2^1a_2^1a_1^1$
Co–Co	2.410	2.385	2.403	2.439	2.455
Co–N_{axial}	2.011	2.089	2.103	2.059	2.071
Co_{middle}–N	1.927	1.934	1.916	1.937	1.920
$Co_{terminal}$–N	2.003	2.004	1.988	2.017	2.005
ΔE/eV	0.000	0.253	0.293	0.750	0.756
$\langle S^2 \rangle$	0.79	0.75	0.76	3.78	3.78

Table 4 Relevant geometrical parameters (distances in Å) and results computed for $[Co_3(dpa)_4(NCS)_2]$

	$S = 1/2$				$S = 3/2$	
	$^2A_2$ $e^4b_2^2a_2^1$	$^2E_2$ $e^3b_2^2a_2^2$	$^2B_2$ $e^4b_2^1a_2^2$	Expt.[a] —	^4E $e^3b_2^2a_2^1a_1^1$	$^4B_1$ $e^4b_2^1a_2^1a_1^1$
Co–Co	2.337	2.313	2.341	2.316	2.359	2.382
Co–N_{axial}	2.008	2.088	2.101	2.050	2.060	2.079
Co_{middle}–N	1.928	1.937	1.918	1.896	1.940	1.922
$Co_{terminal}$–N	1.996	1.997	1.981	1.980	2.011	1.996
ΔE/eV	0.000	0.235	0.500	—	0.825	1.036
$\langle S^2 \rangle$	0.79	0.75	0.76	—	3.78	3.78

[a] Averaged bond distances obtained from ref. 20.

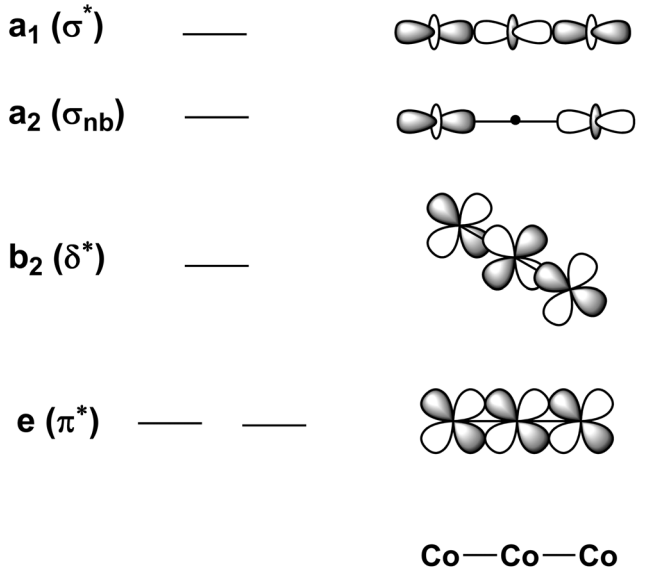

Scheme 6 Schematic molecular orbitals of tricobalt strings near the Fermi level.

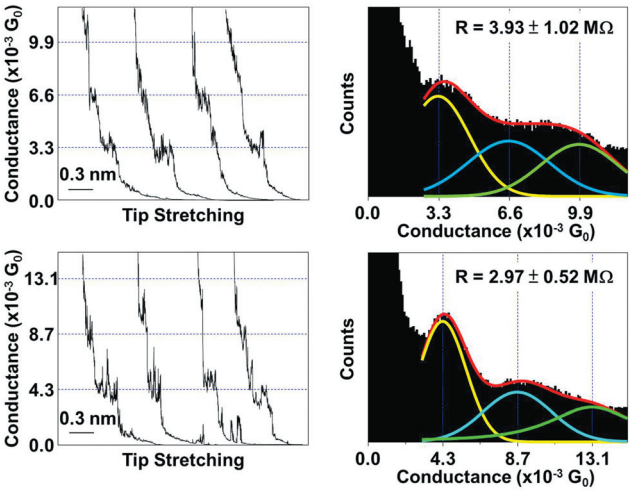

Fig. 6 Typical conductance traces and histograms of **2** (upper panels) and **3** (lower panels). The histograms are subjected to Gaussian fitting to locate the positions of the fundamental peaks. Each histogram is composed of more than 400 conductance traces. The traces from controlled experiments carried out in solutions which do not contain **2** and **3** show exponential decay and thus no conductance peaks in the histograms.

smaller doublet–quartet gap in comparison with that of **4**, which is in agreement with the experimental results. The origin of the decrease of the doublet–quartet gap of **3** can be attributed to its longer Co–Co bond distances. Since the a_1 orbital shows σ antibonding character, the elongation of the Co–Co distances stabilizes significantly the a_1 orbital. The energy gap between e and a_1 orbitals therefore decreases when the Co–Co distance increases. DFT calculations show that the gap between e and a_1 β-spin orbitals of **4** is 1.60 eV. As the nominal Co–Co distances increase from 2.33 Å (in **4**) to 2.40 Å (in **3**), the gap of **3** decreases to 1.44 eV. Because of this smaller energy gap in **3**, the corresponding spin-crossover of **3** occurs even at low temperature as what we observed in the magnetic measurements.

Single-molecule conductance

For the future application as molecular wires, the electron transport property in single molecule was also investigated by the method of STM-bj (scanning tunneling microscopy break junction), which repeatedly creates a nano-gap between the STM tip and the substrate to host the molecule of interest.[29,30] Upon the two axial ligands of isothiocyanate bridging the tip-substrate junction under a small bias potential (E_{bias}, 30 mV for **2** and 25 mV for **3**), the measured current through the molecule will be used to estimate the single-molecule conductance by simple Ohmic law. The left panels of Fig. 6 show typical conductance traces acquired when the STM tip was stretching away from the substrate. The traces are pooled and utilized to construct the conductance histograms where the unit, $G_0 \sim 77.5$ μS, is the conductance quantum of a gold atom chain with single-atom cross-section.[31,32] The local maxima in the histogram are located on the integer multiples of the fundamental ones, indicative of the presence of one, two, or three molecules bridged in the molecular junction.

The values of single-molecule conductance for **2** and **3** are found to be 3.3 (±0.9) × 10^{-3} G_0 and 4.4 (±0.8) × 10^{-3} G_0, respectively, 13 and 32% less conductive than their analogues ligated with dpa^- ligand. Specifically, the single-molecule conductance is found to be 3.8 (±0.6) × 10^{-3} G_0 for $[Ni_3(dpa)_4(NCS)_2]$ and 6.5 (±1.0) × 10^{-3} G_0 for $[Co_3(dpa)_4(NCS)_2]$.[33] Such decrease in the conductance is attributed to the smaller torsion angle of the new dzp^- ligand which makes the metal–metal bonds longer and hence weakens their interactions.

Summary and outlook

Two trinuclear metal string complexes, $[Ni_3(dzp)_4(NCS)_2]$ (**2**) and $[Co_3(dzp)_4(NCS)_2]$ (**3**), containing the rigid Hdzp ligand (**1**) have been synthesized and studied in this work. Because of the rigidity of Hdzp ligand, compounds **2** and **3** exhibit smaller torsion angles and longer metal–metal distances. The longer metal–metal distances observed for **2** and **3** result in variations in their magnetic properties. The exchange interaction ($J = -160$ cm^{-1}) between two HS Ni(II) ions in **2** decreases slightly in comparison with those of trinickel dpa^- analogues ($J = \sim -210$ cm^{-1}). The doublet–quartet gap of **3** is smaller than that of $[Co_3(dpa)_4(NCS)_2]$, which causes compound **3** to show spin-crossover behavior even at low temperature. It is noteworthy that the aim to develop the shortest rigid Hdzp ligand is to avoid the formation of competitive side product in the synthesis of metal string complexes. Although the resulting compounds **2** and **3** are slightly less conductive than their trinuclear dpa^- analogues, we believe that this study will be a useful basis for developing future longer metal string complexes. Further experiments are currently in progress to extend the potential of this research.

Experimental

Materials

The DMSO was distilled from CaH_2. The ethanol was treated with small amount of sodium, and then distilled. All other

reagents and solvents were purchased from commercial sources and were used as received unless otherwise noted. The 1,9-diazaphenoxazine ligand was prepared by a modification of the previously described method.[11]

Physical measurements

IR spectra were obtained with a Nicolet Fourier-Transform in the range 400–4000 cm^{-1}. FAB mass spectra were obtained with a JEOL HX-110 HF double-focusing spectrometer operating in the positive ion detection mode. ^1H NMR spectra were recorded with a Bruker AMX 400 MHz spectrometer. Magnetic measurements were carried out with a Quantum Design MPMS7 SQUID magnetometer operating at a magnetic field of 3000 G between 4 and 300 K. The diamagnetic corrections were evaluated from Pascal's constants.

Synthesis

1,9-Diazaphenoxazine (Hdzp) (1). KOH (2.41 g, 43 mmol) was dissolved in ethanol (7 ml) and DMSO (30 ml) by stirring at room temperature (N_2 atmosphere). Solid 2-amino-3-hydroxypyridine (2.2 g, 20 mmol) then was added. After the resulting claret solution was stirred at 50 °C for 10 minutes, 2-chloro-3-nitropyridine (3.49 g, 22 mmol) was added. The resulting dark brown mixture was refluxed under N_2 atmosphere for 9 hours, and then cooled to room temperature. 200 ml de-ionized water was added to the mixture which was then stored at 4 °C for 12 hours. Brownish precipitates developed. The brown powder was isolated by filtration, and dried *in vacuo*. The residue was extracted by hot $CHCl_3$ (300 ml) and dried under vacuum to afford a light brown solid. The solid was purified by recrystallization from hot THF to yield **1** as white crystals (1.81 g, 49% yield). IR (KBr, cm^{-1}): 3136 m, 3060 m, 2970 m, 1634 m, 1576 m, 1551 s, 1521 s, 1458 s, 1304 m, 1258 m,1181 m, 1119 m, 775 m, 744 m, 575 m cm^{-1}; ^1H NMR (300 MHz, $CDCl_3$): δ (ppm) 8.43 (b, 1H, NH), 7.68 (dd, 1H), 6.82 (dd, 1H), 6.58 (dd, 1H); MS (FAB): m/z = 186 $[M + H]^+$; Elemental analysis (%) $[C_{10}H_7N_3O]$ calcd C 64.86, H 3.81, N 22.69; found: C 64.73, H 3.37, N 22.43.

$[Ni_3(dzp)_4(NSC)_2]$ (2). A mixture of Hdzp (185 mg, 1 mmol), $Ni(OAc)_2{\cdot}4H_2O$ (249 mg, 1 mmol) and naphthalene (30 g) in a 250 ml Erlenmeyer flask was heated to 220 °C for 6 hours. The solution turned to deep green gradually. The mixture was then cooled to 80 °C, and treated with hexane (300 ml) to precipitate the metal complex. The precipitate was washed with hexane to remove naphthalene. The precipitate was extracted with CH_2Cl_2 (200 ml), and treated with excess NaNCS in CH_2Cl_2. The resulting solution was stirred for 1 hour at room temperature. The green precipitate obtained was isolated by filtration and dried under vacuum (142 mg, 55% yield). Single crystals suitable for X-ray diffraction studies can be obtained by slow diffusion of Et_2O into a CH_2Cl_2 solution of the complex. IR (KBr, cm^{-1}): 2074 s, 1632 s, 1444 s, 1281 m, 1254 s, 1193 s, 1119 m, 780 m, 745m. MS (FAB) m/z (%): 1028 $[M]^+$, 970 $[M - NCS]^+$; Elemental analysis (%) $[Ni_3(dzp)_4(NSC)_2]{\cdot}H_2O$: calcd C 48.18, H 2.50, N 18.73; found: C 47.86, H 2.58, N 18.51.

$[Co_3(dzp)_4(NSC)_2]$ (3). A mixture of Hdzp (185 mg, 1 mmol), $CoCl_2$ (130 mg, 1 mmol) and naphthalene (30 g) in a 250 ml Erlenmeyer flask was heated to 130 °C for 12 hours and then heated to 220 °C. A solution of tBuOK (112 mg, 1 mmol) in *n*-butanol (7 ml) was added dropwise. The resulting dark brown mixture was continually refluxed for another 6 hours. The mixture was then cooled to 80 °C, and treated with hexane (300 ml) to precipitate the metal complex. The precipitate was washed with hexane to remove naphthalene. The precipitate was extracted with CH_2Cl_2 (200 ml), and treated with excess NaNCS in CH_2Cl_2. The resulting solution was stirred for 1 hour at room temperature. The yellowish green precipitate obtained was isolated by filtration and dried under vacuum (116 mg, 45% yield). Single crystals suitable for X-ray diffraction studies can be obtained by layering hexane with a CH_2Cl_2 solution of the complex. IR (KBr, cm^{-1}): 2068 s, 1636 s, 1457 s, 1278 m, 1254 s, 1197 s, 1116 m, 775 m, 744m; MS (FAB) m/z (%): 1028 $[M]^+$, 970 $[M - NCS]^+$; Elemental analysis (%) $[Co_3(dzp)_4(NSC)_2]$: calcd C 48.99, H 2.35, N 19.04; found: C 49.16, H 2.67, N 18.57.

X-ray crystallographic determinations

The crystals were mounted on a glass fiber. Crystal data were collected on a NONIUS Kappa CCD diffractometer with monochromatized Mo-Kα radiation (λ = 0.71073 Å) at T = 150(2) K for **1**, **2**, **3**. Cell parameters were retrieved and refined using *DENZO-SMN* software on all observed reflections. Data reduction was performed with the *DENZO-SMN* software.[34–36] An empirical absorption was based on the symmetry-equivalent reflections and absorption corrections were applied with the SORTAV program. All the structures were solved by using the *SHELXS-97*[37] and refined with *SHELXL-97* by full-matrix least squares on F^2 values. The hydrogen atoms were included in calculated positions and refined with a riding model.

Computational methods

All calculations and geometry optimizations reported in this article were carried out by using density functional theory (DFT) methods[38] with the ADF 2006.01 program package.[39] The local spin density (LSD) exchange correlation potential[38] was used with the local density approximation (LDA) of the correlation energy (Vosko, Wilk, Nusair).[40] Becke's nonlocal corrections[41] to the exchange energy and Perdew's nonlocal corrections[42] to the correlation energy were used. Within the ADF program slater type orbitals (STO) with the following basis sets were used: SZ for H, DZP for C, N, O and S, and TZP for Co.[39] The inner shells were treated within the frozen-core approximation (1s for C, N and O, 1s–2p for S, 1s–3p for Co). Full geometry optimizations were carried out within the idealized D_4 symmetry constraints. The z-axis is assumed to be collinear with the Co_3 framework.

Measurement of single-molecule conductance

The method of STM break-junction for the measurement of single-molecule conductance was carried out using a NanoScopeIIIa controller (Veeco, Santa Barbara, CA). The STM tips were

prepared from a freshly cut 0.25 mm gold wire (99.95%, Leesan, Tainan, Taiwan). The substrate was a 100 nm-thick gold film with a 5 nm Cr adhesive layer thermally evaporated onto a glass slide. Before the evaporation, the glass slides were cleaned with piranha solution, a 1 : 3 (v/v) mixture of 30% H_2O_2 and concentrated H_2SO_4. *Piranha solution reacts violently with organics and must be handled carefully.* Compound **2** and **3** were dissolved in toluene (TEDIA) and were introduced to a Teflon STM cell prior to the measurements of single-molecule conductance. Before the data acquisition of conductance traces, images of smooth gold were employed to indicate the quality of the STM tip and substrate. The instrument was then switched to the I(s) mode of STS (scanning tunneling spectroscopy), where the tip was brought into and out of the gold substrate repeatedly and the current *versus* the tip displacement along the *z* direction was recorded. For those junctions with molecules sitting in between the tip and the substrate, the I(s) plot exhibited a plateau. I(s) traces with simple exponential decay were discarded. Each histogram consisted of more than 400 I(s) plots. The standard deviations of single-molecule conductance of **2** and **3** were determined by using Gaussian fitting to the fundamental peaks in the histograms.

Acknowledgements

The authors acknowledge the National Science Council and the Ministry of Education of Taiwan for financial support.

References

1 *Extended Linear Chain Compounds*, ed. J. S. Miller, Plenum, New York, 1982, vols. 1–3.
2 *One-Dimensional Metals*, ed. S. Roth, VCH, New York, 1995.
3 J. K. Bera and K. R. Dunbar, *Angew. Chem., Int. Ed.*, 2002, **41**, 4453–4457.
4 (*a*) J. F. Berry, F. A. Cotton, P. Lei, T. B. Lu and C. A. Murillo, *Inorg. Chem.*, 2003, **42**, 3534–3539; (*b*) J. F. Berry, *Struct. Bonding*, 2010, **136**, 1–26.
5 L.-G. Zhu and S.-M. Peng, *Chin. J. Inorg. Chem.*, 2002, **18**, 117–124.
6 C.-Y. Yeh, C.-C. Wang, C.-h. Chen and S.-M. Peng, in *Nano Redox Sites: Nano-Space Control and its Applications*, ed. T. Hirao, Springer, Berlin, 2006, ch. 5, pp. 85–117.
7 I. P.-C. Liu, W.-Z. Wang and S.-M. Peng, *Chem. Commun.*, 2009, 4323–4331.
8 (*a*) G.-C. Huang, PhD thesis, National Taiwan University, 2008; (*b*) F. A. Cotton, H. Chao, C. A. Murillo and Q. Wang, *Dalton Trans.*, 2006, 5416–5422.
9 S.-J. Shieh, C.-C. Chou, G.-H. Lee, C.-C. Wang and S.-M. Peng, *Angew. Chem., Int. Ed. Engl.*, 1997, **36**, 56–59.
10 M.-H. Yang, T.-W. Lin, C.-C. Chou, H.-C. Lee, H.-C. Chang, G.-H. Lee, M.-K. Leung and S.-M. Peng, *Chem. Commun.*, 1997, 2279–2280.
11 C. O. Okafor, *J. Heterocycl. Chem.*, 1976, **13**, 107–110.
12 I. P.-C. Liu, M. Bénard, H. Hasanov, I-W. P. Chen, W.-H. Tseng, M.-D. Fu, M.-M. Rohmer, C.-h. Chen, G.-H. Lee and S.-M. Peng, *Chem.–Eur. J.*, 2007, **13**, 8667–8677.
13 R. H. Ismayilov, W.-Z. Wang, G.-H. Lee, R.-R. Wang, I. P.-C. Liu, C.-Y. Yeh and S.-M. Peng, *Dalton Trans.*, 2007, 2898–2907.
14 M.-Y. Huang, C.-Y. Yeh, G.-H. Lee and S.-M. Peng, *Dalton Trans.*, 2006, 5683–5690.
15 S.-M. Peng, C.-C. Wang, Y.-L. Jang, Y.-H. Chen, F.-Y. Li, C.-Y. Mou and M.-K. Leung, *J. Magn. Magn. Mater.*, 2000, **209**, 80–83.
16 F. A. Cotton, L. M. Daniels, G. T. Jordan and C. A. Murillo, *J. Am. Chem. Soc.*, 1997, **119**, 10377–10381.
17 M. M. Warnke, F. A. Cotton and D. W. Armstrong, *Chirality*, 2007, **19**, 179–183.
18 F. A. Cotton, L. M. Daniels, P. Lei, C. A. Murillo and X. P. Wang, *Inorg. Chem.*, 2001, **40**, 2778–2784.
19 C.-H. Cheng, R.-D. Hung, W.-Z. Wang, S.-M. Peng and I. C. Chen, *ChemPhysChem*, 2010, **11**, 517–524.
20 R. Clerac, F. A. Cotton, S. P. Jeffery, C. A. Murillo and X. P. Wang, *Inorg. Chem.*, 2001, **40**, 1265–1270.
21 E.-C. Yang, M.-C. Cheng, M.-S. Tsai and S.-M. Peng, *Chem. Commum.*, 1994, 2377–2378.
22 R. Clerac, F. A. Cotton, L. M. Daniels, K. R. Dunbar, K. Kirschbaum, C. A. Murillo, A. A. Pinkerton, A. J. Schultz and X. P. Wang, *J. Am. Chem. Soc.*, 2000, **122**, 6226–6236.
23 J. F. Berry, F. A. Cotton, T. B. Lu, C. A. Murillo and X. P. Wang, *Inorg. Chem.*, 2003, **42**, 3595–3601.
24 (*a*) J. F. Berry, F. A. Cotton and C. A. Murillo, *Dalton Trans.*, 2003, 3015–3021; (*b*) P. Kiehl, M.-M. Rohmer and M. Bénard, *Inorg. Chem.*, 2004, **43**, 3151–3158; (*c*) X. López, M. Bénard and M.-M. Rohmer, *J. Mol. Struct. (THEOCHEM)*, 2006, **777**, 53–60.
25 O. Kahn and C. J. Martinez, *Science*, 1998, **279**, 44–48.
26 E. Coronado, F. P. Prins, F. M. Monrabal-Capilla, E. A. Osorio and H. S. J. van der Zant, *Adv. Mater.*, 2011, **23**, 1545–1549.
27 M.-M. Rohmer, A. Strich, M. Bénard and J. P. Malrieu, *J. Am. Chem. Soc.*, 2001, **123**, 9126–9134.
28 D. A. Pantazis and J. E. McGrady, *J. Am. Chem. Soc.*, 2006, **128**, 4128–4135.
29 (*a*) B. Xu and N. J. Tao, *Science*, 2003, **301**, 1221–1223; (*b*) B. Kim, J. M. Beebe, C. Olivier, S. Rigaut, D. Touchard, J. G. Kushmerick, X.-Y. Zhu and C. D. Frisbie, *J. Phys. Chem. C*, 2007, **111**, 7521–7526; (*c*) R. Mas-Ballesté, J. Gómez-Herrero and F. Zamora, *Chem. Soc. Rev.*, 2010, **39**, 4220–4233; (*d*) A. K. Mahapatro, J. Ying, T. Ren and D. B. Janes, *Nano Lett.*, 2008, **8**, 2131–2136; (*e*) A. Szuchmacher Blum, T. Ren, D. A. Parish, S. A. Trammell, M. H. Moore, J. G. Kushmerick, G.-L. Xu, J. R. Deschamps, S. K. Pollack and R. Shashidhar, *J. Am. Chem. Soc.*, 2005, **127**, 10010–10011.
30 X. Li, J. He, J. Hihath, B. Xu, S. M. Lindsay and N. Tao, *J. Am. Chem. Soc.*, 2006, **128**, 2135–2141.
31 H. Ohnishi, Y. Kondo and K. Takayanagi, *Nature*, 1998, **395**, 780–783.
32 A. I. Yanson, G. R. Bollinger, H. E. van der Brom, N. Agrait and J. M. Ruitenbeek, *Nature*, 1998, **395**, 783–785.
33 I-W. P. Chen, M.-D. Fu, W.-H. Tseng, J.-Y. Yu, S.-H. Wu, C.-J. Ku, C.-h. Chen and S.-M. Peng, *Angew. Chem., Int. Ed.*, 2006, **45**, 5814–5818.
34 Z. Otwinowski and W. Minor, *Macromol. Crystallogr. A*, 1997, **276**, 307–326.
35 R. H. Blessing, *Acta Crystallogr. A*, 1995, **51**, 33–38.
36 G. M. Sheldrick, *Acta Crystallogr. A*, 1990, **46**, 467–473.
37 G. M. Sheldrick, SHELXL-97, University of Göttingen, Germany, 1997
38 R. G. Parr and W. Yang, *Density Functional Theory of Atoms and Molecules*, Oxford University Press, New York, 1989.
39 E. J. Baerends, *et al.* ADF 2006.01 SCM; Theoretical Chemistry, Vrije Universiteit, Amsterdam, The Netherlands; http://www.scm.com
40 S. H. Vosko, L. Wilk and M. Nusair, *Can. J. Phys.*, 1980, **58**, 1200–1211.
41 A. D. Becke, *Phys. Rev. A*, 1988, **38**, 3098–3100.
42 J. P. Perdew, *Phys. Rev. B*, 1986, **33**, 8822–8824.

C. R. Chimie 15 (2012) 159–162

Contents lists available at ScienceDirect

Comptes Rendus Chimie

www.sciencedirect.com

Preliminary communication/Communication

Further studies of $[Ni_4(DAniDANy)_4]$ ($DAniDANy^{2-}$ = *N*,*N*'-bis-*p*-anisyl-2,7-diamido-1,8-naphthyridine) and its one-electron oxidation product: Metal-metal sigma bonding in Ni_4^{9+} complex

Gin-Chen Huang [a], Shao-An Hua [a], Isiah Po-Chun Liu [a,*], Chih-Hsien Chien [a], Jau-Huei Kuo [a], Gene-Hsiang Lee [a], Shie-Ming Peng [a,*,b]

[a] *Department of Chemistry, National Taiwan University, Taipei, Taiwan*
[b] *Institute of Chemistry, Academia Sinica, Taipei, Taiwan*

ARTICLE INFO

Article history:
Received 7 April 2011
Accepted after revision 5 May 2011
Available online 23 June 2011

Dedicated to Pr Marie-Madeleine Rohmer.

Keywords:
Molecular wire
Metal-metal bond
DFT calculation
Molecular switch
Even-numbered metal sting

ABSTRACT

The linear tetranickel strings, $[Ni_4(DAniDANy)_4]$ (**1**), and its one-electron oxidation product, $[Ni_4(DAniDANy)_4](PF_6)$ (**2**), have been synthesized and studied extensively ($DAniDANy^{2-}$ = N,N'-bis-p-anisyl-2,7-diamido-1,8-naphthyridine). Crystal structural analyses and DFT calculations suggest that the chemical oxidation of **1** involves removal of an electron from the σ^* antibonding orbital, which results in the formation of Ni-Ni bonds in **2**.

Metal string complexes that contain a 1D linear transition metal backbone are considered to be potential molecular electronic devices [1]. The general expectation is to transport an electron through the continua of metal wire-like frameworks that are similar to the electric wires in our macroscopic world. In addition to this potential application, the studies of metal strings can also provide useful information for understanding the metal-metal bonds [2]. Because of these significances, numerous metal string complexes have been synthesized and studied in the past two decades [1].

Among the family of metal strings, the linear metal framework of most reported complexes consists of an odd number of metal atoms [1]. The physical properties and electric conductance of odd-numbered metal strings therefore have been studied fruitfully. Compared with the odd-numbered metal stings, research on even-numbered metal stings remains relatively underdeveloped.

The even-numbered metal strings, however, show different physical properties than odd-numbered analogues do [3]. For example, two axial coordinated water molecules of the tetranuclear nickel string, $[Ni_4(Tsdpda)_4(H_2O)_2]$, can be removed by one-electron oxidation ($Tsdpda^{2-}$ = N-(p-toluenesulfonyl)dipyridyldiamido) [3a]. The flexibility of the axial interactions suggests that the geometry and electronic structure of even-numbered metal strings may be tuned by carefully modifying the axial interactions, which was rarely observed in the middle of odd-numbered metal strings. Because of this interesting character, one research goal in our group is to synthesize and to study new even-numbered metal stings, which can help scientists to gain more insights into the design of future molecular wires.

* Corresponding authors.
E-mail addresses: isiahliu@yahoo.com.tw (I.-C. Liu), smpeng@ntu.edu.tw (S.-M. Peng).

1631-0748/$ – see front matter © 2011 Académie des sciences. Published by Elsevier Masson SAS. All rights reserved.
doi:10.1016/j.crci.2011.05.002

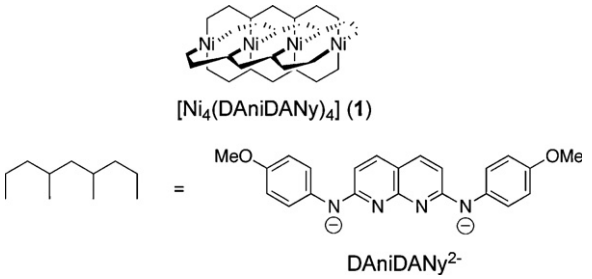

Scheme 1. $[Ni_4(DAniDANy)_4]$ (**1**) and $DAniDANy^{2-}$.

In our previous report, the $[Ni_4(Tsdpda)_4(H_2O)_2]$ and its one-electron oxidized product, $[Ni_4(Tsdpda)_4]^+$, show different electronic structure due to both the oxidation states and the leaving of axial coordinated water molecules [3a]. These concurrent factors result in difficulties for studying the variation of electronic structures of tetranickel strings upon one-electron oxidation. Before we proceed to develop more even-numbered metal strings, we think it is worth understanding the details of tetranickel strings. In this study, we thus report the synthesis, crystal structure, magnetic properties and DFT calculations of $[Ni_4(DAniDANy)_4](PF_6)$ (**2**), which is the one-electron oxidized product of the previously reported $[Ni_4(DAniDANy)_4]$ (**1**) compound [3a]. Since both compounds possess no axial ligands, the $[Ni_4(DAniDANy)_4](PF_6)$ directly shows the variations of geometry and electronic structure upon one-electron oxidation.

The $H_2DAniDANy$ ligand and tetranickel string, $[Ni_4(DAniDANy)_4]$, were prepared according to the literature procedures (Scheme 1) [3a]. The one-electron oxidized product, $[Ni_4(DAniDANy)_4](PF_6)$, was obtained by reacting $[Ni_4(DAniDANy)_4]$ with $FcPF_6$ in CH_2Cl_2 [4]. The crystal structure of **2** is shown in Fig. 1 [5]. The core structure of **1** and **2** are similar. Both compounds consist in a linear tetranickel chain helically wrapped by four $DAniDANy^{2-}$ ligands, which display approximate D_4 symmetry.

Selected bond lengths observed for **2** are reported in Table 1, together with the corresponding values reported for **1** [3a]. The terminal and internal Ni–N bond distances of **2** are 2.326 and 2.309 Å, respectively, which are ~0.03 Å shorter than those in **1**. Considering the oxidation of **1** increases the electrostatic repulsion between Ni ions, the Ni–Ni distances in **2** should be elongated. The contraction of Ni–Ni bond lengths in **2** thus indicates that the formation of significant attractions between Ni ions instead of electrostatic repulsions. Such structural variations are similar to those of the oxidation of $[Ni_4(Tsdpda)_4(H_2O)_2]$, which suggests the formation of Ni–Ni bonds [3a]. However, the oxidation of $[Ni_4(Tsdpda)_4(H_2O)_2]$ accompanies the loss of axial coordinated water molecules, which also shorten the Ni–Ni bond lengths due to the trans effect. The contraction of Ni–Ni bond lengths in **1** upon oxidation clearly indicates that the one-electron oxidation of tetranickel string mainly results in Ni–Ni bond formation.

Table 1
Selected bond distances (Å) of **1**[a] and **2**.

	1	**2**
Ni-Ni terminal	2.356 (1)	2.326 (1)
Ni-Ni internal	2.332 (1)	2.309 (2)
Ni-N terminal	1.912 (3)	1.898 (9)
Ni-N internal	1.912 (3)	1.903 (11)

[a] Reference [3a].

Magnetic susceptibility measurements for compounds **1** and **2** were made on polycrystalline samples in the temperature range 5–300 K. As previously reported, compound **1** is diamagnetic [3a]. The magnetic behaviour of **2** is different from that of **1**. Temperature-dependent $\chi_m T$ versus T is displayed for **2** in Fig. 2. The $\chi_m T$ value for **2** is ca. 0.368 $cm^3\,K\,mol^{-1}$ at 300 K and remains constant down to 15 K. This value indicates that compound **2** possesses one unpaired electron (theoretical value: 0.375 $cm^3\,K\,mol^{-1}$). Furthermore, the axial EPR spectrum ($g_\perp = 2.17$ and $g_\parallel = 2.03$) obtained at 77 K for **2** is coincident with the feature of the $3d^7$ Ni(III) ion ($S = 1/2$) in an elongated octahedral geometry, which supports the previous oxidation reaction and magnetism (Fig. 2, insert) [4].

Cyclic voltammetry of compound **1** in CH_2Cl_2 solution showed three reversible one-electron oxidation processes at potentials of 0.13, 0.87 and 1.02 V, respectively (Fig. 3). The first oxidation process is assigned to the loss of one

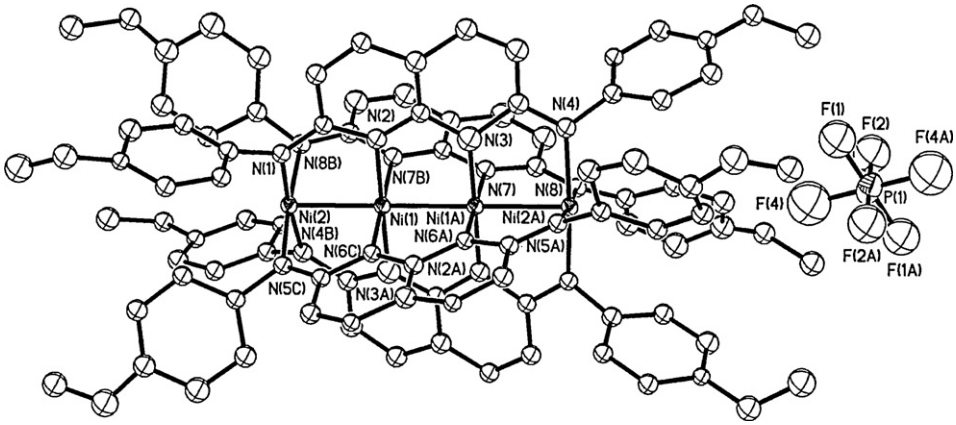

Fig. 1. Crystal structure of **2**. Thermal ellipsoids are drawn at the 30% probability level. Hydrogen atoms and solvent molecules are omitted for clarity.

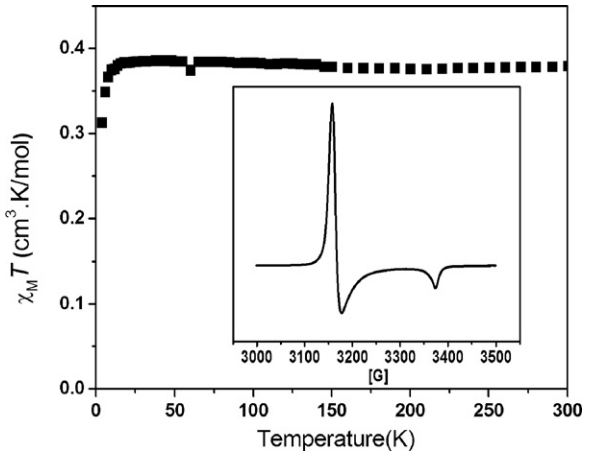

Fig. 2. Plot of $\chi_m T$ versus T of complex **2**. Insert: powder X-band EPR spectrum of **2** at 77 K.

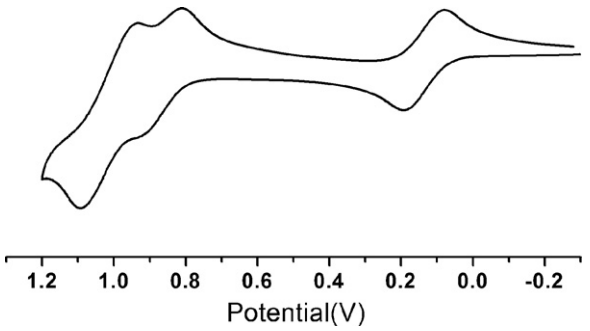

Fig. 3. Cyclic voltammograms of **1** in CH_2Cl_2 containing 0.1 M TBAP with scan rate = 100 mVS^{-1}.

electron from **1**, leading to the formation of **2**. Fig. 4 shows the spectral changes in the near-IR range observed for compound **1** at applied potential from 0 to 0.30 V in CH_2Cl_2 containing 0.1 TMAP. A new broad band at 1150 nm appears as the applied potential increases, which is

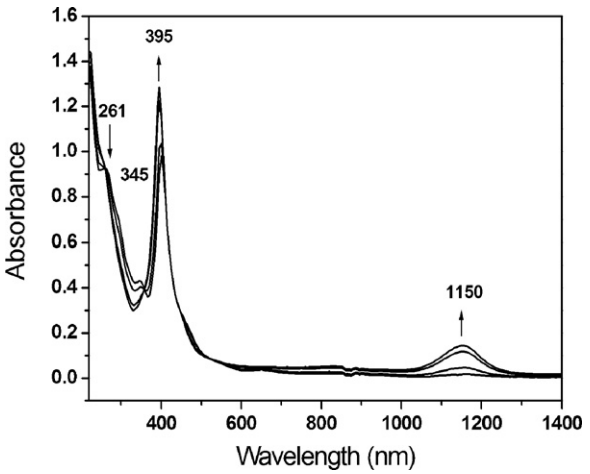

Fig. 4. UV-Vis and near-IR spectral changes for the first oxidation of compound **1** in CH_2Cl_2 with 0.1 M TBAP at various applied potentials form 0 to +0.30 V.

Table 2
Selected DFT calculated bond lengths (Å) of compounds **1** and **2** in the gas phase.

	1	**2**
Ni-Ni terminal	2.366	2.338
Ni-Ni internal	2.350	2.331
Ni-N terminal	1.911	1.908
Ni-N internal	1.938	1.936

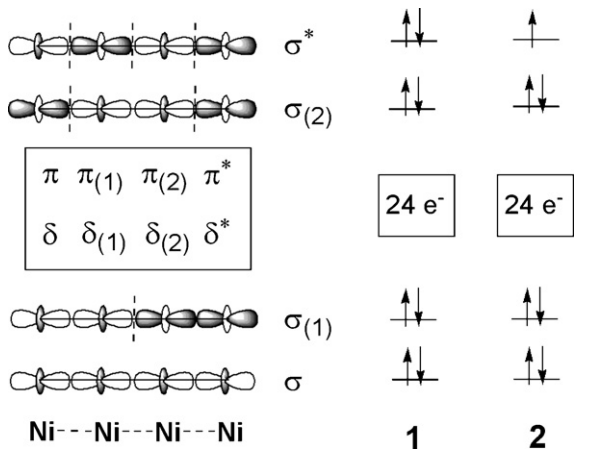

Fig. 5. The qualitative molecular orbital diagram of the linear tetranickel system (left). The computed electronic configuration of compounds **1** and **2** (right).

attributed to the inter-valence charge transfer (IVCT) transition [5]. This IVCT band is a character of the electron delocalization within the mixed-valence complex **2** [2h,6].

To obtain further insight into the electronic structures of compounds **1** and **2**, a series of DFT/BP86 calculations was performed using ORCA [7,8]. For the sake of simplicity, the anisyl groups of the ligand DAniDANy^{2-} are replaced by methyl groups. The geometries of compounds **1** and **2** were optimized on the singlet state for **1** and doublet state for **2**. The z-axis is assumed to be collinear with the tetranickel framework. Some relevant geometrical parameters and results from DFT calculations are listed in Table 2. The optimized geometrical parameters are in good agreement with the experimental data.

In a linear tetranickel system, the d orbitals of the transition metals generate three types of molecular orbitals: (1) σ-type MOs (σ, $\sigma_{(1)}$, $\sigma_{(2)}$ and σ*), composed of d_{z2} combinations; (2) π-type MOs (π, $\pi_{(1)}$, $\pi_{(2)}$ and π*), composed of d_{xz} and d_{yz} orbitals; (3) δ-type MOs (δ, $\delta_{(1)}$, $\delta_{(2)}$ and δ*), composed of d_{xy} orbitals [3a]. The qualitative molecular orbital diagram is shown in Fig. 5. The computed electronic configuration of **1** is $(\sigma)^2(\sigma_{(1)})^2$ (π and δ block)^{24} $(\sigma_{(2)})^2$ $(\sigma^*)^2$. Since all the bonding and antibonding orbitals

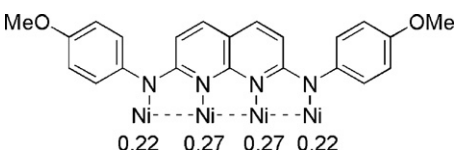

Scheme 2. Computed mulliken atomic spin densities of compound **2**.

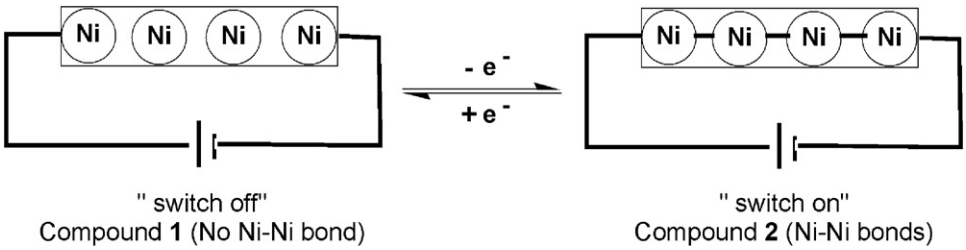

Scheme 3. The proposed redox-controlled molecular switch.

of **1** are doubly occupied, there are no Ni-Ni bonding interactions in **1**. On the contrary, calculations indicate that the electronic configuration of **2** is $(\sigma)^2(\sigma_{(1)})^2$ (π and δ block)^{24} $(\sigma_{(2)})^2$ $(\sigma^*)^1$, which suggests that the removal of one electron from the σ^* antibonding orbital occurs upon oxidation. The one-electron oxidation of **1** gives the product **2** with partial Ni–Ni σ-bonds, which supports the observed shortening in the Ni-Ni distances from **1** to **2**. The electrons on the σ orbitals are proposed to delocalize over the tetranickel framework through Ni–Ni σ-bonds, which is confirmed by the mulliken atomic spin densities (Scheme 2). Moreover, the observed IVCT band of **2** may be assigned qualitatively to the transition from lower doubly occupied σ, $\sigma_{(1)}$ or $\sigma_{(2)}$ orbitals to the highest singly occupied σ^* orbital [9].

In summary, in order to study the structural change of tetranickel string which results from one-electron oxidation, we have oxidized the $[Ni_4(DAniDANy)_4]$ (**1**) and isolated its one-electron oxidized product $[Ni_4(DAniDANy)_4](PF_6)$ (**2**). The magnetic measurements show that **1** and **2** exhibit singlet and doublet ground states, respectively, which were confirmed by EPR spectra. DFT calculations suggest that the chemical oxidation of **1** involves removal of the electron from the σ^* antibonding orbital (Fig. 5), which leads **1** to form Ni-Ni bonds upon oxidation. Considering this oxidation process is reversible (Fig. 3), these tetranickel strings are along the line toward potential applications in molecular switches (Scheme 3) [10]. The studies of the shortest even-numbered tetranickel string, **1** and **2**, therefore, provide more insights into not only the development of future longer even-numbered metal strings but also the design of molecular switches.

Acknowledgment

The authors thank the National Science Council and the Ministry of Education of the Republic of China (Taiwan, ROC) for financial support.

Appendix A. Supporting information

X-ray crystallographic files for compound **2**, experimental details and computational methods are available with the electronic version of this article. CCDC-670782 contains the supplementary crystallographic data for this paper. These data can be obtained free of charge from the Cambridge Crystallographic Data Centre via http://www.ccdc.cam.ac.uk/datarequest.cif.

References

[1] (a) J.S. Miller (Ed.), Extended linear chain compounds, Vols. 1–3, Plenum, NewYork, 1982;
(b) S. Roth, One-dimensional metals, VCH, New York, 1995;
(c) J.K. Bera, K.R. Dunbar, Angew. Chem. Int. Ed 41 (2002) 4453;
(d) C.Y. Yeh, C.C. Wang, C.H. Chen, S.M. Peng, in: T. Hirao (Ed.), Nano redox sites: nano-space control and its applications, Springer, Berlin, 2006, pp. 85–117;
(e) I.P.C. Liu, W.Z. Wang, S.M. Peng, Chem. Commun. (2009) 4323.
[2] (a) J.F. Berry, F.A. Cotton, L.M. Daniels, C.A. Murillo, X. Wang, Inorg. Chem. 42 (2003) 2418;
(b) M.M. Rohmer, M. Bénard, J. Am. Chem. Soc. 120 (1998) 9372;
(c) M.M. Rohmer, A. Strich, M. Bénard, J.P. Malrieu, J. Am. Chem. Soc. 123 (2001) 9126;
(d) N. Benbellat, M.M. Rohmer, M. Bénard, Chem. Commun. (2001) 2368;
(e) M.M. Rohmer, M. Bénard, Chem. Soc. Rev. 30 (2001) 340;
(f) M.M. Rohmer, M. Bénard, J. Cluster Sci. 13 (2002) 333;
(g) P. Kiehl, M.M. Rohmer, M. Bénard, Inor. Chem. 43 (2004) 3151;
(h) I.P.C. Liu, M. Bénard, H. Hasanov, I.W.P. Chen, W.H. Tseng, M.D. Fu, M.M. Rohmer, C.H. Chen, G.H. Lee, S.M. Peng, Chem. Eur. J. 13 (2007) 8667;
(i) G.C. Huang, M. Bénard, M.M. Rohmer, L.A. Li, M.J. Chiu, C.Y. Yeh, G.H. Lee, S.M. Peng, Eur. J. Inorg. Chem. (2008) 1767;
(j) R.H. Ismayilov, W.Z. Wang, G.H. Lee, C. Yu Yeh, S.A. Hua, Y. Song, M.M. Rohmer, M. Bénard, S.M. Peng, Angew. Chem. Int. Ed. 50 (2011) 2045.
[3] (a) X. López, M.Y. Huang, G.C. Huang, S.M. Peng, F.Y. Li, M. Bénard, M.M. Rohmer, Inorg. Chem. 45 (2006) 9075;
(b) S.Y. Lai, T.W. Lin, Y.H. Chen, C.C. Wang, G.H. Lee, M.H. Yang, M.K. Leung, S.M. Peng, J. Am. Chem. Soc. 121 (1999) 250;
(c) C.H. Chien, J.C. Chang, C.Y. Yeh, L.M. Fang, Y. Song, S.M. Peng, Dalton Trans. (2006) 3249;
(d) C.H. Chien, J.C. Chang, C.Y. Yeh, G.H. Lee, L.M. Fang, S.M. Peng, Dalton Trans. (2006) 2106;
(e) T.B. Tsao, S.S. Lo, C.Y. Yeh, G.H. Lee, S.M. Peng, Polyhedron 26 (2007) 3833;
(f) I.P.C. Liu, C.F. Chen, S.A. Hua, C.H. Chen, H.T. Wang, G.H. Lee, S.M. Peng, Dalton Trans. (2009) 3571;
(g) C.W. Yeh, I.P.C. Liu, R.R. Wang, C.Y. Yeh, G.H. Lee, S.M. Peng, Eur. J. Inorg. Chem. (2010) 3153.
[4] R.S. Drago, Physical methods for chemists, 2nd ed, Saunders College Publishing, New York, 1992, , Chapter 13.
[5] D.M. Brown, in: D. Reidel (Ed.), Mixed valence compounds, Dordrecht, Holland, 1980.
[6] G.C. Huang, I.P.C. Liu, J.H. Kuo, Y.L. Huang, C.Y. Yeh, G.H. Lee, S.M. Peng, Dalton Trans. (2009) 2623.
[7] R.G. Parr, W. Yang, Density functional theory of atoms and molecules, Oxford University Press, New York, 1989.
[8] F. Neese, *ORCA*-an ab initio. Density Functional and Semiempirical Program Package Version 2. 8-20 2010 ed, Universität Bonn, Bonn, Germany, 2010.
[9] A. Bencini, E. Berti, A. Caneschi, D. Gatteschi, E. Giannasi, I. Invernizzi, Chem. Eur. J. 8 (2002) 3660.
[10] J. Otsuki, T. Akasaka, K. Araki, Coord. Chem. Rev. 252 (2008) 32.

Inorganic Chemistry

Article

pubs.acs.org/IC

Diruthenium(III,III) Bis(alkynyl) Compounds with Donor/Acceptor-Substituted *geminal*-Diethynylethene Ligands

William P. Forrest, Zhi Cao, Kerry M. Hassell, Boone M. Prentice, Phillip E. Fanwick, and Tong Ren*

Department of Chemistry, Purdue University, West Lafayette, Indiana 47907, United States

Supporting Information

ABSTRACT: Reported in this contribution are the preparation and characterization of a series of $Ru_2(DMBA)_4$ (DMBA = *N*,*N*′-dimethylbenzamidinate) bis(alkynyl) compounds, *trans*-$Ru_2(DMBA)_4$(X-*gem*-DEE)$_2$ [*gem*-DEE = *σ*-*geminal*-diethynylethene; X = H (**1**), Si^iPr_3 (**2**), Fc (**3**); 4-$C_6H_4NO_2$ (**4**), and 4-$C_6H_4NMe_2$ (**5**)]. Compounds **1**−**5** were characterized by spectroscopic and voltammetric techniques as well as the single-crystal X-ray diffraction studies of **2** and **3**. Both the single-crystal structural data of compounds **2** and **3** and the spectroscopic/voltammetric data indicate that the *gem*-DEE ligands are similar to simple acetylides in their impact on the molecular and electronic structures of the $Ru_2(DMBA)_4$ core. Furthermore, density functional theory calculations revealed more extensive *π* delocalization in aryl-donor-substituted *gem*-DEEs and that the hole-transfer mechanism will likely dominate the charge delocalization in Ru_2-*gem*-DEE-based wires.

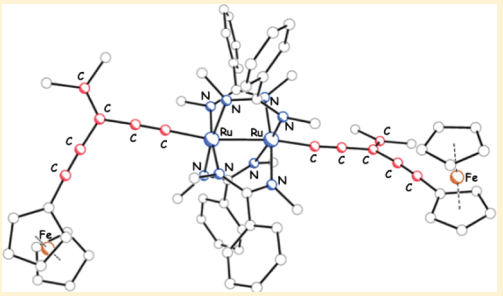

INTRODUCTION

During the past several decades, a great deal of research has been directed toward the design and synthesis of conjugated organic compounds having extensive *π* delocalization and highly polarizable *π*-electron systems. These compounds continue to be sought-after materials because of their interesting optical and conductive properties as well as their nonlinear optical responses (NLOs) or large molecular first- and second-order hyperpolarizabilities (*β* and *γ*, respectively).[1] By far, linearly conjugated *π*-electron systems [Chart 1; polyacetylene (**I**), polydiacetylene (**II**), and polytriacetylene (**III**)] are the most researched and well-known. In addition, several other types of conjugation also display interesting electronic features, i.e., *σ* conjugation in polysilanes,[2] *σ*−*π* conjugation in oligo(cyclohexylidene),[3] and homoconjugation in diphenylpropanes and diphenylsilianes.[4] A type of conjugation that is of significant interest to physical organic chemists but far is less investigated is *cross-conjugation*, which is defined as the conjugation of two unsaturated moieties to a third unsaturated fragment without being directly conjugated to each other.[5] The most apparent difference between linearly conjugated and *cross-conjugated* organic molecules is that the *π*-electron density is not as easily delocalized along the carbon framework within *cross-conjugated* molecules, which is in concurrence with classical resonance theory.[5] The rapid progress in the synthesis of nonlinear eneyne and enediyne scaffolds, notably the contributions from Nielsen and Diederich,[6] Tykwinski and co-workers,[7] and Hopf,[8] make it possible to explore *cross-conjugated* organic and organometallic compounds based on scaffolds of mixed acetylene and ethene units.

Chart 1. *π*-Conjugated Eneyne and Enediyne Oligomers

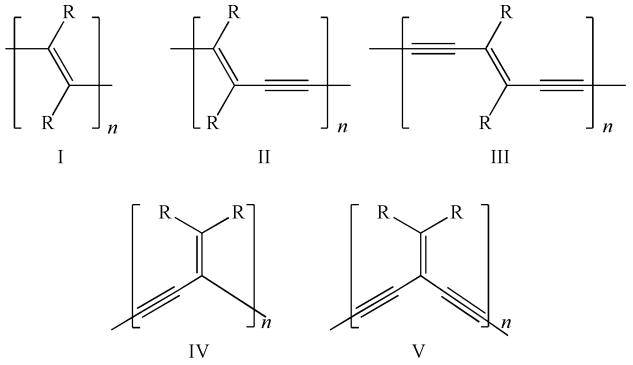

Cross-conjugated oligomers based on the eneyne framework, such as isopolydiacetylenes (Chart 1, **IV**)[9,10] and isopolytriacetylenes (Chart 1, **V**),[11,12] have been previously studied and have shown that electronic communication is observed along the eneyne framework.[13] Organic compounds containing the *geminal*-diethynylethene unit (or isotriacetylene, abbreviated as *gem*-DEE) are of particular interest because it has been recently suggested on the basis of computational modeling that oligomers of *gem*-DEE may function as molecular wires with conductance attenuated by quantum interference effects.[14] We hypothesize that the combination of a redox-rich transition metal with donor/acceptor-substituted *gem*-DEE frameworks will provide a set of organometallic compounds for the experimental exploration of *cross-conjugation* and quantum interference effects.

Received: December 19, 2011
Published: February 10, 2012

   dx.doi.org/10.1021/ic202720c | *Inorg. Chem.* 2012, 51, 3261−3269

Transition-metal compounds containing linear arylacetylide and polyynyl ligands have been studied for several decades with efforts focusing on the linear π conjugation therein,[15,16] and efficient charge transfer has been documented for polyynyl/polyenyl compounds of metal centers such as iron,[17] rhenium,[18] and ruthenium.[19] However, transition-metal compounds with nonlinear eneynes or enediynes as σ-acetylide ligands are relatively rare, and ones based on *gem*-DEE are strictly limited to platinum(II) species.[20] It is worth noting that the coordination of tetraethynylethene, a ligand related to *gem*-DEE, to metal centers such as platinum(II),[21] gold(I),[22] and iron(II)[23] and a trimetallic cluster (μ_3-C)Co_3[24] have been documented as well. While the platinum(II) examples demonstrate the feasibility of metalation, the π conjugation between *gem*-DEE and the platinum(II) center is limited because of the electronic saturation of a d^8 configuration in a square-planar environment. Hence, there is the need to prepare *gem*-DEE complexes of redox-active transition metals, which will help to elucidate the effect of *cross-conjugation* in metal-*gem*-DEE systems. Previously, we communicated the syntheses of two *trans*-Ru_2(DMBA)$_4$(X-*gem*-DEE)$_2$ compounds [X = H (**1**) and Si^iPr_3 (**2**), DMBA = *N*,*N*′-dimethylbenzamidinate, and *gem*-DEE = σ-*geminal*-diethynylethene], which were the first examples of redox-active transition-metal complexes containing *gem*-DEE ligands.[25] In this contribution, we expand the investigation of Ru_2(DMBA)$_4$(X-*gem*-DEE)$_2$-type complexes to those containing electron-donor, ferrocenyl (Fc) and 4-(dimethylamino)phenyl (DMAP), or electron-acceptor, 4-nitrophenyl (NP), substituted *gem*-DEEs as the axial σ-acetylide ligands (Scheme 1).

Scheme 1. Ru_2(DMBA)$_4$ Compounds of *gem*-DEE Ligands

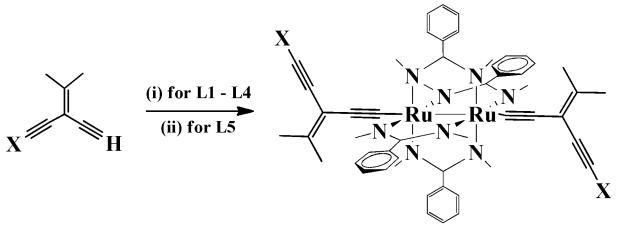

RESULTS AND DISCUSSION

Synthesis. The X-*gem*-DEE ligands **L1**−**L5**, as shown in Scheme 1, were prepared according to the literature methods. The initial synthesis of metal compounds started with 1-(trimethylsilyl)-3-(trimethylsilyl)ethynyl-4-methylpent-3-en-1-yne,[10] which was converted to 3-ethynyl-4-methylpent-3-en-1-yne (**L1**) upon desilylation using K_2CO_3. Ligands **L2** and **L3** were desilylated using methanolic K_2CO_3, while ligands **L4** and **L5** were desilylated using aqueous *n*-Bu_4NF. Ligands **L1**, **L2**, and **L5** were isolated as clear oils, while ligands **L3** and **L4** were isolated as orange and yellow solids, respectively.

The *trans*-Ru_2(DMBA)$_4$(X-*gem*-DEE)$_2$-type compounds were prepared using the weak-base-assisted reaction.[26,27] The reaction between Ru_2(DMBA)$_4$(NO$_3$)$_2$[26] and **L1** in the presence of Et_3N readily yielded a red solution that is characteristic of Ru_2(DMBA)$_4$(C_2R)$_2$-type compounds.[27] Thin-layer chromatography (TLC) analysis of the reaction mixture after 3 h, however, revealed that, in addition to a red species [R_f = 0.72, 1:3 (v/v) EtOAc/hexanes], there was a long, reddish-brown band not far from the baseline. The red species was isolated via recrystallization in 20% yield and unambiguously identified as *trans*-Ru_2(DMBA)$_4$(H-*gem*-DEE)$_2$ (**1**) through both ^{1}H NMR and high-resolution nano-electrospray ionization mass spectrometry (HR-nESI-MS). We surmised that the appearance of very polar byproducts in the synthesis of **1** is likely due to the formation of oligomerized species attributed to the presence of the free ethynyl (−C≡CH) in **1**, which may displace a coordinated **L1** to yield a dimer bridged by μ-C,C′-*gem*-DEE, and subsequently trimer, etc. To eliminate the possibility of oligomerization, our attention turned to 1-(triisopropylsilyl)-3-(trimethylsilyl)ethynyl-4-methylpent-3-en-1-yne,[10] which retains the triisopropylsilyl (TIPS) group to yield 1-(triisopropylsilyl)-3-ethynyl-4-methylpent-3-en-1-yne (**L2**) upon treatment with methanolic K_2CO_3. The ensuing reaction between Ru_2(DMBA)$_4$(NO$_3$)$_2$ and **L2** under weak base conditions yielded a red compound as the sole product (isolated yield 77%) after 3 h, while no residual Ru_2(DMBA)$_4$(NO$_3$)$_2$ was detected. The red product was unambiguously identified as *trans*-Ru_2(DMBA)$_4$(^{i}Pr$_3$Si-*gem*-DEE)$_2$ (**2**) through ^{1}H NMR, HR-nESI-MS, and a single-crystal X-ray diffraction study.

A similar reaction between Ru_2(DMBA)$_4$(NO$_3$)$_2$ and H-*gem*-DEE-Fc (**L3**) progressed slower than those with **L1** and **L2**: while the formation of Ru_2(DMBA)$_4$(Fc-*gem*-DEE)$_2$ (**3**) was significant, residual Ru_2(DMBA)$_4$(NO$_3$)$_2$ remained present after 3 h. The desired compound **3** was isolated via recrystallization from tetrahydrofuran (THF)/hexanes in 48% yield and was positively identified through ^{1}H NMR, HR-nESI-MS, and a single-crystal X-ray diffraction study. On the other hand, the reaction between Ru_2(DMBA)$_4$(NO$_3$)$_2$ (1 equiv) and H-*gem*-DEE-NP (**L4**; 2.2 equiv) proceeded to completion in 3 h, and *trans*-Ru_2(DMBA)$_4$(NP-*gem*-DEE)$_2$ (**4**) was isolated in 68% yield after recrystallization from THF/hexanes.

The preparation of *trans*-Ru_2(DMBA)$_4$(DMAP-*gem*-DEE)$_2$ (**5**), a strong donor-substituted compound, proved to be challenging. When H-*gem*-DEE-DMAP (**L5**; 2.2 equiv) and Ru_2(DMBA)$_4$(NO$_3$)$_2$ (1 equiv) reacted in the presence of Et_2NH in THF, substantial quantities of starting materials remained after 5 h. The desired product **5** was isolated via recrystallization from THF/hexanes in 27% yield and was positively identified through ^{1}H NMR and HR-nESI-MS. Alternatively, the Me_3Si-protected DMAP ligand (Me_3Si-*gem*-DEE-DMAP) and 1 equiv of Ru_2(DMBA)$_4$(NO$_3$)$_2$ were reacted in the presence of excess K_2CO_3 in THF/MeOH (2:1, v/v), where K_2CO_3 was used for both desilylation and as a base for metalation. Compound **5** was obtained in a similar yield after reaction overnight. Finally, a high-yield preparation of **5** was achieved from the reaction between Ru_2(DMBA)$_4$Cl$_2$ and 2.2 equiv of Li-*gem*-DEE-DMAP (Li-**L5**), a method that was successful in affording Ru_2(DMBA)$_4$(C≡CC_6H_4-4-NMe_2)$_2$ in high yield.[28] The reaction between Li-**L5** and Ru_2(DMBA)$_4$Cl$_2$ was almost instantaneous based on the color change, and subsequent recrystallization of the reaction mixture from EtOAc/hexanes resulted in **5** in high yield (74%).

Molecular Structures of 2 and 3. Further confirmation of the identity of *trans*-Ru_2(DMBA)$_4$(X-*gem*-DEE)$_2$-type compounds came from the single-crystal X-ray diffraction study of **2** and **3**.

dx.doi.org/10.1021/ic202720c | *Inorg. Chem.* 2012, 51, 3261−3269

The molecular structures determined for **2** and **3** are shown in Figures 1 and 2, respectively, and the selected bond lengths and

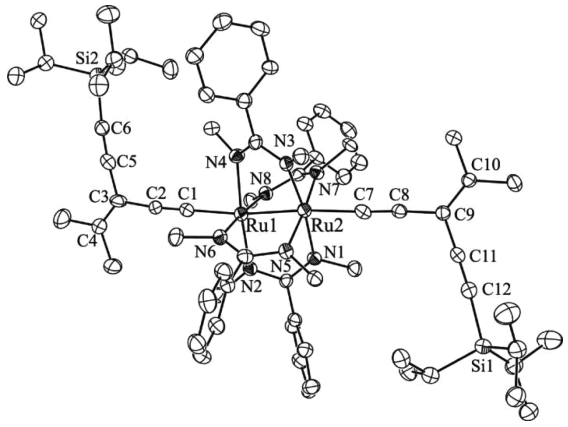

Figure 1. ORTEP plot of **2** at 20% probability. H atoms were omitted for clarity.

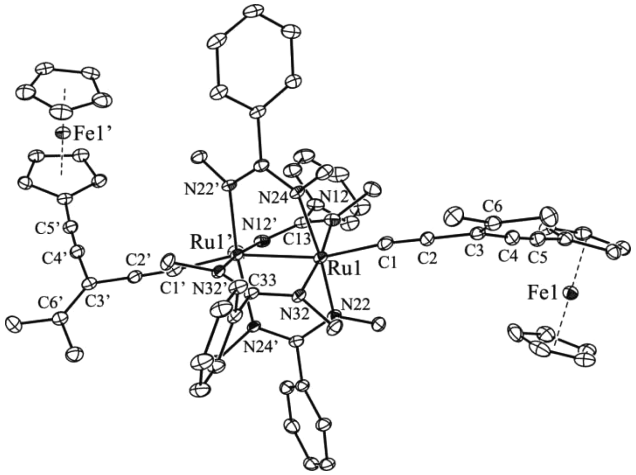

Figure 2. ORTEP plot of **3** at 20% probability. H atoms were omitted for clarity.

angles are listed in Table 1. While the asymmetric unit of crystal **2** contains a complete Ru_2 molecule, the asymmetric unit of **3** contains only half of the Ru_2 molecule, which is related to the other half through a crystallographic 2-fold axis defined by the C13 and C33 atoms. The geometric parameters around the first coordination sphere of the Ru_2 core are comparable to those of other $Ru_2(DMBA)_4(C{\equiv}CR)_2$-type compounds.[29] The Ru−Ru bond lengths are 2.4624(9) and 2.4569(4) Å for **2** and **3**, respectively, while those of $Ru_2(DMBA)_4(C{\equiv}CR)_2$ are in the range of 2.441−2.476 Å. The Ru−C bond distances in **2** and **3** are 1.981 and 1.974 Å, respectively, which are in agreement with those determined for other $Ru_2(DMBA)_4(C{\equiv}CR)_2$ compounds (1.95−2.00 Å). These data indicate that the *gem*-DEE ligand behaves similarly to simple acetylides in bonding to the Ru_2 core. Typical of diruthenium(III,III) compounds bearing strong axial donor ligands, the arrangement of the equatorial N-donor atoms deviates significantly from the eclipsed D_{4h} symmetry.[30] The eight N atoms fall into two distinct groups, those of elongated Ru−N bonds and those of shortened Ru′−N′ bonds, which also span a large torsional angle N−Ru−Ru′−N′ (avg. 19.2°). The electronic origin of such structural distortion has been attributed to both a second-order Jahn−Teller effect and the formation of a partial σ(Ru−Ru)

Table 1. Selected Bond Lengths (Å) and Angles (deg) for Compounds 2 and 3

2		**3**	
Ru1−Ru2	2.4624(9)	Ru1−Ru1′	2.4569(4)
Ru1−C1	1.982(9)	Ru1−C1	1.974(4)
Ru2−C7	1.979(9)		
Ru1−N2	2.105(6)	Ru1−N12	2.025(2)
Ru2−N1	2.004(7)	Ru1−N22	2.043(2)
Ru1−N4	1.973(6)	Ru1−N32	1.991(2)
Ru2−N3	2.074(6)	Ru1−N24	2.133(2)
Ru1−N6	2.001(6)		
Ru2−N5	2.127(6)		
Ru1−N8	2.101(6)		
Ru2−N7	1.977(6)		
C1−C2	1.198(11)	C1−C2	1.224(5)
C3−C4	1.321(14)	C3−C6	1.353(5)
C5−C6	1.209(12)	C4−C5	1.188(5)
C7−C8	1.215(11)		
C9−C10	1.343(10)		
C11−C12	1.190(11)		
Ru1−C1−C2	176.1(8)	Ru1−C1−C2	174.0(3)
Ru2−C7−C8	176.6(8)		
C2−C3−C5	110.5(8)	C2−C3−C4	124.0(3)
C8−C9−C11	113.2(7)		
C1−Ru1−N6	96.8(3)	C1−Ru1−N32′	100.3(12)
C1−Ru1−N8	89.0(3)	C1−Ru1−N12′	86.40(11)
C1−Ru1−Ru2	165.3(3)	C1−Ru1−Ru1′	164.64(9)
N2−Ru1−Ru2−N1	19.55(0.26)	N24′−Ru1′−Ru1−N22	20.80[a]
N4−Ru1−Ru2−N3	18.15(0.27)	N22′−Ru1′−Ru1−N24	17.68[a]
N6−Ru1−Ru2−N5	19.47(0.26)		
N8−Ru1−Ru2−N7	19.67(0.26)		

[a]Determined in *PLUTON*.

bond based on dπ-type orbitals[30,31] and will be elaborated in the density functional theory (DFT) calculation section.

While both TIPS-*gem*-DEE ligands are approximately coplanar with the framework defined by the N1−N2−N4−N3 linkage in **2**, only one of the Fc-*gem*-DEE ligands in **3** is coplanar and the second is perpendicular to the N22−N24′−N24−N22′ framework. In compound **2**, the two (triisopropylsilyl)ethynyl fragments are oriented in the opposite directions. In compound **3**, the two Fc's are approximately in an orthogonal orientation.

The bond lengths and angles of the TIPS-*gem*-DEE ligands in **2** are in close agreement with those determined for a free *gem*-DEE ligand (TMS-*gem*-DEE-TMS).[12] Both the ruthenium-bound acetylene bond (C1−C2) and the "free" alkyne bond (C5−C6) are of length similar to those in TMS-*gem*-DEE-TMS [1.191(6) and 1.215(6) Å, respectively]. There are two notable bond angles: (1) the alkylidene angle C2−C3−C5 at 110.5(8)°, which is less than the anticipated angle of 120° for an sp^2-hybridized C atom and (2) the Ru−C≡C angle of 176°, which is slightly distorted from linearity, demonstrating the inherent flexibility that the alkynyl bonds often show in the solid state.[16] Tykwinski and co-workers reported the X-ray structures of a series of donor/acceptor-substituted *gem*-DEEs,[32] and the geometric parameters of the diethynylethene framework were quite constant regardless of the nature of the substituents.

Electrochemistry. Typically, $Ru_2(DMBA)_4(C_2R)_2$-type compounds undergo at least two diruthenium-centered one-electron couples: an oxidation (**A**) and a reduction (**B**), as can be clearly seen in the voltammograms of $Ru_2(DMBA)_4(C_2TIPS)_2$ (**6**)

dx.doi.org/10.1021/ic202720c | *Inorg. Chem.* 2012, 51, 3261−3269

in Figure 3 and the electrode potentials in Table 2. For unsubstituted *gem*-DEE compounds **1** and **2**, both couples **A**

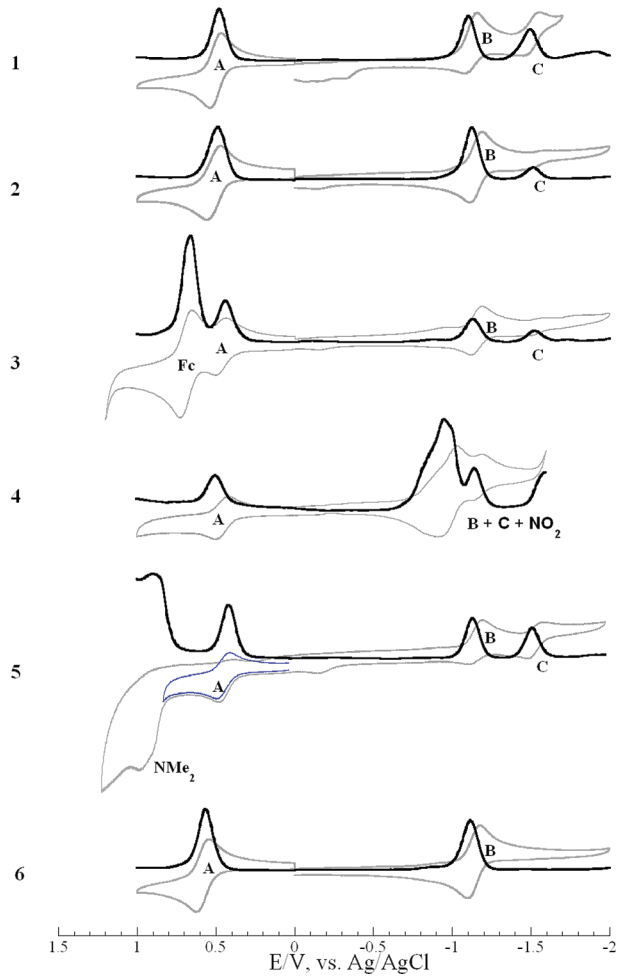

Figure 3. Cyclic (CV; gray) and differential-pulse voltammograms (DPV; black) recorded for compounds **1**–**6** in a 0.20 M THF solution of Bu_4NPF_6 at a scan rate of 0.10 V s^{-1} for CV and a pulse width of 0.05 s for DPV. The blue inset in **5** indicates the anodic CV sweep between 0 and 0.80 V.

Table 2. Electrochemical Potentials (V, vs Ag/AgCl) of Compounds 1–6

compound	*E*(**A**)	*E*(**B**)	*E*(**C**)
1	0.502	−1.154	−1.514[a]
2	0.496	−1.159	−1.496[a]
3	0.467	−1.156	−1.552[a]
4	0.485	NA	NA
5	0.448	−1.165	−1.541
6	0.585	−1.138	NA

[a]The irreversible couple, E_{pc}, is reported.

and **B** can be easily discerned from their voltammograms. The potentials of the oxidation couple (**A**) in **1** and **2** were cathodically shifted by ca. 90 mV from that of **6**, reflecting the stronger donor nature of *gem*-DEE. Unlike **6**, compounds **1** and **2** also exhibit an irreversible reduction (**C**) at ca. −1.5 V, which cannot be attributed to a second one-electron reduction of the diruthenium center in **1**/**2** because this reduction typically occurs at electrode potential < −2.0 V.[33] Instead, the partial dissociation of one of the *gem*-DEE ligands upon the first reduction resulted in a mono-*gem*-DEE-$Ru^{II,III}_2$ species, which, as a neutral species, was reduced at a mild potential (Scheme 1). Facile degradation of **1**/**2** under reducing conditions reflects a weakened Ru–C bond with the *gem*-DEE ligand compared with simple linear acetylides. The direct detection of the proposed mono-*gem*-DEE-$Ru^{II,III}_2$ species in a voltammetric experiment is challenging because it is only produced in a minute quantity at or near the electrode surface. Nevertheless, the fragile nature of the Ru–C(*gem*-DEE) bond is evident from MS experiments: the mono-*gem*-DEE-$Ru^{II,III}_2$ peak is very pronounced in the nESI spectrum of compound **2**, while the mono-TIPS-acetylide peak is negligible in the nESI spectrum of compound **6** under identical electrospray parameters (see Figure S6 in the Supporting Information).

Having two Fc-substituted *gem*-DEE ligands, compound **3** undergoes a reversible, two-electron oxidation that is ascribed to the simultaneous oxidation of both Fc units, in addition to the diruthenium-centered couples that were observed in **1** and **2**. The simultaneous oxidation of Fc in **3** is in stark contrast with the behavior of *trans*-$Ru_2(DMBA)_4(C_{2n}Fc)_2$-type compounds reported earlier by our laboratory, where pairwise oxidations of the two Fc termini were observed for compounds of n = 1–4 and were taken as evidence of long-distance electronic coupling between two Fc centers.[34,35] Clearly, the *cross-conjugated* nature of the *gem*-DEE linker severely limited the degree of electronic coupling. In comparison with compounds **1**/**2**, the couple **A** in **3** is cathodically shifted slightly, while **B** occurs at nearly identical potential. Hence, Fc's as moderate electron donors destabilized the highest occupied molecular orbital (HOMO) but had no impact on the lowest unoccupied molecular orbital (LUMO; δ^*; see the Results and Discussion section).

The behaviors of the acceptor (donor)-substituted *gem*-DEE compounds **4** (**5**) are somewhat complicated compared with those of **1**–**3**. Compound **4**, with nitrophenyl-substituted *gem*-DEE ligands, displays a reversible oxidation **A** at an electrode potential comparable to those of **1** and **2**, indicating minimal influence of an acceptor substituent on the HOMO. The cathodic region of **4** is quite complex with an early onset of multiple reduction processes (ca. −0.7 V), and significant deposition of greenish materials on the working electrode was observed upon completion of a single sweep. It is likely that the reduction of one of the nitro groups initiated some oligomerization reaction. For compound **5**, the oxidation couple (**A**) is cathodically shifted by 50 mV from that of **2**, which is consistent with DMAP-*gem*-DEE being the most electron-rich among all of the *gem*-DEE ligands. The electron richness of DMAP-*gem*-DEE also makes its C–Ru bond very prone to cleavage, as evidenced by the large current of couple **C**. In the case of *trans*-$Ru_2(DMBA)_4(C_2C_6H_4\text{-}4\text{-}NMe_2)_2$, oxidations of the two $-NMe_2$ groups were stepwise and quasi-reversible.[28] The oxidation wave of the two $-NMe_2$ groups in **5** was broad and irreversible and accompanied by degradation of **5**. The latter resulted in the disappearance of the cathodic wave of couple **A** on the backward sweep. However, when the potential sweep window was limited to +0.80 V, a perfectly reversible oxidation was recorded in CV (shown as a blue inset in Figure 3).

Vis–Near-IR (NIR) Spectroscopy. Shown in Figure 4 are the vis–NIR absorption spectra of compounds **2**, **4**, and **5**, while those of **1**, **3**, and **6** are provided as Figure S1 in the Supporting Information. The absorption spectrum of **2** features peaks at ca. 510 ($\varepsilon \sim 15\,000$ M^{-1} cm^{-1}) and 890 nm ($\varepsilon \sim 3000$ M^{-1} cm^{-1}). The low-energy transition is attributed to the dipole-allowed

dx.doi.org/10.1021/ic202720c | *Inorg. Chem.* 2012, 51, 3261–3269

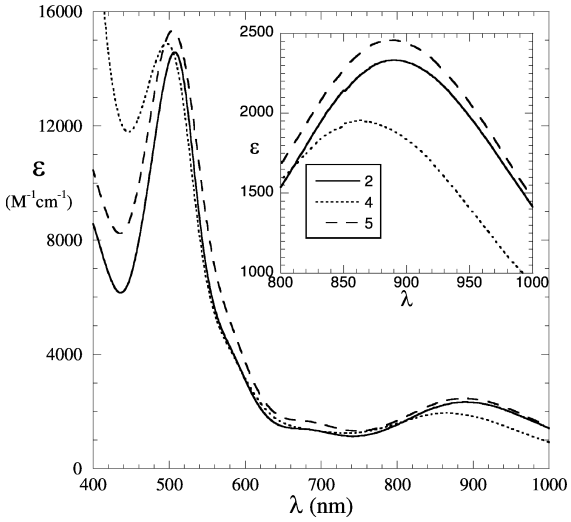

Figure 4. Vis−NIR spectra of **2** (solid), **4** (dotted), and **5** (dashed) in THF; the NIR region is magnified in the inset.

HOMO [π_{yz}*(Ru−Ru)]−LUMO [δ*(Ru−Ru)] transition, while the high-energy transition is likely due to the ligand-to-metal charge transfer from the amidinate π(N) orbital to δ*(Ru−Ru).[35] The absorption spectrum of compound **5** is very similar to that of **2** and consists of peaks at 505 nm ($\varepsilon \sim 15\,400$ M^{-1} cm^{-1}) and 890 nm (2460 M^{-1} cm^{-1}), indicating that the introduction of electron-donor aryl substituents such as DMAP do little to alter the electronic structure of **5** compared to **2**. The spectrum of **4** [497 nm (14 900 M^{-1} cm^{-1}) and 865 nm (1960 M^{-1} cm^{-1})] has both peaks blue-shifted from those of **2** and **5**.

Electronic Structures via DFT Analysis. In order to gain further insight into the electronic interactions between the donor/acceptor-substituted *gem*-DEE ligands and the Ru_2 core, DFT calculations at the B3LYP/LanL2DZ level (*Gaussian03* program)[36] were performed. In the previously reported DFT study of *trans*-$Ru_2(DMBA)_4$(*gem*-$DEE)_2$, DMBA ligands were reduced to $(HNC(H)NH)^{-1}$. In the current study, the model compound **2′** was fully optimized from the crystal structure of **2** without truncation, while the model compounds of **7**, **4′**, and **5′** were built based on the modification of **2**. Both Si^iPr_3 groups of **2** were replaced with either $-C_6H_5$ (**7**), 4-$C_6H_4NO_2$ (**4′**), or 4-$C_6H_4NMe_2$ (**5′**), which were followed by full optimizations. The optimized bond lengths and angles for **2′** are in good agreement with the crystal structural data of **2**, while comparable bond lengths and angles for the first coordination sphere of the Ru_2 core were obtained for **7**, **4′**, and **5′** (see Tables S1−S4 in the Supporting Information). The computed energies and counterplots of the most relevant molecular orbitals (MOs) for the model compounds **2′**, **7**, **4′**, and **5′** are given in Figure 5.

Compared with our prior DFT study of the simplified model compound of *trans*-$Ru_2(DMBA)_4$(*gem*-$DEE)_2$,[25] spin-restricted DFT calculations for model **2′** yielded a comparable distribution of valence MOs. The optimized Ru−Ru bond length (2.525 Å) in **2′** is longer than the experimental value of 2.462 Å in **2** but significantly shorter than that of the oversimplified model (2.611 Å) reported in the previous communication. The lengthening of the optimized Ru−Ru bond in comparison with the experimental data can be attributed to the underestimation of weak metal−metal interactions by the DFT (B3LYP) method. Similar to **2′**, the geometries optimized for **7**, **4′**, and **5′** exhibit features unique to diruthenium(III,III) bis(alkynyl) species: the nonlinearity of the −C≡C−Ru−Ru−C≡C− linkage and a distorted $Ru_2(N-N)_4$ coordination sphere (D_4 to C_2 symmetry).[30,31] The optimized Ru−Ru bond lengths for **7** (2.525 Å), **4′** (2.525 Å), and **5′** (2.521 Å) are approximately the same as that of **2′** (2.525 Å).

As shown in Figure 5, the four HOMOs of **2′**, namely, HOMO−3 to HOMO, are the combinations of $\pi(Ru_2)$ and π(*gem*-DEE). The HOMO−3 is the antibonding combination of π_{xz}(Ru−Ru) and two $\pi_{\|}$(DEE) (in-plane π orbitals of *gem*-DEE).[37] The HOMO−2 is an antibonding combination of π_{xz}*(Ru−Ru) and two $\pi_{\|}$(DEE). The π_{xz}*(Ru−Ru) component in HOMO−2 exhibits significant σ-type overlap because of the severe twisting of the equatorial DMBA ligands around the Ru_2 core, as noted in the prior study.[31] HOMO−1 and HOMO are the antibonding combinations of two $\pi_{\perp}$(DEE) (out-of-plane π orbitals of *gem*-DEE) with π_{yz}(Ru−Ru) and π_{yz}*(Ru−Ru), respectively. The LUMO is dominated by δ*(Ru−Ru) with no contribution from *gem*-DEE because of the orbital orthogonality. The LUMO+1 is mostly the contribution of two σ*(Ru−C) bonds, where the two Ru d_{z^2} orbitals have the appearance of σ-type bonding. In addition, the HOMO−4 is identified as the δ(Ru−Ru) orbital in **2′**. Furthermore, the nominal σ(Ru−Ru) is nonexistent because the d_{z^2}(Ru) orbitals are primarily used for the formation of σ(Ru−C) bonds. Hence, the ground-state configuration of the Ru_2 core is $\delta^2\pi^4\pi^{*4}$, corresponding to an effective Ru−Ru single bond.

The distribution of the valence MOs in **7** follows the same pattern as that of **2′**, albeit with a slightly enhanced HOMO−LUMO gap (1.99 in **7** vs 1.92 eV in **2′**). Compared with **2′**, both HOMO and HOMO−1 in **7** are stabilized as a result of π delocalization onto the phenyl ring, which reduces the antibonding interaction between π(DEE) and π/π*(Ru−Ru). With the introduction of a strong electron-withdrawing phenyl substituent ($-NO_2$ in **4′**), HOMO and LUMO in **4′** are further stabilized, with the HOMO−LUMO gap increasing from 1.99 eV in **7** to 2.15 eV. Both the composition and energetic order of the metal-based MOs in **4′** (with minimum contribution from nitrophenyl ligands) are almost the same as those for **7**, indicating that the electronic effect of nitro substitution is mostly inductive. In compound **5′**, the presence of a strong donating substituent ($-NMe_2$) significantly destabilized all valence MOs in comparison with those of **7** and **4′**. The electronic effect of $-NMe_2$ substitution goes beyond simply inductive: it has resulted in the substantial participation of the aryl π component in the high-lying occupied MOs. Specifically, the σ-type (in-plane) and π-type (out-of-plane) bondings of the $-C\equiv C-Ru_2-C\equiv C-$ component are apt to extensively interact with the dimethylamino-substituted phenyl rings in HOMO−2 and HOMO−1. The computed HOMO−LUMO gaps for all model compounds are in the range from 1.90 to 2.15 eV, which are comparable to that of *trans*-$Ru_2(DMBA)_4(C_2Fc)_2$.[35] Current results strongly support that the hole-transfer mechanism will likely dominate the charge delocalization in Ru_2-*gem*-DEE-based wires.

■ CONCLUSION

A new family of $Ru_2(DMBA)_4$ compounds based on substituted *gem*-DEE axial ligands were prepared under mild conditions in relatively good yields. The work described herein demonstrated the feasibility of preparing *gem*-DEE compounds of transition-metal ions beyond platinum(II). The electronic properties of

dx.doi.org/10.1021/ic202720c | *Inorg. Chem.* 2012, 51, 3261−3269

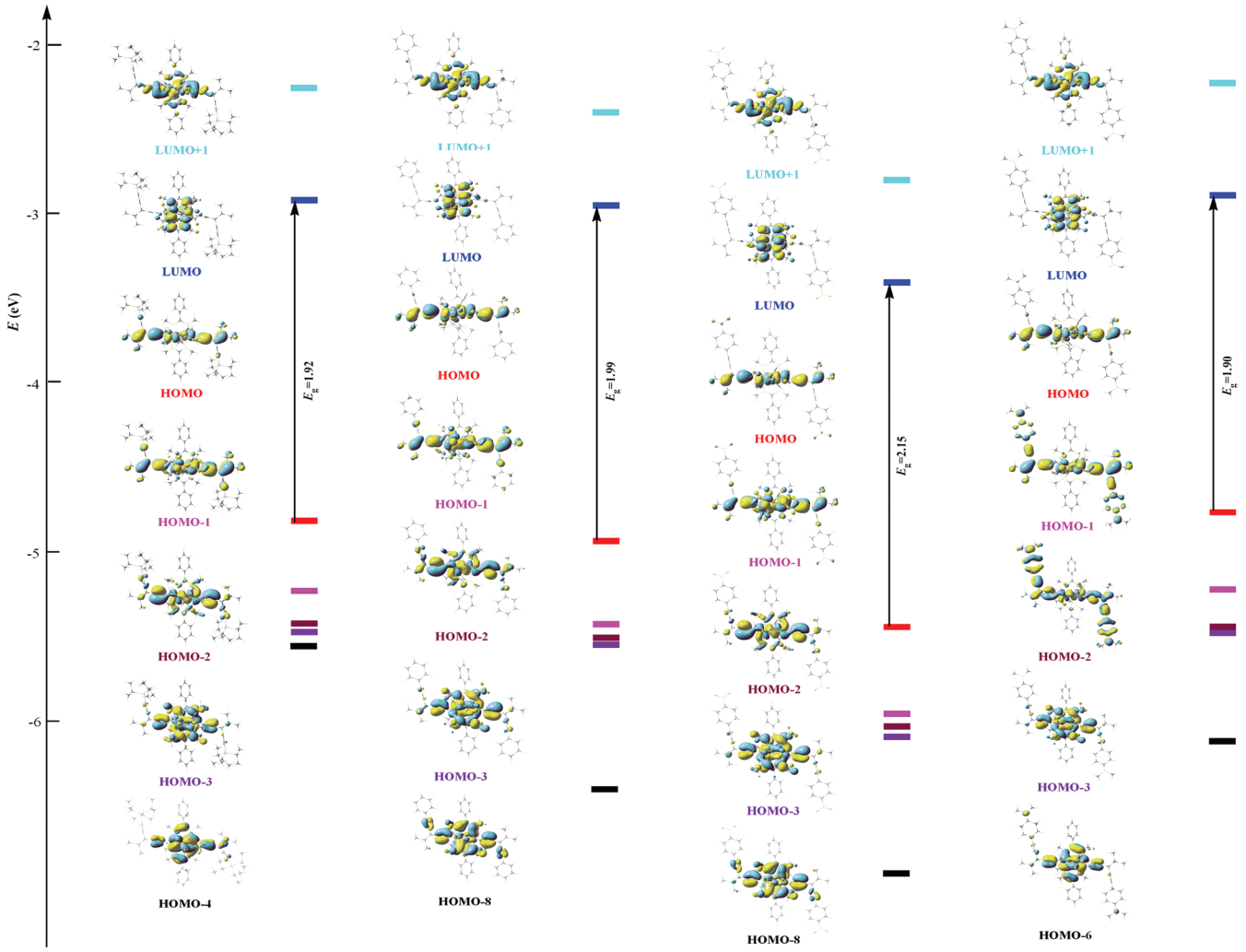

Figure 5. MO diagrams for (from left to right) **2′**, **7**, **4′**, and **5′** obtained from DFT calculations.

these new $Ru_2(DMBA)_4$ compounds having *cross-conjugated* σ-alkynyl ligands resemble those of the previously studied $Ru_2(DMBA)_4(C_2R)_2$ compounds. DFT analysis provided a better understanding of both the molecular and electronic properties for the $Ru_2(DMBA)_4$(*gem*-DEE)$_2$-type compounds. While most of the terminal substituents of *gem*-DEE manifest a minimal π interaction with the Ru_2 center, the strong donor $-NMe_2$ enables an extensive interaction between π(*gem*-DEE) and $\pi(Ru_2)$ orbitals.

EXPERIMENTAL SECTION

General Procedures. X-*gem*-DEE ligands (**L1**−**L5**) were prepared according to previously reported literature procedures.[10,38] $Ru_2(DMBA)_4(NO_3)_2$ and $Ru_2(DMBA)_4Cl_2$ were prepared as previously described.[26,33] ^{1}H NMR spectra were obtained using a Varian Mercury 300 NMR spectrometer, with chemical shifts (δ) referenced to the residual $CHCl_3$. Vis−NIR spectra were obtained with a Jasco V-670 spectrophotometer in THF solutions. Fourier transform infrared (FT-IR) spectra were measured on neat samples with a Jasco FT/IR-6300 spectrometer. nESI-MS spectra were performed on a QqQ tandem mass spectrometer in CH_2Cl_2 (QTRAP4000; Applied Biosystems/MDS Sciex, Concord, Ontario, Canada). For compounds **1**−**5**, the HR-nESI-MS spectra were performed on a modified QqTOF tandem mass spectrometer in CH_2Cl_2 (QSTAR XL; Applied Biosystems/MDS Sciex, Concord, Ontario, Canada). Masses were calculated by isotopic distribution utilizing Analyst 1.4 software (Applied Biosystems/MDS Sciex, Concord, Ontario, Canada). CV and DPV were recorded in a 0.2 M $(n\text{-Bu})_4NPF_6$ solution (THF, N_2-degassed) on a CHI620A voltammetric analyzer with a glassy carbon working electrode (diameter = 2 mm), a platinum wire auxiliary electrode, and a Ag/AgCl reference electrode. The concentration of Ru_2 species is always 1.0 mM. The ferrocenium/ferrocene couple was observed at 0.570 V (vs Ag/AgCl) at the noted experimental conditions.

Preparation of *trans*-Ru_2(DMBA)$_4$(H-*gem*-DEE)$_2$ (1). $Ru_2(DMBA)_4(NO_3)_2$ (0.092 g, 0.101 mmol) was dissolved in THF (20 mL), to which were added **L1** (0.023 g, 0.220 mmol) and Et_3N (1 mL). Upon the addition of Et_3N, the reaction mixture turned from green to wine red in ca. 3 min and was stirred for an additional 3 h. TLC analysis (1:3 EtOAc/hexanes) revealed a red product (**1**) and a reddish-brown species just above the baseline. After removal of the solvent, the resulting red residue was purified via column chromatography (1:6 → 1:1 EtOAc/hexanes) followed by recrystallization from THF/MeOH (1:3, v/v) to yield **1** as a red crystalline solid. Yield: 0.020 g (0.020 mmol, 20% based on Ru). Data for **1**. R_f = 0.72 (1:3 EtOAc/hexanes). ^{1}H NMR ($CDCl_3$, δ): 7.41−7.38 (12H, Ph*H*), 6.98−6.95 (8H, Ph*H*), 3.23 (24H, N*Me*), 2.86 (2H, C_2H), 2.10 (12H, *Me* (*gem*-DEE)). nESI-MS (*m*/*e*, based on ^{101}Ru): 998, corresponding to $[M + H]^+$. HR-nESI-MS (*m*/*e*, based on ^{101}Ru): 997.826, corresponding to $[M + H]^+$ ($C_{52}H_{58}N_8Ru_2$, calcd 997.834). Vis−NIR [λ_{max}, nm (ε, M^{-1} cm^{-1})]: 890 (2210), 506 (14 600). FT-IR (neat, ν, cm^{-1}): 2076 (−C≡C−H), 2057 (Ru−C≡C−). CV [$E_{1/2}$/V, ΔE_p/V, $i_{backward}/i_{forward}$]: **B**, 0.502, 0.034, 0.903; **C**, −1.154, 0.036, 0.935; E_{pc} (**D**), −1.514.

dx.doi.org/10.1021/ic202720c | *Inorg. Chem.* 2012, 51, 3261−3269

Preparation of *trans*-$Ru_2(DMBA)_4(^iPr_3Si$-*gem*-DEE)$_2$ (2). $Ru_2(DMBA)_4(NO_3)_2$ (0.151 g, 0.165 mmol) was dissolved in THF (30 mL), to which were added **L2** (0.094 g, 0.363 mmol) and Et_2NH (1 mL). Upon the addition of Et_2NH, the reaction mixture turned from green to wine red in ca. 3 min and was stirred for an additional 3 h. TLC analysis (1:3 EtOAc/hexanes) revealed compound **2** as the sole product formed. The reaction mixture was then filtered through a 2 cm silica gel plug to remove any residual $Ru_2(DMBA)_4(NO_3)_2$. After removal of the solvent, the resulting red residue was purified via recrystallization from THF/MeOH (1:4, v/v) to yield a red crystalline solid. Yield: 0.166 g (0.127 mmol, 77% based on Ru). Data for **2**. R_f = 0.83 (1:3 EtOAc/hexanes). ^{1}H NMR ($CDCl_3$, δ): 7.39−7.36 (12H, Ph*H*), 6.96−6.94 (8H, Ph*H*), 3.22 (24H, N*Me*), 2.12 (12H, *Me* (*gem*-DEE), 0.95 (21H, $^iPr_3$Si). nESI-MS (*m*/*e*, based on ^{101}Ru): 1310, corresponding to $[M + H]^+$. HR-nESI-MS (*m*/*e*, based on ^{101}Ru): 1309.620, corresponding to $[M + H]^+$ ($C_{70}H_{98}N_8Si_2Ru_2$, calcd 1309.613). Vis−NIR [λ_{max}, nm (ε, M^{-1} cm^{-1})]: 890 (2330), 507 (14 600). FT-IR (neat, ν, cm^{-1}): 2140 (−C≡C−Si^{i}Pr$_3$), 2065 (Ru−C≡C−). CV [$E_{1/2}$/V, ΔE_p/V, $i_{backward}/i_{forward}$]: **B**, 0.496, 0.034, 0.905; **C**, −1.159, 0.037, 0.931; E_{pc}(**D**), −1.496.

Preparation of *trans*-$Ru_2(DMBA)_4$(Fc-*gem*-DEE)$_2$ (3). $Ru_2(DMBA)_4(NO_3)_2$ (0.230 g, 0.251 mmol) was dissolved THF (40 mL), to which were added 2.2 equiv of **L3** (0.160 g, 0.552 mmol) of **L3** and 5 mL of Et_2NH. Upon the addition of Et_2NH, the reaction mixture began to turn from green to red in ca. 15 min. The reaction was stirred for an additional 3 h. TLC analysis (1:3 EtOAc/hexanes) revealed the formation of **3** along with unreacted ligand (**L3**) and $Ru_2(DMBA)_4(NO_3)_2$. Removal of the solvent yielded a red residue, which was redissolved in EtOAc/hexanes (1:6, v/v) and filtered through a 3 cm silica gel plug to remove the residual **L3** ligand and $Ru_2(DMBA)_4(NO_3)_2$. After removal of the solvent, the resulting red residue was further purified via recrystallization from THF/hexanes (1:9, v/v) to yield a red crystalline solid. Yield: 0.164 g (0.120 mmol, 48% based on Ru). Data for **3**. R_f = 0.66 (1:3 EtOAc/hexanes). ^{1}H NMR ($CDCl_3$, δ): 7.37−7.35 (12H, Ph*H*), 6.99−6.96 (8H, Ph*H*), 4.25 (4H, Cp*H*), 4.04 (14H, Cp*H*), 3.29 (24H, N*Me*), 2.12 (12H, *Me* (*gem*-DEE). nESI-MS (*m*/*e*, based on ^{101}Ru): 1366, corresponding to $[M + H]^+$. HR-nESI-MS (*m*/*e*, based on ^{101}Ru): 1366.285, corresponding to $[M + H]^+$ ($C_{72}H_{74}N_8Fe_2Ru_2$, calcd 1366.275). Vis−NIR [λ_{max}, nm (ε, M^{-1} cm^{-1})]: 890 (2290), 504 (15 400). FT-IR (neat, ν, cm^{-1}): 2140 (−C≡C−Fc)), 2070 (Ru−C≡C−). CV [$E_{1/2}$/V, ΔE_p/V, $i_{backward}/i_{forward}$]: **Fc**, 0.690, 0.035, 0.100; **A**, 0.467, 0.033, 0.500; **B**, −1.156, 0.033, 0.870; E_{pc}(**C**), −1.552.

Preparation of *trans*-$Ru_2(DMBA)_4$(NP-*gem*-DEE)$_2$ (4). $Ru_2(DMBA)_4(NO_3)_2$ (0.101 g, 0.110 mmol) was dissolved in THF (35 mL), to which were added **L4** (0.054 g, 0.242 mmol) and 2 mL of Et_2NH. Upon the addition of Et_2NH, the reaction mixture turned from green to red in ca. 6 min and the reaction was stirred for an additional 3 h. TLC analysis (1:3 EtOAc/hexanes) revealed compound **4** as the sole product formed. The reaction mixture was then filtered through a 2 cm silica gel plug to remove any residual $Ru_2(DMBA)_4(NO_3)_2$. After removal of the solvent, the resulting red residue was purified via recrystallization from 1:9 THF/hexanes to yield a red crystalline solid. Yield: 0.094 g (0.076 mmol, 68% based on Ru). Data for **4**. R_f = 0.58 (1:3 EtOAc/hexanes). ^{1}H NMR ($CDCl_3$, δ): 8.18−8.15 (4H, O_2NPh*H*), 7.58−7.55 (4H, Ph*H*), 7.42−7.39 (12H, Ph*H*), 6.98−6.96 (8H, Ph*H*), 3.26 (24H, N*Me*), 2.17 (12H, *Me* (*gem*-DEE). nESI-MS (*m*/*e*, based on ^{101}Ru): 1240, corresponding to $[M + H]^+$. HR-nESI-MS (*m*/*e*, based on ^{101}Ru): 1240.436, corresponding to $[M + H]^+$ ($C_{64}H_{64}N_{10}O_4Ru_2$, calcd 1240.425). Vis−NIR [λ_{max}, nm (ε, M^{-1} cm^{-1})]: 865 (1960), 497 (14 900). FT-IR (neat, ν, cm^{-1}): 2195 (−C≡C−NP), 2065 (Ru−C≡C−). CV [$E_{1/2}$/V, ΔE_p/V, $i_{backward}/i_{forward}$]: **A**, 0.485, 0.041, 0.870.

Preparation of *trans*-$Ru_2(DMBA)_4$(DMAP-*gem*-DEE)$_2$ (5). *Method A.* $Ru_2(DMBA)_4(NO_3)_2$ (0.106 g, 0.116 mmol) was dissolved in THF [or 2:1 (v/v) THF/MeOH], to which were added **L5** (or TMS-**L5**) (2.2 equiv, 0.255 mmol) and 5 mL of Et_2NH (or excess K_2CO_3). Upon the addition of a base, the reaction mixture began to turn from green to red in ca. 30 min. The reaction was stirred for an additional 3 h. Ensuing TLC analysis (1:1:3 CH_2Cl_2/Et_3N/hexanes) revealed the formation of **5** along with a brown-red product (R_f = 0.45) and unreacted starting materials. The reaction mixture was then filtered through a plug of Celite to remove the residual $Ru_2(DMBA)_4(NO_3)_2$. After removal of the solvent, the resulting red residue was purified via recrystallization from THF/hexanes (1:15, v/v) to yield a red crystalline solid. Yield: 0.038 g (0.031 mmol, 27% based on Ru).

Method B. **L5** (0.116 g, 0.520 mmol) was lithiated with *n*-BuLi (1.1 equiv of **L5**) in a THF solution to form Li-**L5** *in situ*. Li-**L5** was then transferred via a cannula to a THF solution of $Ru_2(DMBA)_4Cl_2$ (0.207 g, 0.240 mmol). Following transfer, the reaction mixture changed immediately from brown to deep red-purple. The reaction was stirred overnight to ensure complete reaction. Ensuing TLC analysis (1:1:3 CH_2Cl_2/Et_3N/hexanes) revealed compound **5** as the sole product. The solvent was then removed, and the resulting red-purple residue was redissolved in CH_2Cl_2/hexanes (1:3, v/v) and filtered quickly through a plug of Celite. After removal of the solvent, the resulting red residue was recrystallized from EtOAc/hexanes (1:5, v/v) to yield a red-purple crystalline solid. Yield: 0.220 g (0.180 mmol, 74% based on Ru).

Data for **5**. R_f = 0.64 (1:1:3 CH_2Cl_2/Et_3N/hexanes). ^{1}H NMR ($CDCl_3$, δ): 7.39−7.37 (16H, Ph*H*), 6.98−6.95 (8H, Ph*H*), 6.53−6.51 (4H, Ph*H*), 3.26 (24H, N*Me*), 2.90 (12H, PhN*Me*), 2.24 (12H, *Me* (*gem*-DEE). nESI-MS (*m*/*e*, based on ^{101}Ru): 1236, corresponding to $[M + H]^+$. HR-nESI-MS (*m*/*e*, based on ^{101}Ru): 1236.557, corresponding to $[M + H]^+$ ($C_{68}H_{76}N_{10}Ru_2$, calcd 1236.566). Vis−NIR [λ_{max}, nm (ε, M^{-1} cm^{-1})]: 890 (2460), 505 (15 400). FT-IR (neat, ν, cm^{-1}): 2193 (−C≡C−DMAP), 2071 (Ru−C≡C−). CV [$E_{1/2}$/V, ΔE_p/V, $i_{backward}/i_{forward}$]: **A**, 0.434, 0.041, 0.780; **B**, −1.165, 0.038, 0.360; **C**, −1.541, 0.049, 1.000; E_{pa}(-**NMe$_2$**), 0.944.

Preparation of *trans*-$Ru_2(DMBA)_4(C{\equiv}CSi^iPr_3)_2$ (6). $Ru_2(DMBA)_4(NO_3)_2$ (0.180 g, 0.197 mmol) was dissolved in THF (30 mL), to which was added HC≡CSi^{i}Pr$_3$ (0.097 mL, 0.432 mmol) and Et_3N (2 mL). Upon the addition of Et_3N, the reaction mixture turned from green to wine red in ca. 2 min and was stirred for an additional 3 h to yield **6** as the sole product. The reaction mixture was then filtered through a 2 cm silica gel plug to remove any residual $Ru_2(DMBA)_4(NO_3)_2$. After removal of the solvent, the resulting red residue was purified via recrystallization from THF/MeOH (1:3, v/v) to yield a red crystalline solid. Yield: 0.191 g (0.166 mmol, 84% based on Ru). Data for **6**. R_f = 0.85 (1:3 EtOAc/hexanes). ^{1}H NMR ($CDCl_3$, δ): 7.45−7.43 (12H, Ph*H*), 7.00−6.97 (8H, Ph*H*), 3.28 (24H, N*Me*), 0.97 (21H, $^iPr_3$Si). nESI-MS (*m*/*e*, based on ^{101}Ru): 1155, corresponding to $[M + H]^+$. FT-IR (neat, ν, cm^{-1}): 1996 (Ru−C≡C−Si^{i}Pr$_3$). CV [$E_{1/2}$/V, ΔE_p/V, $i_{backward}/i_{forward}$]: **A**, 0.585, 0.041, 0.858; **B**, −1.138, 0.038, 1.000.

X-ray Data Collection, Processing, and Structure Analysis and Refinement for Crystals **2** *and* **3**. Single crystals of compounds **2** and **3** were grown via the slow cooling of a THF/MeOH solution (1:3, v/v) and the slow evaporation of a THF/benzene/hexanes solution (1:1:9, v/v/v), respectively. X-ray diffraction data were collected on a Rigaku RAPID-II image plate diffractometer using Cu Kα radiation (λ = 1.541 84 Å) at 150 K, and the structures were solved using the structure solution program *DIRDIF2008*[39] and refined using *SHELX-TL*.[40] Relevant information on the data collection and figures of merit of the final refinement is listed in Table 3.

Computational Methods. Ground-state geometries of model compounds **2′**, **7**, **4′**, and **5′** were fully optimized using the DFT method B3LYP (Becke's three-parameter hybrid functional using the Lee−Yang−Parr correlation functional).[41] The geometry of model compound **2′** was fully optimized from the crystal structure of **2**, while those of **7**, **4′**, and **5′** were assembled based on the truncated crystal structure of **2**. Both Si^{i}Pr$_3$ ligands in **2** were replaced by $-C_6H_5$ (**7**), 4-$C_6H_4NO_2$ (**4′**), or 4-$C_6H_4NMe_2$ (**5′**), followed by full optimization. In the calculations, quasi-relativistic pseudopotentials of the 16 ruthenium valence electrons were employed and the LanL2DZ basis sets associated with the pseudopotential were adopted. All of the calculations were performed using the *Gaussian03* program package.[36] No negative frequency was observed in the vibrational frequency analysis, which

dx.doi.org/10.1021/ic202720c | *Inorg. Chem.* 2012, 51, 3261−3269

Table 3. Crystal Data for Compounds 2 and 3

	2·THF	3
molecular formula	$C_{74}H_{106}N_8ORu_2Si_2$	$C_{72}H_{74}Fe_2N_8Ru_2Si_2$
fw	1382.03	1365.28
space group	$P\bar{1}$	$C2/c$(No. 15)
a, Å	10.626(2)	25.4583(9)
b, Å	16.654(3)	20.7805(7)
c, Å	21.360(3)	13.8410(4)
α, deg	80.51(8)	
β, deg	79.91(10)	120.020(2)
γ, deg	87.79(12)	
V, Å^3	3671(1)	6340.1(4)
Z	2	4
ρ_{calcd}, g cm^{-3}	1.250	1.430
μ, mm^{-1}	4.071	7.754
T, K	150	150
no. of rflns collected	58683	34760
no. of indep rflns	9274 [R(int) = 0.097]	5977 [R(int) = 0.048]
final R indices [$I > 2\sigma(I)$]	R1 = 0.078, wR2 = 0.218	R1 = 0.037, wR2 = 0.096

indicates that these *gem*-DEE-substituted diruthenium complexes are metastable equilibrium structures.

■ ASSOCIATED CONTENT

Supporting Information

Vis−NIR spectra for **1**, **3**, and **6**, equilibrium structures and optimized bond lengths and angles from DFT calculations for model compounds **2′**, **4′**, **5′**, and **7**, nESI-MS spectra for **2** and **6**, and X-ray crystallographic files in CIF format for the structure determination of compounds **2** and **3**. This material is available free of charge via the Internet at http://pubs.acs.org.

■ AUTHOR INFORMATION

Corresponding Author

*E-mail: tren@purdue.edu.

Notes

The authors declare no competing financial interest.

■ ACKNOWLEDGMENTS

We gratefully acknowledge financial support from the National Science Foundation (Grant CHE 1057621) and Purdue University.

■ REFERENCES

(1) Bosshard, C.; Sutter, K.; Pretre, P.; Hulliger, J.; Florsheimer, M.; Kaatz, P.; Gunter, P. *Organic Nonlinear Optical Materials*; Gordon and Breach: Amsterdam, The Netherlands, 1995. Gubler, U.; Bosshard, C. *Adv. Polym. Sci.* **2002**, *158*, 123. Klokkenburg, M.; Lutz, M.; Spek, A. L.; van der Maas, J. H.; van Walree, C. A. *Chem.—Eur. J.* **2003**, *9*, 3544. Prasad, P. N.; Williams, D. J. *Introduction to Nonlinear Optical Effects in Molecules and Polymers*; Wiley: New York, 1991. van Walree, C. A.; Kaats-Richters, V. E. M.; Veen, S. J.; Wieczorek, B.; van der Wiel, J. H.; van der Wiel, B. C. *Eur. J. Org. Chem.* **2004**, *2004*, 3046. Zhao, Y.; Slepkov, A. D.; Akoto, C. O.; McDonald, R.; Hegmann, F. A.; Tykwinski, R. R. *Chem.—Eur. J.* **2005**, *11*, 321. Skotheim, T. A., Elsenbaumer, R. L., Reynolds, J. R., Eds. *Handbook of Conducting Polymers*; Marcel Dekker: New York, 1998. Mullen, K., Wegner, G., Eds. *Electronic Materials: The Oligomer Approach*; VCH: Weinheim, Germany, 1997. Martin, R. E.; Diederich, F. *Angew. Chem., Int. Ed.* **1999**, *38*, 1350. Zhou, G.-J.; Wong, W.-Y. *Chem. Soc. Rev.* **2011**, *40*, 2541.

(2) Miller, R. D.; Michl, J. *Chem. Rev.* **1989**, *89*, 1359.

(3) Bakkers, E. P. A. M.; Marsman, A. W.; Jenneskens, L. W.; Vanmaekelbergh, D. L. *Angew. Chem., Int. Ed.* **2000**, *39*, 2297. Hoogesteger, F. J.; van Walree, C. A.; Jenneskens, L. W.; Roest, M. R.; Verhoeven, J. W.; Schuddeboom, W.; Piet, J. J.; Warman, J. M. *Chem.—Eur. J.* **2000**, *6*, 2948.

(4) van Walree, C. A.; Kooijman, H.; Spek, A. L.; Zwikker, J. W.; Jenneskens, L. W. *J. Chem. Soc., Chem. Commun.* **1995**, 35. van Walree, C. A.; Roest, M. R.; Schuddeboom, W.; Jenneskens, L. W.; Verhoeven, J. W.; Warman, J. M.; Kooijman, H.; Spek, A. L. *J. Am. Chem. Soc.* **1996**, *118*, 8395.

(5) Phelan, N. F.; Orchin, M. *J. Chem. Educ.* **1968**, *45*, 633.

(6) Nielsen, M. B.; Diederich, F. *Chem. Rev.* **2005**, *105*, 1837.

(7) Tykwinski, R. R.; Zhao, Y. M. *Synlett* **2002**, 1939. Gholami, M.; Tykwinski, R. R. *Chem. Rev.* **2006**, *106*, 4997.

(8) Hopf, H. *Classics in Hydrocarbon Chemistry*; Wiley-VCH: Weinheim, Germany, 2000.

(9) Zhao, Y.; Tykwinski, R. R. *J. Am. Chem. Soc.* **1999**, *121*, 458.

(10) Zhao, Y. M.; Campbell, K.; Tykwinski, R. R. *J. Org. Chem.* **2002**, *67*, 336.

(11) Burri, E.; Diederich, F.; Brandsted-Nielsen, M. *Helv. Chim. Acta* **2002**, *85*, 2169. Zhao, Y.; McDonald, R.; Tykwinski, R. R. *Chem. Commun.* **2000**, 77.

(12) Zhao, Y.; McDonald, R.; Tykwinski, R. R. *J. Org. Chem.* **2002**, *67*, 2805.

(13) Bruschi, M.; Giuffreda, M. G.; Luthi, H. P. *Chem.—Eur. J.* **2002**, *8*, 4216.

(14) Solomon, G. C.; Andrews, D. Q.; Goldsmith, R. H.; Hansen, T.; Wasielewski, M. R.; Van Duyne, R. P.; Ratner, M. A. *J. Am. Chem. Soc.* **2008**, *130*, 17301.

(15) Hagihara, N.; Sonogashira, K.; Takahashi, S. *Adv. Polym. Sci.* **1980**, *40*, 149. Nast, R. *Coord. Chem. Rev.* **1982**, *47*, 89. Paul, F.; Lapinte, C. *Coord. Chem. Rev.* **1998**, *178−180*, 431. Wong, W.-Y.; Ho, C.-L. *Coord. Chem. Rev.* **2006**, *250*, 2627.

(16) Szafert, S.; Gladysz, J. A. *Chem. Rev.* **2006**, *106*, 1.

(17) Lenarvor, N.; Toupet, L.; Lapinte, C. *J. Am. Chem. Soc.* **1995**, *117*, 7129. Hamon, P.; Justaud, F.; Cador, O.; Hapiot, P.; Rigaut, S.; Toupet, L.; Ouahab, L.; Stueger, H.; Hamon, J.-R.; Lapinte, C. *J. Am. Chem. Soc.* **2008**, *130*, 17372.

(18) Brady, M.; Weng, W.; Zou, Y.; Seyler, J. W.; Amoroso, A. J.; Arif, A. M.; Bohme, M.; Frenking, G.; Gladysz, J. A. *J. Am. Chem. Soc.* **1997**, *119*, 775.

(19) Bruce, M. I.; Low, P. J.; Costuas, K.; Halet, J.-F.; Best, S. P.; Heath, G. A. *J. Am. Chem. Soc.* **2000**, *122*, 1949. Fox, M. A.; Roberts, R. L.; Baines, T. E.; Guennic, B. L.; Halet, J.-F.; Hartl, F.; Yufit, D. S.; Albesa-Jové, D.; Howard, J. A. K.; Low, P. J. *J. Am. Chem. Soc.* **2008**, *130*, 3566. Olivier, C.; Costuas, K.; Choua, S.; Maurel, V.; Turek, P.; Saillard, J.-Y.; Touchard, D.; Rigaut, S. *J. Am. Chem. Soc.* **2010**, *132*, 5638. Liu, S. H.; Chen, Y.; Wan, K. L.; Wen, T. B.; Zhou, Z.; Lo, M. F.; Williams, I. D.; Jia, G. *Organometallics* **2002**, *21*, 4984. Li, F.; Cheng, J.; Chai, X.; Jin, S.; Wu, X.; Yu, G.-A.; Liu, S. H.; Chen, G. Z. *Organometallics* **2011**, *30*, 1830. Ren, T.; Zou, G.; Alvarez, J. C. *Chem. Commun.* **2000**, 1197. Xu, G.-L.; Zou, G.; Ni, Y.-H.; DeRosa, M. C.; Crutchley, R. J.; Ren, T. *J. Am. Chem. Soc.* **2003**, *125*, 10057. Xi, B.; Liu, I. P. C; Xu, G.-L.; Choudhuri, M. M. R.; DeRosa, M. C.; Crutchley, R. J.; Ren, T. *J. Am. Chem. Soc.* **2011**, *133*, 15094.

(20) Campbell, K.; Johnson, C. A.; McDonald, R.; Ferguson, M. J.; Haley, M. M.; Tykwinski, R. R. *Angew. Chem., Int. Ed.* **2004**, *43*, 5967. Campbell, K.; McDonald, R.; Ferguson, M. J.; Tykwinski, R. R. *J. Organomet. Chem.* **2003**, *683*, 379. Campbell, K.; McDonald, R.; Ferguson, M. J.; Tykwinski, R. R. *Organometallics* **2003**, *22*, 1353.

(21) Diederich, F.; Faust, R.; Gramlich, V.; Seiler, P. *Chem. Commun.* **1994**, 2045. Faust, R.; Diederich, F.; Gramlich, V.; Seiler, P. *Chem.—Eur. J.* **1995**, *1*, 111.

(22) Lu, W.; Zhu, N.; Che, C.-M. *J. Organomet. Chem.* **2003**, *670*, 11.

(23) Akita, M.; Tanaka, Y.; Naitoh, C.; Ozawa, T.; Hayashi, N.; Takeshita, M.; Inagaki, A.; Chung, M.-C. *Organometallics* **2006**, *25*, 5261.

(24) Bruce, M. I.; Zaitseva, N. N.; Low, P. J.; Skelton, B. W.; White, A. H. *J. Organomet. Chem.* **2006**, *691*, 4273.

(25) Forrest, W. P.; Cao, Z.; Fanwick, P. E.; Hassell, K. M.; Ren, T. *Organometallics* **2011**, *30*, 2075.
(26) Xu, G.-L.; Jablonski, C. G.; Ren, T. *Inorg. Chim. Acta* **2003**, *343*, 387.
(27) Xu, G.-L.; Jablonski, C. G.; Ren, T. *J. Organomet. Chem.* **2003**, *683*, 388. Ying, J.-W.; Cordova, A.; Ren, T. Y.; Xu, G.-L.; Ren, T. *Chem.—Eur. J.* **2007**, *13*, 6874.
(28) Hurst, S. K.; Xu, G.-L.; Ren, T. *Organometallics* **2003**, *22*, 4118.
(29) Ren, T. *Organometallics* **2005**, *24*, 4854.
(30) Lin, C.; Ren, T.; Valente, E. J.; Zubkowski, J. D. *J. Chem. Soc., Dalton Trans.* **1998**, 571.
(31) Liu, I. P.-C.; Ren, T. *Inorg. Chem.* **2009**, *48*, 5608.
(32) Zhao, Y. M.; Zhou, N. Z.; Slepkov, A. D.; Ciulei, S. C.; McDonald, R.; Hegmann, F. A.; Tykwinski, R. R. *Helv. Chim. Acta* **2007**, *90*, 909.
(33) Xu, G.-L.; Campana, C.; Ren, T. *Inorg. Chem.* **2002**, *41*, 3521.
(34) Xu, G.-L.; DeRosa, M. C.; Crutchley, R. J.; Ren, T. *J. Am. Chem. Soc.* **2004**, *126*, 3728. Xi, B.; Xu, G.-L.; Fanwick, P. E.; Ren, T. *Organometallics* **2009**, *28*, 2338.
(35) Xu, G.-L.; Crutchley, R. J.; DeRosa, M. C.; Pan, Q.-J.; Zhang, H.-X.; Wang, X.; Ren, T. *J. Am. Chem. Soc.* **2005**, *127*, 13354.
(36) Frisch, M. J.; Trucks, G. W.; Schlegel, H. B.; Scuseria, G. E.; Robb, M. A.; Cheeseman, J. R.; Montgomery, J. A., Jr.; Vreven, T.; Kudin, K. N.; Burant, J. C.; Millam, J. M.; Iyengar, S. S.; Tomasi, J.; Barone, V.; Mennucci, B.; Cossi, M.; Scalmani, G.; Rega, N.; Petersson, G. A.; Nakatsuji, H.; Hada, M.; Ehara, M.; Toyota, K.; Fukuda, R.; Hasegawa, J.; Ishida, M.; Nakajima, T.; Honda, Y.; Kitao, O.; Nakai, H.; Klene, M.; Li, X.; Knox, J. E.; Hratchian, H. P.; Cross, J. B.; Bakken, V.; Adamo, C.; Jaramillo, J.; Gomperts, R.; Stratmann, R. E.; Yazyev, O.; Austin, A. J.; Cammi, R.; Pomelli, C.; Ochterski, J. W.; Ayala, P. Y.; Morokuma, K.; Voth, G. A.; Salvador, P.; Dannenberg, J. J.; Zakrzewski, V. G.; Dapprich, S.; Daniels, A. D.; Strain, M. C.; Farkas, O.; Malick, D. K.; Rabuck, A. D.; Raghavachari, K.; Foresman, J. B.; Ortiz, J. V.; Cui, Q.; Baboul, A. G.; Clifford, S.; Cioslowski, J.; Stefanov, B. B.; Liu, G.; Liashenko, A.; Piskorz, P.; Komaromi, I.; Martin, R. L.; Fox, D. J.; Keith, T.; Al-Laham, M. A.; Peng, C. Y.; Nanayakkara, A.; Challacombe, M.; Gill, P. M. W.; Johnson, B.; Chen, W.; Wong, M. W.; Gonzalez, C.; Pople, J. A. *Gaussian03*, revision D.02; Gaussian, Inc.: Wallingford, CT, 2003.
(37) Cao, Z.; Ren, T. *Organometallics* **2011**, *30*, 245.
(38) Zhao, Y.; Zhou, N.; Slepkov, A. D.; Ciulei, S. C.; McDonald, R.; Hegmann, F. A.; Tykwinski, R. R. *Helv. Chim. Acta* **2007**, *90*, 909.
(39) Beurskens, P. T.; Beurskens, G.; deGelder, R.; Garcia-Granda, S.; Gould, R. O.; Smits, J. M. M. *The DIRDIF2008 Program System*; Crystallography Laboratory, University of Nijmegen: Nijmegen, The Netherlands, 2008.
(40) Sheldrick, G. M. *Acta Crystallogr., Sect. A* **2008**, *64*, 112.
(41) Becke, A. D. *J. Chem. Phys.* **1993**, *98*, 5648. Stephens, P. J.; Devlin, F. J.; Chabalowski, C. F.; Frisch, M. J. *J. Phys. Chem.* **1994**, *98*, 11623.

Inorganic Chemistry

Article

pubs.acs.org/IC

Diruthenium(III,III) Ethynyl-phenyleneimine Molecular Wires: Preparation via On-Complex Schiff Base Condensation

Steven P. Cummings, Zhi Cao, Phillip E. Fanwick, Anastasia Kharlamova, and Tong Ren*

Department of Chemistry, Purdue University, West Lafayette, Indiana 47907, United States

Supporting Information

ABSTRACT: The diruthenium compound *trans*-$Ru_2(DMBA)_4(C{\equiv}C{-}C_6H_4\text{-}4\text{-}CHO)_2$ (**1**; DMBA is *N*,*N*′-dimethylbenzamidinate) was prepared from the reaction between $Ru_2(DMBA)_4(NO_3)_2$ and $HC{\equiv}C{-}C_6H_4\text{-}4\text{-}CHO$ under the weak base conditions. The aldehyde groups of **1** undergo a condensation reaction with $NH_2C_6H_4$-4-Y (Y = H and NH_2) to afford new compounds *trans*-$Ru_2(DMBA)_4(C{\equiv}C{-}C_6H_4\text{-}4\text{-}CH{=}N{-}C_6H_4\text{-}4'\text{-}Y)_2$ (Y = H (**2**) and NH_2 (**3**)). A related compound, $Ru_2(DMBA)_4(C{\equiv}C{-}C_6H_4\text{-}4\text{-}N{=}C(Me)Fc)_2$ (**4**), was also prepared from the reaction between $Ru_2(DMBA)_4(NO_3)_2$ and $HC{\equiv}C{-}C_6H_4{-}N{=}C(Me)Fc$. X-ray structural studies of compounds **1** and **2** revealed significant deviation from an idealized D_{4h} geometry in the coordination sphere of the Ru_2 core. Voltammetric measurements revealed four one electron redox processes for compounds **1**−**3**: the Ru_2 centered oxidation and reduction, and a pair of reductions of the imine or aldehyde groups. Compound **4** displays an additional oxidation attributed to the Fc groups. DFT calculations were performed on model compounds to gain a more thorough understanding of the interaction of the organic functional groups across the diruthenium bridge.

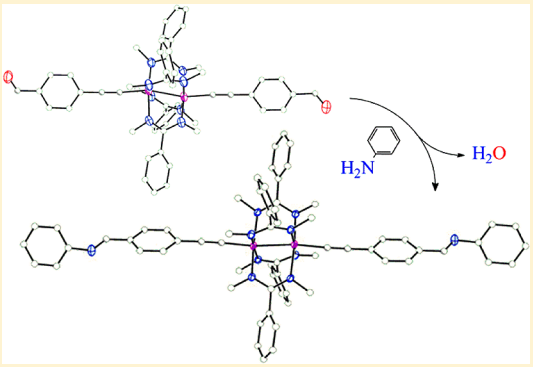

INTRODUCTION

For decades, metal alkynyl and alkenyl complexes have been investigated as building blocks for molecular wires,[1,2] nonlinear optical chromophores,[3] and photovoltaic materials.[4] Excellent charge transfer and molecular switching characteristics of molecular wires based on Fe,[5] Re,[6] Ru,[7] and Ru_2[8] compounds have been demonstrated through current−voltage (I−V) measurements at the single or few molecule level.[9] Among several types of diruthenium polyynyl and polyenyl compounds, those based on $Ru_2(DMBA)_4$ (DMBA is *N*,*N*′-dimethylbenzamidinate) are particularly attractive due to their rich and robust redox properties as well as the facile formation of bis-alkynyl adducts.[10,11] In contrast to the aforementioned successes based on polyynyl/polyenyl ligands, organometallic compounds containing heteroatoms in the conjugated pathway are far less common. Frisbie and co-workers recently reported that oligophenyleneimines (OPI) are efficient charge carriers in the donor−bridge−acceptor (D−B−A) scheme, revealing the potential of heteroatom bridges.[12,13] Charge transfer was found to proceed via a superexchange mechanism over short distances (up to 4 nm), and a hopping mechanism at extended distances (4−8 nm) with an exceptionally small attenuation constant (β) of 0.09 $Å^{-1}$ ($R = R_0e^{-\beta L}$; R and L are molecular resistance and length, respectively).[12] Accordingly, there is an interest in incorporating an OPI fragment into the conjugated backbone of $[M]{-}C{\equiv}C{-}R$, which may lead to interesting charge transfer characteristics. Further demonstration of the utility of phenyleneimine in molecular electronics came from the recent reports of Si nanogaps with organic molecular bridges by Ashwell et al.[14] The Si surface of the nanogap was first modified with 4-ethynylbenzaldehyde, which then underwent a Schiff base condensation reaction with an aromatic compound containing two terminal amino groups to complete the molecular bridge.

Transition-metal compounds with an imino-containing acetylide ligand are rare and limited to arylacetylides. As shown in Chart 1, these compounds can be classified as either

Chart 1. Compounds with Imino-Containing Acetylide Ligands

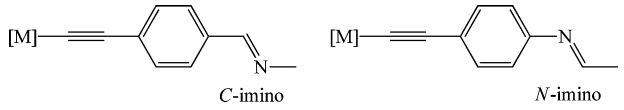

the C-imino or N-imino type based on the imine orientation relative to the arylacetylene fragment. The N-imino type compounds of Ru(II), Au(I), and Ni(II) were prepared by Humphrey and co-workers from the dehydrohalogenation reactions between the imino-containing aryl acetylene and the appropriate Ru, Au, and Ni starting compounds.[15] In contrast, Lapinte and co-workers found that the $(\eta^2\text{-dppe})(\eta^5\text{-Cp*})Fe$ based *N*-imino type compound can be obtained by an on-complex condensation reaction between $(\eta^2\text{-dppe})(\eta^5\text{-Cp*})\text{-}FeC{\equiv}C\text{-}4\text{-}(C_6H_4)NH_2$ and 2-pyridinecarboxaldehyde, while

Received: January 24, 2012
Published: June 22, 2012

   dx.doi.org/10.1021/ic300182h | *Inorg. Chem.* 2012, 51, 7561−7568

preparation via the dehydrohalogenation reaction failed.[16] Pt(II) based *C*-imino type compounds were also prepared from the condensation reaction between the aldehyde substituents of Pt-bound arylacetylides and aniline by Eisenberg and co-workers.[17] Previously, we reported the preparation of N-imino type $Ru_2(ap)_4$-compounds (*ap* = 2-anilinopyridinate) using the on-complex condensation reaction.[18] Described in this contribution are the preparation of *trans*-$Ru_2(DMBA)_4(C{\equiv}C{-}C_6H_4{-}4\text{-}CHO)_2$ (**1**), and subsequent synthesis of its derivatives **2** and **3** (Scheme 1) via condensation

Scheme 1. Synthesis of Ru_2(DMBA)-Alkynyls with Imine Substituent[a]

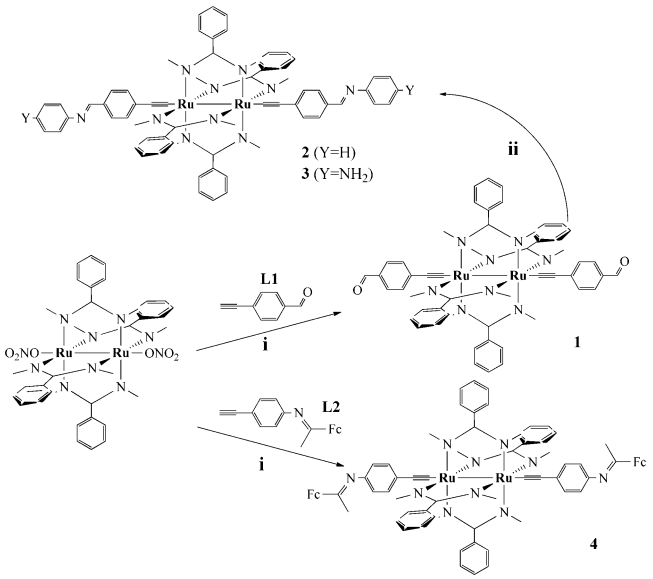

[a]Conditions: (i) $Ru_2(DBMA)_4(NO_3)_2$, $HNEt_2$; (ii) 4-Y-aniline, CF_3CO_2H/CH_3CO_2H.

with the appropriate arylamines. A related compound, $Ru_2(DMBA)_4(C{\equiv}C{-}C_6H_4\text{-}4\text{-}N{=}C(Me)Fc)_2$ (**4**), was prepared from the reaction between $Ru_2(DMBA)_4(NO_3)_2$ and $HC{\equiv}C{-}C_6H_4{-}N{=}C(Me)Fc$. While the synthesis of **1**–**3** is similar to that of $Ru_2(ap)_4$-based compounds, the resultant compounds are diamagnetic and of significantly different physical properties. Furthermore, the condensation reaction occurs simultaneously on both axial directions of $Ru_2(DMBA)_4$ core and hence permits faster extension than that of $Ru_2(ap)_4$-based compounds, where the extension is unidirectional. The impact of the imine moiety on the electronic structure of the diruthenium species was examined through structural, voltammetric, and computational studies.

RESULTS AND DISCUSSION

Synthesis. As a continuation of the study on peripheral modification of diruthenium paddlewheel species,[19] on-complex Schiff base condensations were previously carried out between the terminal amino group in $Ru_2(ap)_4(C{\equiv}C\text{-}3/4\text{-}C_6H_4{-}NH_2)$[20] and an arylaldehyde.[18] However, attempts to obtain an analogous $Ru_2(DMBA)_4(L_{ax})_2$ precursor, *trans*-$Ru_2(DMBA)_4(C{\equiv}C{-}C_6H_4{-}4\text{-}NH_2)_2$, from the reaction between $Ru_2(DMBA)_4(NO_3)_2$ and $4\text{-}HC{\equiv}C{-}C_6H_4{-}NH_2$ only led to intractable precipitates. Alternatively, the reaction between $Ru_2(DMBA)_4(NO_3)_2$ and 4-ethynylbenzaldehyde (**L1**, see Supporting Information) in the presence of diethylamine yielded compound **1** as shown in Scheme 1.[21] Both aldehyde groups of **1** undergo a simultaneous condensation reaction with aniline or *p*-phenylenediamine resulting in compounds **2** or **3**, respectively, with the *C*-imino linkage. To facilitate Schiff base condensation, both trifluoroacetic acid and acetic acid were tested as a Brønsted acid catalyst. The use of acetic acid allows for yields between 75 and 80% with a reaction time of ca. 3 h, while the use of trifluoroacetic acid led to significantly shortened reaction times (<5 min) and yields around 60 to 65% due to product degradation. As an oligomerization reaction between **1** and *p*-phenylenediamine could occur, a large excess of *p*-phenylenediamine was used to reduce the possibility of an oligomeric product. Compound **4** (Scheme 1) was prepared from the reaction between $Ru_2(DMBA)_4(NO_3)_2$ and $Fc\text{-}C(Me){=}N\text{-}4\text{-}C_6H_4{-}C{\equiv}CH$ (**L2**), the latter of which already contains a C-imino moiety, which will result in an N-imino Ru_2 product. The C-imino substitution in **2** and **3** has an electron withdrawing effect (σ_p = 0.42), while the N-imino substitution in **4** has an electron donating effect, and is described in more detail below. As the imine group in **4** was derived from an acetyl rather than aldehyde, this required the use of alumina to catalyze the reaction. The resulting imine potentially provides a more stable environment for the C=N bond by reducing the chance of hydrolysis; yet it should have minimal impact on the electronic structure.

Compounds **1**–**4** are all diamagnetic, and were readily characterized using ^1H NMR spectroscopy. Compound **1** has a distinct peak at 9.8 ppm that is indicative of an aldehyde, whereas the spectra of **2** and **3** feature a singlet at 8.3 ppm due to the methylidine proton of the imine group. FT-IR spectroscopy was useful in revealing product formation by the detection of an intense peak near 2050 cm^{-1} that is characteristic of the C≡C symmetric stretch in *trans*-$Ru_2(DMBA)_4$-acetylide compounds. A weak peak near 1619 cm^{-1} in compounds **2**, **3**, and **4** is attributed to the C=N stretch, while **1** has a strong peak at 1683 cm^{-1} indicative of a C=O stretch. Disappearance of the latter is an excellent indicator of the product purity for Schiff base condensation reactions.

Molecular Structures. Single crystals of **1** and **2** were grown via slow cooling of a THF:hexanes solution (1:5) and vapor diffusion of hexanes into a saturated THF solution, respectively. ORTEP plots of **1** and **2** are displayed in Figures 1 and 2, respectively, with selected bond lengths and angles given in Table 1. In both **1** and **2**, a crystallographic inversion center is present bisecting the Ru–Ru bond, and the asymmetric unit

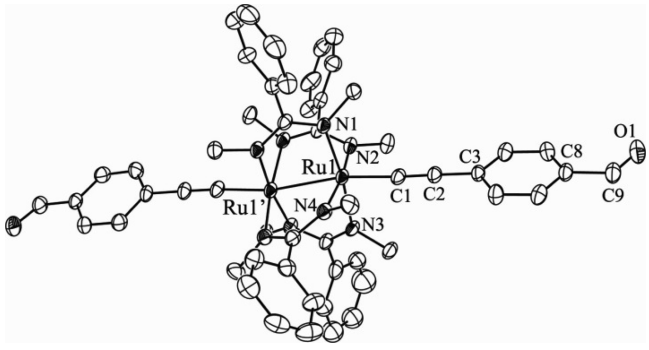

Figure 1. ORTEP plot of **1** at the 20% probability level. Hydrogen atoms were omitted for clarity.

dx.doi.org/10.1021/ic300182h | *Inorg. Chem.* 2012, 51, 7561–7568

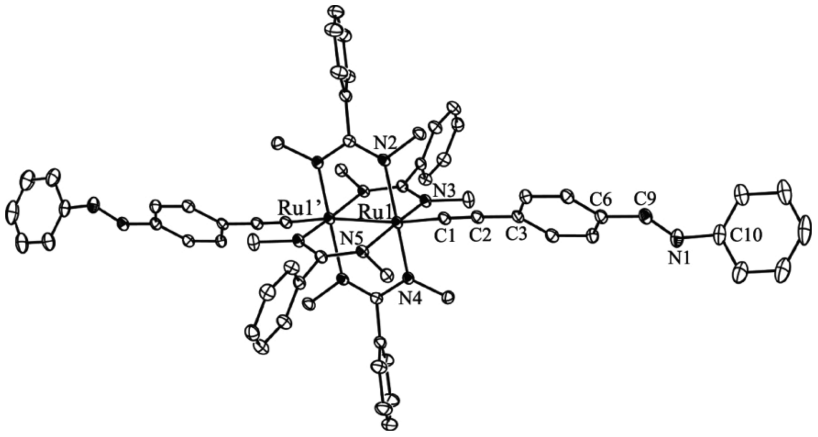

Figure 2. ORTEP plot of **2** at the 20% probability level. Hydrogen atoms were omitted for clarity.

Table 1. Selected Bond Lengths (Å) and Angles (deg) for 1 and 2

1		2	
Ru1−Ru1′	2.459(1)	Ru1−Ru1′	2.456(1)
Ru1−C1	1.970(7)	Ru1−C1	1.984(3)
Ru1−N1	2.051(5)	Ru1−N2	1.994(2)
Ru1−N2	2.142(5)	Ru1−N3	2.135(2)
Ru1−N3	2.038(5)	Ru1−N4	2.132(2)
Ru1−N4	1.981(6)	Ru1−N5	1.993(2)
C1−C2	1.22(1)	C1−C2	1.208(4)
C2−C3	1.44(1)	C2−C3	1.423(4)
C9−O1	1.22(1)	C9−N1	1.268(4)
		N1−C10	1.431(4)
Ru1−Ru1′−C1	163.8(2)	Ru1−Ru1′−C1	160.9(1)
Ru1−C1−C2	175.1(7)	Ru1−C1−C2	170.8(2)
C1−C2−C3	178.7(7)	C1−C2−C3	177.4(3)
C6−C9−O1	123.6(8)	C9−N1−C10	116.8(3)

contains one-half of the diruthenium molecule. The coordination sphere of $Ru_2(DMBA)_4$ in **1** and **2** are comparable to several previously reported $Ru_2(DMBA)_4(alkynyl)_2$ compounds.[22,23] The Ru−Ru bond lengths for **1** and **2** are in good agreement with *trans*-$Ru_2(DMBA)_4(C{\equiv}CPh{-}4\text{-}NO_2)_2$.[22,24] The observed elongation of the Ru−Ru bond is caused by the electron deficiency of the aldehyde and imine substituents, which further polarizes the Ru d_{z2} orbital toward C1.[11,22] A second-order Jahn−Teller distortion from a D_{4h} geometry is evident in the coordination sphere of the Ru_2 centers: (i) large variations among the Ru−N and Ru′−Ru−N bond lengths and angles, and (ii) the Ru−Ru−C angle being significantly bent from linear to 163.8 and 160.9° for **1** and **2**, respectively.[25,26] A detailed DFT study into the origin of the Ru−Ru−C bond angles deviation from linear for *trans*-$Ru_2(L)_4(C{\equiv}C{-}R)_2$ compounds resulted in an ideal angle of 158.7°,[27] which is exceptionally close to those obtained experimentally, especially for **2**.

The C9−N1 and C10−N1 bond lengths in **2** are consistent with lengths previously published for imino-phenylacetylides bound to ruthenium,[18] nickel,[28] platnium[17] and iron,[16] while the C9−N1−C10 bond angle (116.8°) is slightly smaller than other imino-phenylacetylide compounds which range from 119.1 to 121.7°. The imine bound aryl rings of **2** contain a significant dihedral angle (59.4°) around the imine moiety, of which is coplanar with the aryl-aldehyde derived phenyl.[17,28,29] The majority of secondary aldimine structures have a torsional angle between 29 and 41°, which is attributed primarily to a steric hindrance of the ortho hydrogen on the aniline ring and the methylidine hydrogen.[30] An evaluation of Humphery and co-workers' series of phenylacetylides on gold, nickel, and ruthenium containing isoelectronic -ene, -imine, and -azo linkers supports steric hindrance being a primary cause for the dihedral angle.[28,29] In general, the aryl rings linked by an -azo group tend to have smaller dihedral angles (4−20°), while the aryl linked -imine and -ene (*E* conformation) have increased torsional angles (8−50°). A packing diagram shows that the terminal aryl rings of two independent molecules of **2** are within 3.5 Å at their nearest point, signifying that this increase of the dihedral angle is electronic in origin and not due to π-interactions.

Electrochemistry. Previously reported *trans*-$Ru_2(DMBA)_4(C{\equiv}CR)_2$ compounds display one reversible oxidation (**A**, (III,III) to (III,IV)) and one reversible reduction (**B**, (III,III) to (III,II)) that are Ru_2 centered.[2,23,24,26,31−33] As described in Scheme 2 and Table 2, compounds **1**−**4** exhibit

Scheme 2. Redox Couple Assignments for Compounds 1−4

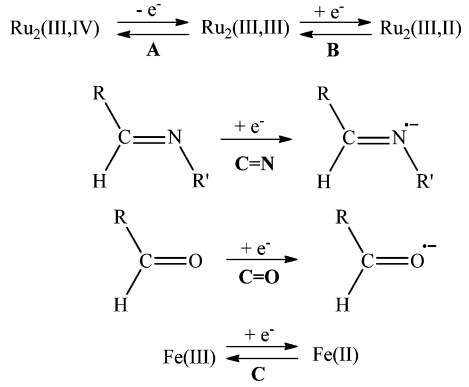

Table 2. Electrochemical Potentials (V, vs Ag/AgCl) of Compounds 1−4

	$E_{1/2}$ (C)	$E_{1/2}$ (A)	$E_{1/2}$ (B)	E_{pc} (C═N/O)[a]
1		0.609	−0.976	−1.860, −2.052
2		0.548	−1.017	−1.888, −1.986
3		0.545	−1.016	−1.815, −1.900
4	0.693	0.433	−1.140	−2.120

[a] E_{pc}(C═N/O) were obtained from DPV.

dx.doi.org/10.1021/ic300182h | *Inorg. Chem.* 2012, 51, 7561−7568

(Figure 3) analogous Ru_2 based redox couples. In addition, they display a second set of reductions which are assigned to the

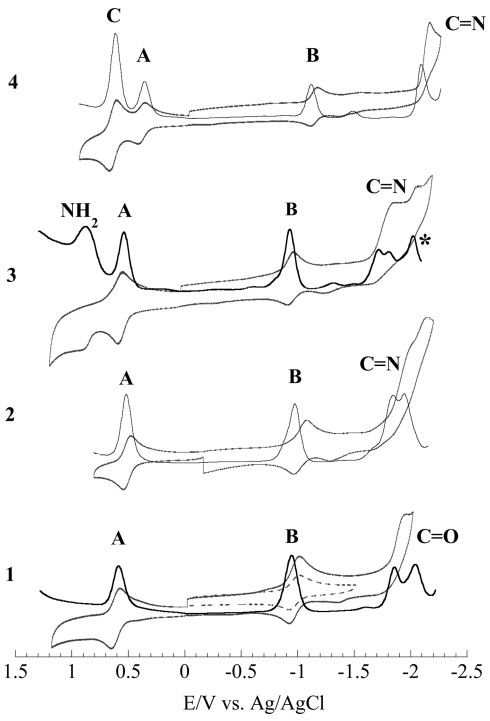

Figure 3. Cyclic and differential pulse voltammograms of **1**–**4**; * indicates degradation.

axial ligand functional groups (**C═O** and **C═N**). Compounds **3** and **4** display an additional $2e^-$ oxidation process, which is assigned to the simultaneous oxidation of the amino (**NH_2**) and ferrocenyl (**C**, Fc to Fc^+) groups, respectively. Few electrochemical studies have been carried out on imino-phenylacetylides bound to a transition metal, and to the best of our knowledge this marks the first one in which an imine orientation effect is studied.

The first oxidations of **1**–**4** occur between 433 and 609 mV and are Ru_2-based for all compounds. Compound **1** is the most difficult to oxidize with the electrode potential being 60 mV higher than those of **2** and **3.** However, compound **4** is the easiest to oxidize with the electrode potential cathodically shifted by 176 mV from that of **1**. The first reduction of **1**–**4** is also Ru_2 centered, and its electrode potentials range from −0.976 to −1.140 V. The variation in reduction potentials follows the same trend as that of the oxidation with **4** being the most difficult to reduce and **1** being the easiest.

The changes in the Ru_2 redox potentials are in general accordance with the Hammett parameters of the substituents of arylacetylide ligands: **1** exhibits the most anodically shifted oxidation and reduction due to the aldehyde substituent being the strongest electron withdrawing group (σ_p = 0.42) among the compounds considered here.[34,35] $Ru_2(DMBA)_4$ bound to the C-imino moiety, as with **2** and **3**, displays similar oxidation and reduction potentials, as the 4-CH═N−C_6H_4−R is a substituent of comparable electron withdrawing ability (σ_p = 0.42) to an aldehyde. Although the C-imino and aldehyde groups have equivalent electron withdrawing strengths, there is a 60 mV difference in redox potentials, indicating that the substituent effect is not purely inductive. When the $Ru_2(DMBA)_4$ moiety is bound by an N-imino ligand, as with compound **4**, the Ru_2-based oxidation (**A**) and reduction couples (**B**) undergo a significant cathodic shift from those of compounds **1**–**3**, which is consistent with the strong electron donating nature of 4-N═CH−C_6H_4−R (σ_p = −0.55).[34] The strong electron donating effect of N-imino was also observed by both Lapinte and Shaabani,[16,36] where significant cathodic shifts of the Fe(II/III) couple were noticed when the amino precursor was converted to an *N*-imino substituent. It is also worth mentioning that the ferrocenyl group of **4** is C-imino bound and as a result the ferrocene/ferrocenium couple was observed at a potential 140 mV more positive than free ferrocene due to the *C*-imino group being an electron acceptor.

The cyclic voltammograms (CV) of compounds **1**–**4** display one or more $1e^-$ reductions from −1.80 to −2.10 V in addition to the Ru_2 centered couple (**B**). For **1**–**3**, the differential pulse voltammograms (DPV) clearly show two $1e^-$ reductions, while compound **4** has a single reduction peak that is greater than a one electron area. Previous studies in our lab have suggested this is a ligand based reduction.[18] It is well established that the imine and aldehyde groups are capable of being reduced, yet very little has been documented on their redox potentials when bound to metal centers. The cause of the variation in the imine reduction potentials is unclear, as evidenced by **3**, where **C═N** reduction couple is shifted positively when compared to that of **2**, despite the electron donating amino group which should increase the potential required for the imine reduction. One possible explanation, proposed in detail by Lapinte, is that an amino group in the para position is capable of manifesting a quinoidal resonance structure allowing for accommodation of the added electron.[37] According to the DPV for compounds **1**–**3**, the second reduction observed in CV occurs as two separate one-electron reductions. The stepwise reduction of two equivalent C═O (C═N) moieties may imply a long distance electronic coupling across the entire molecule, which was previously documented for the $Ru_2(DMBA)_4(C_{2n}Fc)_2$ type compounds.[23,31,38] Interestingly, in **4**, with the reversal of the imine group, this long distance coupling is not observed for either ferrocene or the imine group.

vis-NIR Electronic Spectroscopy. The vis-NIR spectra were recorded in THF for **1**–**4**. Compounds **1**–**4** have a low energy band with λ_{max}(nm) centered near 875 for **1**–**3** and 857 for **4** as shown in Figure 4. In the high energy region, compound **4** has a well-defined peak at 502 nm that is characteristic of $Ru_2(DMBA)_4(CCAr)_2$-type compounds.[22−24,31,33,39] Compounds **1**–**3**, however, exhibit an intense peak between 390 and 420 nm and a shoulder at 490 nm. The low energy transitions from 850 to 870 nm are ascribed to the HOMO−LUMO gap of a $\pi^*(Ru_2) \rightarrow \delta^*(Ru)_2$ and are in good agreement with the electrochemical gap of ca. 1.56 V obtained from cyclic voltammetry. This transition does have some axial ligand influence as seen with **4**, which is blue-shifted by 20 nm due to an increase in the antibonding overlap between π(C≡C) and $\pi^*(Ru_2)$ occurring from the electron donating character of the imine.[26,33] The well-defined high energy absorption band of **4** is tentatively assigned to a mixture of $\pi(N) \rightarrow \delta^*(Ru_2)$ and $\delta\ (Ru_2) \rightarrow \delta^*(Ru_2)$ transitions as in previous $Ru_2(DMBA)_4(C{\equiv}C{-}R)_2$ systems and corroborated by a previously published TD-DFT calculation.[23] The $\pi(N) \rightarrow \delta^*(Ru_2)/\delta\ (Ru_2) \rightarrow \delta^*(Ru_2)$ transition for **1**–**3** is overshadowed by a more intense and broad peak at ca. 400 nm, resulting in a shoulder at 490 nm that accounts for the orange-red color observed. The intense high energy transitions observed for **1**–**3** at 390 to 420 nm are likely a mixture of

dx.doi.org/10.1021/ic300182h | *Inorg. Chem.* 2012, 51, 7561−7568

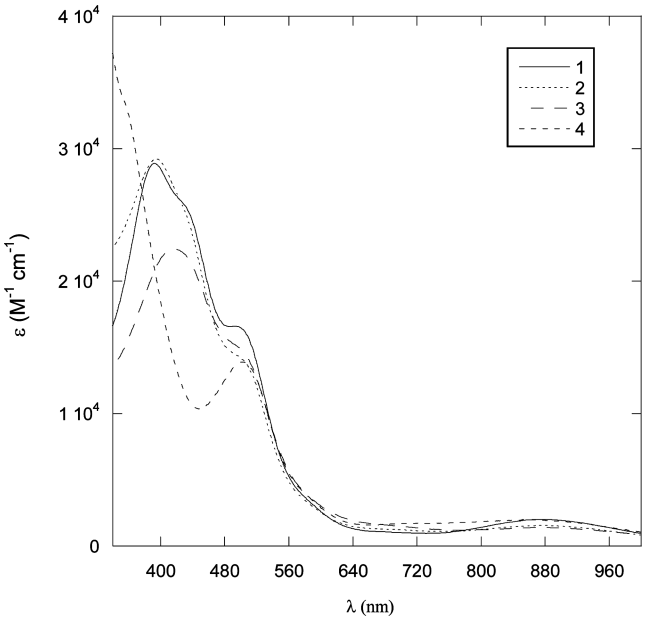

Figure 4. Vis-NIR spectra of **1**–**4** in THF.

ligand based $\pi \rightarrow \pi^*$ and MLCT transitions, similar to Pt-arylacetylide compounds bearing imino-substituents by Eisenberg.[17]

Density Functional Theory (DFT) Calculations. In an effort to better understand the unique electronic characteristics that these compounds display, spin-restricted DFT calculations were carried out for molecules **1** and **2** using optimized geometries based on the crystal structures without truncation. As electrochemistry revealed a significant difference in the ligand reduction in compounds **2**/**3** compared to that in **4**, a calculation of model **4**′ was also carried out to determine if these differences were of an electronic origin. Model **4**′ was built on the optimized structure of **2**, with the C═N bond being inverted to reflect the C-imino nature of **4** and the ferrocene group being replaced by the phenyl group to simplify calculations. DFT calculations were performed at the B3LYP/LanL2DZ level (by the Gaussian 03 suite).[40−42] For the purpose of comparison, a calculation consisting of polarization functions was carried out on **1** with the application of a 6-31G** basis set for H, C, N, and O, and a LanL2DZ(f) basis set for Ru resulting in **1**′.[43] Comparison of the calculations with and without polarization functions revealed no significant discrepancy. Hence, polarization functions were not applied for the remaining model calculations due to the significant increase in computation time considering the size of the system. The results of **1**′ are detailed in the Supporting Information Table S1 and Figure S1. A qualitative discussion of the MO contribution is provided below, while a natural bond orbital (NBO) analysis for **1**, **2**, and **4**′ was carried out with the percent contribution for distinct functional groups detailed in Table S2 of the Supporting Information.

The bond lengths of the optimized structures were in good agreement (Table S1 of the Supporting Information) with the crystal structures of **1** and **2**. The optimized Ru−Ru bond lengths (2.54−2.56 Å) are ca. 0.10 Å longer than the experimental bond lengths (2.46 Å), which is likely due to the underestimation of metal−metal interactions by the B3LYP method. The introduction of polarization functions does result in a slightly improved bond length of 2.52 Å.[23] It is worth noting that previous DFT calculations had put the Ru−Ru bond length between 2.61 and 2.65 Å using calculations without polarization, but based on a truncated DMBA ligand model.[27,39] The bond angles of **1** and **2** are also in good agreement with experimental values, except for the Ru1−C1−C2 and C9−N1−C10 of **2** where C9−N1−C10 increases from 116.8 to 122° putting the nitrogen in a more trigonal planar orientation. The Ru1−C1−C2 angle of **2** was 175°, which is a 5° increase from the experimental value.

Since the DFT results for **1**, **2**, and **4**′ are quite similar, the valence MOs of **1** are discussed in detail with the contour plots and energy levels shown in Figure 5. Contour plots of the

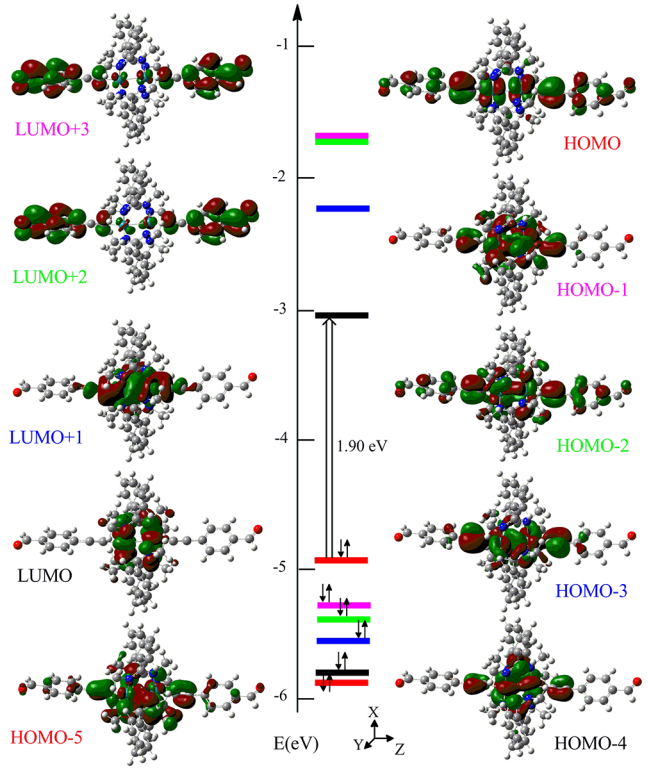

Figure 5. MO diagram of **1** based on spin-restricted DFT calculations.

valence MOs for **2** and **4**′ can be found in the Supporting Information as Figures S2 and S3, respectively. The HOMO of **1** is an antibonding combination of π_{xz}*(Ru−Ru) and π(C≡C) with some contribution from the imine/aldehyde moiety, while the HOMO-1 is an antibonding combination of the π_{xz}(Ru−Ru) and π(C≡C). The HOMO-2 of **1** is an antibonding combination of π(C≡C) and π_{xz}(Ru−Ru) with additional contribution from π*(aryl), while the contribution from π_{xz}(Ru−Ru) decreases slightly in **2** and **4**′. Although the HOMO-3 is formally an antibonding combination of π_{yz}*(Ru−Ru) and π(C≡C), there is a significant σ-type overlap between two d_{yz} orbitals due to the distortion of the Ru_2 coordination sphere, which results in a partial σ-bond between two Ru centers.[39] The HOMO-4 is δ(Ru−Ru), though only weak orbital overlap is present, due to the small underestimation of the metal−metal interaction in conjunction with distortion of the coordination sphere. On the basis of formal molecular orbital assignments of the HOMO to the HOMO-4, the ground state electronic configuration is $\pi^4\delta^2\pi^{*4}$, which is in agreement with previous studies of *trans*-Ru_2(III,III)$(L_{ax})_2$ type compounds.[23,27] The LUMO and LUMO+1 are primarily

dx.doi.org/10.1021/ic300182h | Inorg. Chem. 2012, 51, 7561−7568

metal in character being the δ^*(Ru−Ru) and σ^*(Ru−C) orbitals, respectively. The LUMO+2 and LUMO+3 are primarily the antibonding interactions between π (aldehyde/imine) and π (aryl) orbitals of the ligand with a minimal presence of π_{yz} and π_{yz}^*(Ru−Ru). The HOMO-5 is mostly made of the π(N) of the amidinate ligands with a modest contribution with the π_{yz}(Ru−Ru) and π(C≡C).

The HOMO of **1** (−4.92 eV) is the lowest in energy with **4′** being the highest (−4.57 eV) and **2** in-between at −4.73 eV. This energetic order is consistent with electrochemical results, where the one electron-oxidation of **2** is easier than that of **1** but more difficult than **4**. The same trend holds true for the LUMO energies of **1**, **2**, and **4′**, which correlate well with the reduction potentials of the Ru_2(III,III) to Ru_2(III,II) couple. The reduction of **1** is the easiest as well as having the lowest lying LUMO at −3.02 eV followed by **2** and **4′** with the LUMO occurring at −2.75 and −2.64 eV, respectively. The HOMO−LUMO gaps of **1**, **2**, and **4′** are 1.90, 1.98, and 1.93 eV, respectively, and are in good agreement with the energy gaps previously calculated for *trans*-$Ru_2(DMBA)_4(C{\equiv}C{-}R)_2$ models.[23,39] The LUMO+2 and LUMO+3 for **1** and **2** are separated by 0.03 eV, while in **4′** these orbitals are degenerate.

In order to understand the change in the electronic structure for $Ru_2(DMBA)_4$ upon a one electron reduction, a spin-unrestricted DFT calculation was performed for $(\mathbf{2})^-$ which is a Ru_2(III,II) species adapted from the optimized structure of **2**. The calculation was carried out with $S = 1/2$, which provided a molecular geometry (Table S1 of the Supporting Information) and occupied molecular orbitals not too dissimilar to that of the neutral species. Upon reduction, the LUMO in **2** becomes the SOMO of $(\mathbf{2})^-$ as shown in Figure 6. The most marked difference upon reduction is an increase in the Ru−Ru and Ru−N bond lengths, due to the increased electron density on the Ru_2 core. The LUMO+1 of **2** is significantly destabilized, becoming the LUMO+2 for $(\mathbf{2})^-$, while the LUMO+2 and LUMO+3 of **2** become the LUMO and LUMO+1 in $(\mathbf{2})^-$. This gives support to the stepwise reduction of the organic functional group occurring before a second Ru_2 centered reduction. There is a slight but significant increase in the contribution of the $\pi_{xz}^*(Ru_2)$ in the LUMO and LUMO+1 of $(\mathbf{2})^-$, providing support for a superexchange pathway for electronic coupling between of the redox active C═O/C═N groups.

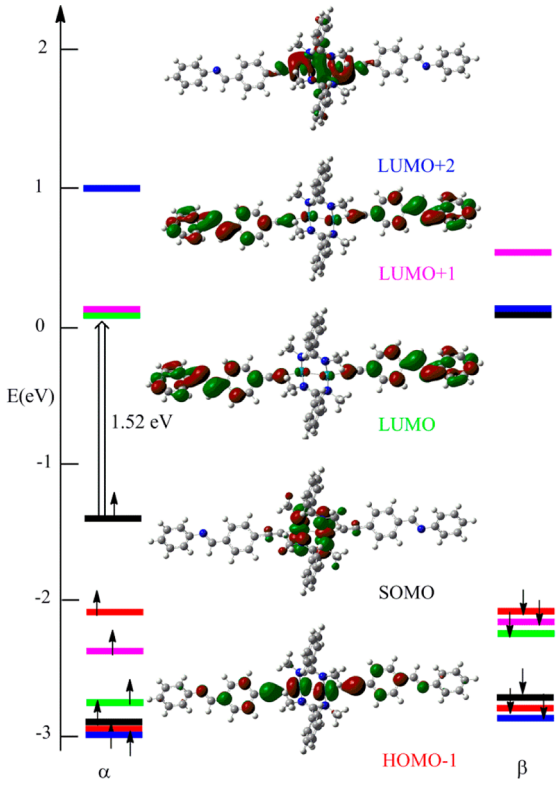

Figure 6. MO diagram of model compound $(\mathbf{2})^-$ based on spin-unrestricted DFT calculations; The α spin Kohn−Sham orbitals are shown with energy levels for both spins.

CONCLUSIONS

The on-complex Schiff base condensation has been successfully expanded from a monoadduct to a bis-adduct phenylimine system using Ru_2(III,III) increasing the scope of peripheral covalent modification chemistry.[19] Electronic interactions between distant organic aldehyde/imine groups in compounds **1**−**3** was inferred from electrochemical data and rationalized with the aid of DFT calculations. While the ligand centered mixed valency was not probed due to highly cathodic reduction potential in this contribution, it is worth noting that ligand-based mixed valency has been confirmed in other dinuclear systems by Chisholm and co-workers.[44] Work is continuing with **1** and **3** to form a monolayer covalently bound to a silicon surface in order to interrogate the electronic interactions of diruthenium and the silicon surface.

EXPERIMENTAL SECTION

General. 4-Bromobenzaldehyde, 4-iodoaniline, aniline, and *p*-phenylenediamine were purchased from Sigma-Aldrich, trimethylsilylacetylene was purchased from GFS chemicals, and acetylferrocene was purchased from STREM chemicals. $Ru_2(DMBA)_4(NO_3)_2$ was synthesized according to a literature procedure.[21] Toluene and diethylamine were distilled over CaH_2; THF was distilled over Na/benzophenone. Phenylenediamine was recrystallized from EtOH and all other reagents were used as received. The synthesis and characterization of 4-ethynylbenzaldehyde (**L1**) and Fe($\eta^5C_5H_5$)-($\eta^5C_5H_4$−C(Me)═N−4-Ph−C≡C−H) (**L2**) can be found in the Supporting Information. Syntheses were carried out using standard Schlenk techniques unless noted otherwise and were monitored by TLC using 3:7 EtOAc:hexanes for all reactions unless otherwise stated. ^{1}H NMR spectra were obtained using a Varian 300 MHz in $CDCl_3$. UV−vis-NIR was collected on a JASCO V-670 spectrophotometer in THF. Infrared spectra were collected on a JASCO FT-IR 6300 spectrometer via ATR on a ZnSe crystal. HR-nESI-MS spectra were performed on a QqQ tandem mass spectrometer in CH_2Cl_2 (QSTAR XL; Applied Biosystems/MDS Sciex, Concord, ON, Canada). Cyclic voltammograms were recorded in a 0.2 M *n*-Bu_4PF_6 and 1.0 mM diruthenium compound solution in N_2 degassed THF by a CHI620A voltammetric analyzer using a glassy carbon electrode (diameter = 2 mm), Pt-wire counter electrode, and a Ag/AgCl reference electrode using ferrocene as an internal reference (corrected to 0.565 V for **1** and **2**).

Attempted Synthesis of *trans*-$Ru_2(DMBA)_4(C{\equiv}C{-}C_6H_4{-}4{-}NH_2)_2$. A 25 mL Schlenk flask containing 0.055 mmol $Ru_2(DMBA)_4(NO_3)_2$ and 0.55 mmol 4-ethynylaniline was thoroughly degassed, to which was added 20 mL THF and 1 mL $HNEt_2$. The solution slowly became yellow-brown in color resulting in a baseline product according to TLC (3:7 EtOAc:hex). No red product was ever detected by TLC and the solid product isolated was soluble in common organic solvents, which made characterization difficult.

***trans*-$Ru_2(DMBA)_4(C{\equiv}C{-}4{-}Ph{-}CHO)_2$ (1).** To a 50 mL Schlenk flask with 0.295 mmol $Ru_2(DMBA)_4(NO_3)_2$ and 0.87 mmol 4-ethynylbenzaldehyde was added 20 mL THF and 3 mL $HNEt_2$; the

dx.doi.org/10.1021/ic300182h | Inorg. Chem. 2012, 51, 7561−7568

solution became orange-red over several hours. The solution was filtered through a diatomaceous earth plug and the solvents were removed on rotovap. Compound **1** was isolated as an orange-red solid (0.256 mmol, 87%) after being recrystallizied from THF/hexanes. Data for **1**: R_f = 0.55; ^{1}H NMR: 3.29 (s − 24H, CH_3), 7.03 (d − 8H, aromatic), 7.12 (d − 4H, aromatic), 7.45 (d − 12 H, aromatic), 7.67 (d − 4H, aromatic), 9.84 (s − 2H, C*H*═O); nESI-HR-MS, $[M+H]^+$ − 1050.248, (calc. 1050.212); visible spectra, λ_{max} (nm, ε (M^{-1} cm^{-1}): 877(2000), 495(16000); IR (cm^{-1}): C≡C − 2053 (s), C═O − 1683(s); Electrochemistry ($E_{1/2}$, V; ΔE_p; $i_{backward/forward}$): **A**, 0.609, 0.039, 0.98; **B**, −0.976, 0.049, 0.86; **C═O** (based on DPV) −1.860, −2.052.

***trans*-Ru$_2$(DMBA)$_4$(C≡C−4-Ph−CH═N−Ph)$_2$ (2).** A 50 mL Schlenk flask was charged with 0.082 mmol **1**, 0.15 mmol aniline, 30 mL dry-THF and 10 mL EtOH. To the solution was added 2 drops of acetic acid, and the reaction was monitored by TLC using 1:3 THF:hexanes. Upon completion, the reaction mixture was filtered through a deactivated silica plug and the solvents were removed under reduced pressure. The solid residue was recrystallized in THF:MeOH to yield 0.062 mmol purple solid (76% based on Ru). Alternatively, the reaction was performed in THF using trifluoroacetic acid with a yield of ca. 65%, but with a significantly shortened reaction time. Data for **2**: R_f = 0.60; ^{1}H NMR: 3.31 (s − 24H, CH_3), 7.03 (d − 8H, aromatic), 7.17 (t − 12H, aromatic), 7.41 (m − 14H, aromatic), 7.71 (d − 4H, aromatic), 8.34 (s − 2H, C*H*═N); nESI−HR−MS, $[M+H]^+$ − 1200.344, (calc. 1200.433); visible spectra, λ_{max} (nm, ε (M^{-1} cm^{-1}): 492(14000), 875(1500); IR (cm^{-1}): C≡C − 2065(s), C═N − 1619(w); Electrochemistry ($E_{1/2}$, V; ΔE_p; $i_{backward/forward}$): **A**, 0.548, 0.032, 0.88; **B**, −1.017, 0.034, 1.00; E_{pc}: **C═N** (based on DPV), −1.888, −1.986.

***trans*-Ru$_2$(DMBA)$_4$-(C≡C−4-Ph−CH═N−4′-Ph−NH$_2$)$_2$ (3).** Using the same procedure as **2** with trifluoroacetic acid, 0.508 mmol **1** and 3.28 mmol *p*-phenylenediamine were reacted to yield 0.339 mmol purple solid (67% based on Ru). Data for **3**: R_f = 0.1 (THF:hexanes, 1:1); ^{1}H NMR: 3.31 (s − 24H, CH_3), 4.03 (s − 4H, NH_2), 6.70 (d − 4H, aromatic), 7.01 (d − 4H, aromatic), 7.08 (d − 6H, aromatic), 7.15 (d − 6H, aromatic), 7.46 (d − 12H, aromatic), 7.70 (d − 4H, aromatic), 8.30 (s − 2H, C*H*═N); nESI−HR−MS, $[M+2H]^{+2}$ − 615.661, (calc. 615.733), $[M+H]^+$ − 1230.369, (calc. 1230.456); visible spectra, λ_{max} (nm, ε (M^{-1} cm^{-1}): 492(14000), 871(1400); IR (cm^{-1}): NH_2 − 3450, 3378, 3318(m), C≡C − 2071(s), C═N − 1619(w); Electrochemistry ($E_{1/2}$, V; ΔE_p; $i_{backward/forward}$): E_{pa}: **NH$_2$**, 0.888; **A**, 0.545, 0.030, 0.80; **B**, −1.016, 0.031, 1.00; E_{pc}: **C═N** (based on DPV), −1.815, −1.900.

***trans*-Ru$_2$(DMBA)$_4$-[(C≡C−4-Ph−N═C(Me)-η^5C$_5$H$_4$)(η^5C$_5$H$_5$)-Fe]$_2$ (4).** Following the procedure for the synthesis of **1**, 0.086 mmol **L2** was reacted with 0.046 mmol Ru$_2$(DMBA)$_4$(NO$_3$)$_2$. Upon completion, the reaction mixture was filtered and recrystallized in EtOAc:hexanes to yield 0.026 mmol (62%, based on Fe). Data for **4**: R_f = 0.40; ^{1}H NMR using C_6D_6: 1.845 (s − 6H, CH_3), 3.288 (s − 24H, CH_3), 3.967 (s − 10H, Cp*), 4.146 (s − 4H, Cp*), 4.584 (s − 4H, Cp*), 6.534 (d − 4H, aromatic), 6.909 (d − 8H, aromatic), 7.053 (d − 8H, aromatic), 7.233 (d − 8H, aromatic), nESI−HR−MS, $[M+H]^+$ − 1444.309, (calc. 1444.329); visible spectra, λ_{max} (nm, ε (M^{-1} cm^{-1}): 502(14000), 707(1700), 858(2000); IR (cm^{-1}): C≡C − 2078(s), C═N − 1621(s); Electrochemistry ($E_{1/2}$, V; ΔE_p; $i_{backward/forward}$): **A**, 0.433, 0.030, 0.63; **C**, 0.693, 0.030, 0.87; **B**, −1.140, 0.032, 0.68; E_{pc} (based on DPV), **C═N**, −2.120.

X-ray Data Collection, Processing, And Structure Analysis and Refinement for Crystal. Preliminary examination and data collection were performed on a Rigaku Rapid II image plate diffractometer with CuKα radiation (λ = 1.5418 Å) and the structures were solved using the structure solution program PATTY in DIRDIF99,[45] and refined using SHELX-07.[46] Cell constants for data collection were obtained from least-squares refinement, using the setting angles of 9536 reflections in the range of 2 < θ < 72° for **1** and 5815 reflections in the range 3 < θ < 72° for **2**. Crystal data for **1**: $C_{54}H_{49}N_8O_2Ru_2\cdot(C_4H_8O)_2$, FW = 1188.40, monoclinic, $C2/c$, a = 21.142(1), b = 17.907(1), c = 16.4044(7) Å, β = 115.188(4)°, V = 5618.0(6) Å^3, Z = 4, $D_{calc.}$ = 1.405 g cm^{-1}, $R1$ = 0.059, $wR2$ = 0.163. Crystal data for **2**: $C_{66}H_{64}N_{10}Ru_2$, FW = 1199.45, monoclinic, $C2/c$, a = 18.5186(7), b = 11.3288(4), c = 29.7899(9) Å, β = 104.300(3)°, V = 6056.1(4) Å^3, Z = 4, $D_{calc.}$ = 1.315 g cm^{-1}, $R1$ = 0.034, $wR2$ = 0.083.

Computational Methods. The full geometry optimizations of structures **1** and **2** were based on obtained crystal structures of **1** and **2** using the density functional theory (DFT) method,[47] which was based on the hybrid B3LYP[40] density functional model. The basis set used for all atoms was the LanL2DZ[48] and considered the involvement of metals. All calculations were carried out with the Gaussian 03 suite programs.[42]

■ ASSOCIATED CONTENT

Ⓢ Supporting Information

Experimental for **L1**, **L2**, and DFT details of model compounds **1**, **1′**, **2**, **4′**, and $(2)^-$. X-ray crystallographic details (CIF) of **1** and **2**. This material is available free of charge via the Internet at http://pubs.acs.org.

■ AUTHOR INFORMATION

Corresponding Author

* Phone. (765) 494-5466. Fax: (765) 494-0239. E-mail: tren@purdue.edu.

Notes

The authors declare no competing financial interest.

■ ACKNOWLEDGMENTS

We gratefully acknowledge financial support from both the National Science Foundation (CHE 1057621) and Purdue Research Foundation (fellowship to Z.C.).

■ REFERENCES

(1) Nast, R. *Coord. Chem. Rev.* **1982**, *47*, 89−124. Hagihara, N.; Sonogashira, K.; Takahashi, S. *Adv. Polym. Sci.* **1981**, *41*, 149−179. Manna, J.; John, K. D.; Hopkins, M. D. *Adv. Organomet. Chem.* **1995**, *38*, 79−154. Paul, F.; Lapinte, C. *Coord. Chem. Rev.* **1998**, *178*−*180*, 431−509. Higgins, S. J.; Nichols, R. J.; Martin, S.; Cea, P.; Zant, H. S. J. v. d.; Richter, M. M.; Low, P. J. *Organometallics* **2011**, *30*, 7−12. Costuas, K.; Rigaut, S. *Dalton Trans.* **2011**, *40*, 5643−5658.

(2) Ren, T. *Organometallics* **2005**, *24*, 4854−4870.

(3) Whittall, I. R.; McDonagh, A. M.; Humphrey, M. G.; Samoc, M. *Adv. Organomet. Chem.* **1998**, *42*, 291−362. Zhou, G.-J.; Wong, W.-Y. *Chem. Soc. Rev.* **2011**, *40*, 2541−2566.

(4) Wong, W.-Y.; Ho, C.-L. *Acc. Chem. Res.* **2010**, *43*, 1246−1256.

(5) Le Narvor, N.; Toupet, L.; Lapinte, C. *J. Am. Chem. Soc.* **1995**, *117*, 7129−7138. Tanaka, Y.; Shaw-Taberlet, J. A.; Justaud, F.; Cador, O.; Roisnel, T.; Akita, M.; Hamon, J.-R.; Lapinte, C. *Organometallics* **2009**, *28*, 4656−4669. Hoffert, W. A.; Rappé, A. K.; Shores, M. P. *J. Am. Chem. Soc.* **2011**, *133*, 20823−20836.

(6) Weng, W.; Ramsden, J. A.; Arif, A. M.; Gladysz, J. A. *J. Am. Chem. Soc.* **1993**, *115*, 3824−3825. Dembinski, R.; Bartik, T.; Bartik, B.; Jaeger, M.; Gladysz, J. A. *J. Am. Chem. Soc.* **2000**, *122*, 810−822.

(7) Bruce, M. I.; Low, P. J.; Costuas, K.; Halet, J.-F.; Best, S. P.; Heath, G. A. *J. Am. Chem. Soc.* **2000**, *122*, 1949−1962. Hamon, P.; Justaud, F.; Cador, O.; Hapiot, P.; Rigaut, S.; Toupet, L.; Ouahab, L.; Stueger, H.; Hamon, J.-R.; Lapinte, C. *J. Am. Chem. Soc.* **2008**, *130*, 17372−17383. Olivier, C.; Costuas, K.; Choua, S.; Maurel, V.; Turek, P.; Saillard, J.-Y.; Touchard, D.; Rigaut, S. *J. Am. Chem. Soc.* **2010**, *132*, 5638−5651. Li, F.; Cheng, J.; Chai, X.; Jin, S.; Wu, X.; Yu, G.-A.; Liu, S. H.; Chen, G. Z. *Organometallics* **2011**, *30*, 1830−1837. Fox, M. A.; Guennic, B. L.; Roberts, R. L.; Brue, D. A.; Yufit, D. S.; Howard, J. A. K.; Manca, G.; Halet, J.-F.; Hartl, F. e.; Low, P. J. *J. Am. Chem. Soc.* **2011**, *133*, 18433−18446.

(8) Xu, G.-L.; Zou, G.; Ni, Y.-H.; DeRosa, M. C.; Crutchley, R. J.; Ren, T. *J. Am. Chem. Soc.* **2003**, *125*, 10057−10065. Ying, J.-W.; Liu, I. P.-C.; Xi, B.; Song, Y.; Campana, C.; Zuo, J.-L.; Ren, T. *Angew. Chem., Int. Ed.* **2010**, *49*, 954−957. Xi, B.; Liu, I. P. C.; Xu, G.-L.; Choudhuri,

M. M. R.; DeRosa, M. C.; Crutchley, R. J.; Ren, T. *J. Am. Chem. Soc.* **2011**, *133*, 15094−15104.
(9) Blum, A. S.; Ren, T.; Parish, D. A.; Trammell, S. A.; Moore, M. H.; Kushmerick, J. G.; Xu, G. L.; Deschamps, J. R.; Pollack, S. K.; Shashidhar, R. *J. Am. Chem. Soc.* **2005**, *127*, 10010−10011. Kim, B.; Beebe, J. M.; Olivier, C.; Rigaut, S.; Touchard, D.; Kushmerick, J. G.; Zhu, X.-Y.; Frisbie, C. D. *J. Phys. Chem. C.* **2007**, *111*, 7521−7526. Mahapatro, A. K.; Ying, J.; Ren, T.; Janes, D. B. *Nano Lett.* **2008**, *8*, 2131−2136. Luo, L.; Benameur, A.; Brignou, P.; Choi, S. H.; Rigaut, S.; Frisbie, C. D. *J. Phys. Chem. C.* **2011**, *115*, 19955−19961. Ballmann, S.; Hieringer, W.; Secker, D.; Zheng, Q.; Gladysz, J. A.; Görling, A.; Weber, H. B. *ChemPhysChem.* **2011**, *11*, 2256−2260. Benameur, A.; Brignou, P.; Piazza, E. D.; Hervault, Y.-M.; Norel, L.; Rigaut, S. *New J. Chem.* **2011**, *35*, 2105−2113.
(10) Xu, G. L.; Campana, C.; Ren, T. *Inorg. Chem.* **2002**, *41*, 3521−3527. Xi, B.; Ren, T. *C. R. Chimie.* **2009**, *12*, 321−331.
(11) Ren, T.; Xu, G. L. *Commun. Inorg. Chem.* **2002**, *23*, 355−380.
(12) Choi, S. H.; Kim, B.; Frisbie, C. D. *Science* **2008**, *320*, 1482−1486.
(13) Choi, S. H.; Risko, C.; Delgado, M. C. R.; Kim, B.; BreÌdas, J.-L.; Frisbie, C. D. *J. Am. Chem. Soc.* **2010**, *132*, 4358−4368.
(14) Ashwell, G. J.; Phillips, L. J.; Robinson, B. J.; Urasinska-Wojcik, B.; Lambert, C. J.; Grace, I. M.; Bryce, M. R.; Jitchati, R.; Tavasli, M.; Cox, T. I.; Sage, I. C.; Tuffin, R. P.; Ray, S. *ACS Nano* **2010**, *4*, 7401−7406. Ashwell, G. J.; Phillips, L. J.; Robinson, B. J.; Barnes, S. A.; Williams, A. T.; Urasinska-Wojcik, B.; Lambert, C. J.; Grace, I. M.; Cox, T. I.; Sage, I. C. *Angew. Chem., Int. Ed.* **2011**, *50*, 8722−8726.
(15) Whittall, I. R.; Humphrey, M. G.; Houbrechts, S.; Persoons, A.; Hockless, D. C. R. *Organometallics* **1996**, *15*, 5738−5745. Whittall, I. R.; Cifuentes, M. P.; Humphrey, M. G.; Luther-Davies, B.; Samoc, M.; Houbrechts, S.; Persoons, A.; Heath, G. A.; Bogsanyi, D. *Organometallics* **1997**, *16*, 2631−2637. Whittall, I. R.; Humphrey, M. G.; Persoons, A.; Houbrechts, S. *Organometallics* **1996**, *15*, 1935−1941.
(16) Ghazala, S. I.; Gauthier, N.; Paul, F.; Toupet, L.; Lapinte, C. *Organometallics* **2007**, *26*, 2308−2317.
(17) Wadas, T. J.; Chakraborty, S.; Lachicotte, R. J.; Wang, Q.-M.; Eisenberg, R. *Inorg. Chem.* **2005**, *44*, 2628−2638.
(18) Cummings, S. P.; Geanes, A. R.; Fanwick, P. E.; Kharlamova, A.; Ren, T. *J. Organomet. Chem.* **2011**, *696*, 3955−3960.
(19) Ren, T. *Chem. Rev.* **2008**, *108*, 4185−4207. Ren, T. *C. R. Chim.* **2008**, *11*, 684−692.
(20) Cummings, S. P.; Cao, Z.; Liskey, C. W.; Geanes, A. R.; Fanwick, P. E.; Hassell, K. M.; Ren, T. *Organometallics* **2010**, *29*, 2783−2788.
(21) Xu, G. L.; Jablonski, C. G.; Ren, T. *Inorg. Chim. Acta* **2003**, *343*, 387−390.
(22) Hurst, S. K.; Xu, G. L.; Ren, T. *Organometallics* **2003**, *22*, 4118−4123.
(23) Xu, G. L.; Crutchley, R. J.; DeRosa, M. C.; Pan, Q. J.; Zhang, H. X.; Wang, X. P.; Ren, T. *J. Am. Chem. Soc.* **2005**, *127*, 13354−13363.
(24) Ying, J. W.; Cordova, A.; Ren, T. Y.; Xu, G. L.; Ren, T. *Chem.—Eur. J.* **2007**, *13*, 6874−6882.
(25) Lin, C.; Ren, T.; J. Valente, E.; D. Zubkowski, J. *J. Chem. Soc., Dalton Trans.* **1998**, 571−576.
(26) Ying, J. W.; Ren, T. *J. Organomet. Chem.* **2006**, *691*, 4021−4027.
(27) Liu, I. P. C.; Ren, T. *Inorg. Chem.* **2009**, *48*, 5608−5610.
(28) Whittall, I. R.; Humphrey, M. G.; Hockless, D. C. R. *Aust. J. Chem.* **1997**, *50*, 991−998.
(29) Whittall, I. R.; Humphrey, M. G.; Hockless, D. C. R. *Aust. J. Chem.* **1998**, *51*, 219−228.
(30) Montalvo-Gonzalez, R.; Ariza-Castolo, A. *J. Mol. Struct.* **2003**, *655*, 375−389.
(31) Xi, B.; Xu, G. L.; Fanwick, P. E.; Ren, T. *Organometallics* **2009**, *28*, 2338−2341.
(32) Ying, J. W.; Sobransingh, D. R.; Xu, G. L.; Kaifer, A. E.; Ren, T. *Chem. Commun.* **2005**, 357−359.
(33) Ying, J. W.; Ren, T. *J. Organomet. Chem.* **2008**, *693*, 1449−1454.
(34) Hansch, C.; Leo, A.; Taft, R. W. *Chem. Rev.* **1991**, *91*, 165−195.
(35) Ren, T. *Coord. Chem. Rev.* **1998**, *175*, 43−58.
(36) Shaabani, B.; Shaghaghi, Z. *Tetrahedron* **2010**, *66*, 3259−3264.
(37) Costuas, K.; Paul, F.; Toupet, L.; Halet, J.-F.; Lapinte, C. *Organometallics* **2004**, *23*, 2053−2068. Paul, F.; Ellis, B. G.; Bruce, M. I.; Toupet, L.; Roisnel, T.; Costuas, K.; Halet, J.-F.; Lapinte, C. *Organometallics* **2006**, *25*, 649−665. Paul, F.; Toupet, L.; Thepot, J. Y.; Costuas, K.; Halet, J. F.; Lapinte, C. *Organometallics* **2005**, *24*, 5464−5478. Denis, R.; Toupet, L.; Paul, F.; Lapinte, C. *Organometallics* **2000**, *19*, 4240−4251.
(38) Xu, G.-L.; DeRosa, M. C.; Crutchley, R. J.; Ren, T. *J. Am. Chem. Soc.* **2004**, *126*, 3728−3729.
(39) Forrest, W. P.; Cao, Z.; Fanwick, P. E.; Hassell, K. M.; Ren, T. *Organometallics* **2011**, *30*, 2075−2078.
(40) Becke, A. D. *J. Chem. Phys.* **1993**, *98*, 5648−5652. Lee, C. T.; Yang, W. T.; Parr, R. G. *Phys. Rev. B.* **1988**, *37*, 785−789.
(41) Stephens, P. J.; Devlin, F. J.; Chabalowski, C. F.; Frisch, M. J. *J. Phys. Chem.* **1994**, *98*, 11623−11627.
(42) Frisch, M. J.; Trucks, G. W.; Schlegel, H. B.; Scuseria, G. E.; Robb, M. A.; Cheeseman, J. R.; Montgomery, J. A., Jr.; Vreven, T.; Kudin, K. N.; Burant, J. C.; Millam, J. M.; Iyengar, S. S.; Tomasi, J.; Barone, V.; Mennucci, B.; Cossi, M.; Scalmani, G.; Rega, N.; Petersson, G. A.; Nakatsuji, H.; Hada, M.; Ehara, M.; Toyota, K.; Fukuda, R.; Hasegawa, J.; Ishida, M.; Nakajima, T.; Honda, Y.; Kitao, O.; Nakai, H.; Klene, M.; Li, X.; Knox, J. E.; Hratchian, H. P.; Cross, J. B.; Bakken, V.; Adamo, C.; Jaramillo, J.; Gomperts, R.; Stratmann, R. E.; Yazyev, O.; Austin, A. J.; Cammi, R.; Pomelli, C.; Ochterski, J. W.; Ayala, P. Y.; Morokuma, K.; Voth, G. A.; Salvador, P.; Dannenberg, J. J.; Zakrzewski, V. G.; Dapprich, S.; Daniels, A. D.; Strain, M. C.; Farkas, O.; Malick, D. K.; Rabuck, A. D.; Raghavachari, K.; Foresman, J. B.; Ortiz, J. V.; Cui, Q.; Baboul, A. G.; Clifford, S.; Cioslowski, J.; Stefanov, B. B.; Liu, G.; Liashenko, A.; Piskorz, P.; Komaromi, I.; Martin, R. L.; Fox, D. J.; Keith, T.; Al-Laham, M. A.; Peng, C. Y.; Nanayakkara, A.; Challacombe, M.; Gill, P. M. W.; Johnson, B.; Chen, W.; Wong, M. W.; Gonzalez, C.; Pople, J. A. *Gaussian 03, Revision D.02*, Wallingford, Ct., 2003.
(43) Hehre, W. J.; Ditchfield, R.; Pople, J. A. *J. Chem. Phys.* **1972**, *56*, 2257−2261. Krishnan, R.; Binkley, J. S.; Seeger, R.; Pople, J. A. *J. Chem. Phys.* **1980**, *72*, 650−654. Hariharan, P. C.; Pople, J. A. *Theor. Chim. Acta* **1973**, *28*, 213−222.
(44) Bunting, P.; Chisholm, M. H.; Gallucci, J. C.; Lear, B. J. *J. Am. Chem. Soc.* **2011**, *133*, 5873−5881. Chisholm, M. H.; Lear, B. J. *Chem. Soc. Rev.* **2011**, *40*, 5254−5265.
(45) Beurskens, P. T.; Beurskens, G.; deGelder, R.; Garcia-Granda, S.; Gould, R. O.; Smits, J. M. M. *The DIRDIF2008 Program System, Crystallography Laboratory*; University of Nijmegen: The Netherlands: 2008.
(46) Sheldrick, G. M. *Acta Crystallogr.. A.* **2008**, *64*, 112−122.
(47) Parr, R. G.; Yang, W. *Density Functional Theory of Atoms and Molecules*; Oxford University Press: New York, 1989.
(48) Hay, P. J.; Wadt, W. R. *J. Chem. Phys.* **1985**, *82*, 270−283. Wadt, W. R.; Hay, P. J. *J. Chem. Phys.* **1985**, *82*, 284−298. Hay, P. J.; Wadt, W. R. *J. Chem. Phys.* **1985**, *82*, 299−310.